TRANSIENT GROUNDWATER FLOW IN A SLOPING AQUIFER WITH SURFACE WATER-GROUNDWATER INTERACTION

A Dissertation

by

XIN LIU

Submitted to the Office of Graduate and Professional Studies of
Texas A&M University
in partial fulfillment of the requirements for the degree of

DOCTOR OF PHILOSOPHY

Chair of Committee,	Hongbin Zhan
Committee Members,	David Sparks
	Peter Knappett
	Huilin Gao
Head of Department,	John R. Giardino

December 2018

Major Subject: Water Management and Hydrological Science

ABSTRACT

The theory of groundwater flow in a sloping aquifer is indispensable to understand water exchange among atmosphere, surface water and an aquifer. However, for various reasons, the theory of groundwater flow in a sloping aquifer is still not understood clearly. In the past decades, several researchers have studied groundwater flow in a sloping aquifer using analytical and numerical methods and laboratory experiments. The purpose of this dissertation is to advance the hydrodynamics of transient groundwater flow in a sloping aquifer with surface water-groundwater interaction. A few new models and their semi-analytical and numerical solutions are developed to study the water table fluctuations and river-aquifer fluxes in the presence of an unconfined sloping aquifer. The first model is built for a sloping aquifer with a river on left side and infinite extent on the other side. The second model is built for a sloping aquifer with two parallel rivers. The two models both provide general considerations about the less permeable sedimentary layer (or clogging layer) between an aquifer and surface water, the time-dependent river stages, and responses of time-dependent recharge by infiltration. Special attention has been paid to the impact of sloping feature, among other parameters, on the evolution of the water table profile and the river-aquifer fluxes. The analytical solutions are developed using a linearized Boussinesq equation modified for a sloping aquifer, and they are compared with a finite element COMSOL program for the same linearized Boussinesq equation. Excellent agreement was found between the analytical solution and the COMSOL program. The analytical solution is subsequently compared with a full scale numerical model using HydroGeoSphere to consider coupled unsaturated-saturated

flow process. The result indicates that the linearized analytical solution can serve as a reliable surrogate of the full scale numerical model when the sloping angle is less than 10 degrees. The flow character of a sloping aquifer is quite different from that of a horizontal aquifer, and the variations of river stages will cause much more variations of water table heights and river-aquifer fluxes in a sloping aquifer. In particular, the water table profile in a sloping aquifer shows some unique features that have never been seen in a horizontal aquifer, as the water table profile may evolve from a straight line parallel with the sloping bed at the beginning to a convex shape, even without any recharge/evaporation. Another new model acknowledging the realistic initial conditions and river stage variation is proposed with the help of sequential Sigmoid functions for describing the river stage. One benefit of using the Sigmoid functions is that it allows enough time for the system to reach its pseudo-steady state before the rapid rising or falling of the river stage. Therefore, this avoids the idealized (and often unrealistic) initial condition of a constant water table height above the impermeable base as was assumed by many previous investigations. Finally, the limitations of the study and future work are outlined.

DEDICATION

To my family

ACKNOWLEDGEMENTS

I would like to express my sincere appreciation to my advisor, Dr. Hongbin Zhan, who has supervised me although my PhD studies. Dr. Zhan pays a lot of attention to my research and personal life during my studies.

I would like to thank my committee members, Dr. Huilin Gao, Dr. David Sparks and Dr. Peter Knappett, for their guidance and improvement throughout this research.

I would like to thank Dr. Xiuyu Liang a lot for your analytical guidance. Dr. Yang Xian, thank you for the guidance of HydroGeoSphere. Dr. Quanrong Wang, thank you for your guidance of numerical model.

Finally, Thanks also to my parents and friends Renjie Zhou, Xin Peng, Kewei Chen, Shuo Yang and Zhenlei Yang for their support and encouragement during my studies.

CONTRIBUTORS AND FUNDING SOURCES

This work was supervised by a dissertation committee consisting of Professor Hongbin Zhan [advisor], Professor Peter Knappett, Professor Huilin Gao of the Department of Water Management and Hydrological Science, and Professor David Sparks of the Department of Geology and Geophysics.

All other work conducted for the dissertation was completed by the student, in collaboration with Professor Xiuyu Liang of Southern University of Science and Technology, Professor Quanrong Wang and Dr. Yang Xian of China University of Geosciences.

Graduate study was supported by financial aid from the Department of Water Management and Hydrological Science, Texas A&M University.

TABLE OF CONTENTS

LIST OF FIGURES

NOMENCLATURE

Symbol	Definition	unit
a_k	A fitting parameter of river stage function in Eq. (4-1)	T^{-1}
b	Thickness of vertical clogging layer	L
b_1	Thickness of vertical clogging layer between aquifer and river 1	L
b_2	Thickness of vertical clogging layer between aquifer and river 2	L
C_1	Constant to determine the steady-state water table height in a sloping aquifer	L
C_2	Constant to determine the steady-state water table height in a sloping aquifer	L
c_k	A fitting parameter of river stage function in Eq. (4-1)	T
D	Hydraulic diffusivity	L/T
e	Euler's number	dimensionless
h	Water table height measured in the vertical direction from the sloping impervious base	L
h_a	Average saturated depth of aquifer	L
h_f	Final stage value of river	L
h_{f_1}	Final stage value of river 1	L
h_{f_2}	Final stage value of river 2	L
h_i	Initial stage of river at t=0	L
h_s	Time-dependent stage of river	L
h_{s_1}	Time-dependent stage of river 1	L
h_{s_2}	Time-dependent stage of river 2	L
k	Hydraulic conductivity of the clogging layer	L/T
k_1	Hydraulic conductivity of the clogging layer between aquifer and river 1	L/T

k_2	Hydraulic conductivity of the clogging layer between aquifer and river 2	L/T
K	Hydraulic conductivity along the bedding direction	L/T
$K(\cdot)$	Fourier transform kernel	dimensionless
L	Horizontal length of aquifer	L
p_k	A fitting parameter of river stage function in Eq. (4-1)	dimensionless
q	Discharge over the entire unconfined aquifer per unit width	L^2/T
Q_1	River-aquifer flux between aquifer and river 1	L^2/T
Q_2	River-aquifer flux between aquifer and river 2	L^2/T
S_y	Specific yield of the aquifer	dimensionless
t	Time	T
T	Characteristic time	T
x	Horizontal coordinate	T
θ	Sloping angle	dimensionless
λ	A fitting parameter of river stage function in Eq. (2-6)	T^{-1}
λ_1	A fitting parameter of river stage function in Eq. (3-1a)	T^{-1}
λ_2	A fitting parameter of river stage function in Eq. (3-1b)	T^{-1}
ω_n	Fourier transform eigenvalue	dimensionless
ODE	Ordinary different equation	
PDE	Partial different equation	
RPD	Relative percentage difference	
a_{kD}	Dimensionless form of a_k	dimensionless
c_{kD}	Dimensionless form of c_k	dimensionless
h_D	Dimensionless form of h	dimensionless
t_D	Dimensionless form of t	dimensionless
x_D	Dimensionless form of x	dimensionless
λ_D	Dimensionless form of λ	dimensionless
λ_{1D}	Dimensionless form of λ_1	dimensionless
λ_{2D}	Dimensionless form of λ_2	dimensionless

CHAPTER 1

INTRODUCTION

The conventional theories concerning groundwater flow in aquifers often assume that aquifers are horizontally oriented (Bear, 1972; Fetter, 1999; Domenico and Schwartz, 1998). However, under certain geological settings, aquifers could be sloping instead of horizontal. Sloping aquifers are widely discovered in regions with volcanic activities (Cabrera and Custodio, 2004; Join et al., 2005), karstic formations (Plan et al., 2009; Sauro et al., 2013), anticline and syncline structures (Ashjari and Raeisi, 2006), coal seams (Zhang and Shen, 2004; Sun and Miao, 2017; Wang et al., 2017), and coastal formations (Dutton et al., 2003; Cabrera and Custodio, 2004). For instance, Join et al. (2005) pointed out that the sloping geological structure of an the active shield volcano in the Piton de la Fournaise volcano provided sufficient hydrological conditions to produce a high water table (as much as 1800 m above sea level) in the interior of the island. This finding bears similarity with the study of Cabrera and Custodio (2004) for the Teide volcano in Canary Islands, Spain, but contrasts with the conventional Hawaiian conceptual models in which the occurrence of high water levels near the volcanos was thought to be caused by groundwater flow barriers such as dikes or other local impervious layers, as observed in Kilauea of Hawaii (Ingebritsen and Scholl, 1993). Ashjari and Raeisi (2006) studied the influences of anticlinal structure on regional flow in Carbonate Karstic formations of Zagros of Iran and showed that regional groundwater flow patterns are closely controlled by the anticlinal structure of aquifers and geometry of bedrock.

Among other features, the inclined angle of a sloping aquifer is one of the most important factors controlling the groundwater dynamics in such an aquifer. Plan et al. (2009) and Sauro et al. (2013) presented case studies of inclined strata in a karstic area in Austria and northeast Italy, respectively, where the inclination of the strata can be as high as 15 to 45 degrees. Wang et al. (2017) studied the CO_2 geological storage in a sloping saline aquifer in Qinshui Basin of China and noticed that the inclined angles of strata angles ranged from 0 to 16 degrees. The CO_2 geological storage is an effective way for CO_2 emission reduction. Wang et al. (2017) studied the influences of sloping angle to the effective storage space for CO_2. Their results show that the greater the dip angle, the greater the effective reservoir space reduces. Sun and Miao (2017) studied the inclined coal seam and stated that the slope angle generally ranged from 0 to 45 degrees. They state that if research based on the horizontal and near-horizontal seams are applied to predict water inrush from an inclined coal seam floor, serious errors may occur, resulting in safety hazards. The Carrizo-Wilcox aquifer underneath central Texas is an aquifer inclining towards Gulf of Mexico with a sloping angle from 0.25º to 2º (Dutton et al., 2003).

Despite the wide distribution of sloping aquifers around the globe, groundwater dynamics in such a ubiquitous system is still poorly understood, particularly when surface water and groundwater interaction is also involved. For instance, it is generally unclear if the conventional theories developed for groundwater flow under the horizontal aquifer assumption are still valid within sloping aquifers. One specific question is: under what slope angles will the horizontal flow theory may be acceptable as an approximation for sloping aquifers, when surface water and groundwater interaction is involved? To

answer this question, we will conduct a brief literature review on groundwater dynamics concerning sloping aquifers under the influence of surface water level fluctuations in the following section and then outline the specific objective of this study, which is to fill a knowledge gap on the sloping aquifer flow concerning surface water and groundwater interaction.

Previous investigations by a number of scientists have formulated and developed corresponding mathematical models to describe water table fluctuations caused by dynamic water exchange between surface water and an unconfined aquifer overlying a horizontal bed, based on the Boussinesq equation (Bouwer, 2002; Ghosh et al., 2015; Glover and Balmer, 1954; Hantush, 1967; Manglik et al., 1997; Mustafa, 1987; Polubarinova and Kochina, 1962; Rai and Singh, 1992; Rai and Singh, 1995; Ram et al., 1994; Schmid and Luthin, 1964; Theis, 1941; Workman et al., 1997). The nonlinear nature of the Boussinesq equation often requires a numerical model to approximate the solution, but approximate analytical solution of the Boussinesq equation is also popular and highly valuable for gaining physical insights into the physical processes involved (Koussis and Lien, 1982; Koussis et al., 1998; Upadhyaya and Chauhan, 1998).

Boussinesq (1877) made the assumption that when the lateral extent of an aquifer is much larger than its thickness, then groundwater flows primarily along the direction of the bedding slope. Many subsequent investigations showed that the Boussinesq assumption was accurate in cases with sloping aquifers (Chauhan et al., 1968; Childs, 1971; Marei and Towner, 1975; Wooding and Chapman, 1966), and this assumption was commonly used to study the sloping aquifer with the modified Darcy's Law (Brutsaert, 1994; Chapman, 1980; Childs, 1971). As a result, most analytical studies concerning the

sloping aquifer were based on this Boussinesq assumption. Shukla et al. (1990) obtained a finite-difference solution of the Boussinesq equation for a sloping aquifer and compared the results with an earlier steady-state analytical solution of Schmid and Luthin (1964) and experiments of Luthin and Guitjens (1967). Shukla et al. (1990) claimed that when the sloping angle was less than 16.7º, the Boussinesq equation can be used to characterize the groundwater table. Verhoest and Troch (2000) developed an analytical solution of the linearized Boussinesq equation with recharge by infiltration for a sloping aquifer, and they focused on the response of groundwater table at the onset of rainfall storm in a hillslope system. Zissis et al. (2001) presented an analytical solution of seepage from a stream with a dynamic stream stage into an adjacent sloping unconfined aquifer of semi-infinite extent, considering the effects of recharge from infiltration. They found an excellent agreement between their analytical solution and a properly crafted numerical solution.

Upadhyaya and Chauhan (2002) developed analytical solutions of the linearized Boussinesq equation for a system with an unconfined sloping aquifer with two canals and constant recharge, but did not consider the changes of canal river stages and the effects of a thin less permeable sedimentary layer lining the bottom and side of the canals. Upadhyaya and Chauhan (2002) compared their analytical solution with a fully implicit finite-difference numerical solution of the Boussinesq equation for various sloping angles of 0º, 2.86º, 5.71º and the solution of Mustafa (1987) for a horizontal aquifer. They found that the point of minimum water table height tended to shift from the middle region toward the lower canal when the sloping angle increased. They also noticed that linearization of the Boussinesq equation resulted in overestimation of the water table

height, a conclusion held true for both sloping and horizontal aquifers. Akylas and Koussis (2007) studied groundwater flow in a sloping aquifer considering a step function increase (or decrease) in stream stage and an impervious boundary on one side, with a mild sloping angle varying within ±3º. They provided a host of analytical solutions for various possible cases that may be seen in the field. Bansal et al. (2016) combined the effects of bed slope, clogging layer, and variable stream stages on one side of a sloping aquifer, and then developed analytical solutions to quantify the interaction of surface water and groundwater, but this article is problematic in treating the boundary condition associated with the vertical clogging layer. Detailed discussion about this issue will be provided later. Troch et al. (2003) studied the influence of the hillslope shape for groundwater flow and interaction of surface water and groundwater, and they discussed different behaviors of hillslope drainage under a number of hillslope types (uniform, convergent, divergent) and hillslope angles.

A careful examination of the above referenced studies suggests that there is still not a general analytical model that considers the most important factors of governing groundwater dynamics in a sloping aquifer is still lacking. These factors include: 1) clogging layers between bounding river and the aquifer; 2) variable vertical recharge; 3) variable river stage. Furthermore, none of the analytical models developed so far have been compared with numerical models incorporating coupled saturated-unsaturated flow processes. Therefore, the overarching objective of this study is to develop a general purpose model that simulates these important processes governing groundwater flow in a dynamically fluctuating, sloped aquifer, under the influence of a dynamically fluctuating river. Specifically, the following objectives will be achieved. First, to develop a general

analytical model to study water table heights and water exchanges in an unconfined sloping aquifer which is connected to a time-dependent river (through a clogging layer). Second, to study different responses of water table fluctuations and lateral fluxes between the aquifer and a river with variable stage, combined with time-dependent infiltrated recharge across the top of a sloping aquifer. Third, to compare the differences of results between the newly developed analytical model and two new numerical models. The first numerical model was a linearized one-dimensional (1D) Boussinesq equation using COMSOL Multiphysics. The second numerical model was a solution to the two-dimensional (2D) Boussinesq equation using HydroGeoSphere (Therrien et al., 2006). A point to note is that the 2D HydroGeoSphere program considers both the saturated and unsaturated flow processes, while the analytical model and the 1D COMSOL program only consider the saturated flow process. Fourth, to investigate the differences in water table heights and river-aquifer fluxes from the newly developed analytical model in section 2 and Bansal's analytical solution. Fifth, to develop a general analytical model to study water table heights and water exchanges between two rivers and the unconfined sloping aquifer (through the clogging layers). Sixth, to compare the water table fluctuations and river-aquifer fluxes in an unconfined sloping aquifer with two rivers from the developed analytical solution, the numerical solution by COMSOL, and the numerical solution including the saturated and unsaturated processes by HydroGeoSphere. Finally, to develop a new method to fill a gap of analytical models in a sloping aquifer. Such a new method can use a new function to describe a realistic river stage. In the study of building ground water model, when an initial water table heights are unknown, identical initial water table heights and initial boundary heads are set in the

horizontal aquifer and sloping aquifer. In the sloping aquifer, the identical initial water table heights and initial boundary heads are not steady-state. The water table may change rapidly at the beginning of time. That function can reconcile the initial condition problem for transient groundwater flow in a sloping aquifer.

CHAPTER 2

TRANSIENT GROUNDWATER FLOW IN A SLOPING AQUIFER WITH ONE RIVER

2.1 Introduction

A river connected to an unconfined aquifer is a very general phenomenon in the hydrological cycle. The impermeable beds defining the lower boundary of unconfined aquifers are commonly gently inclined. In Chapter 1, we have mentioned that an unconfined aquifer with a connected river on one side and semi-infinite on the other side was studied by Zissis et al. (2001) and Bansal et al. (2016). Zissis et al. (2001) considered the influences of recharges from the various river stages and precipitation, but they did not consider the influences of a river bed clogging layer between river and aquifer. Bansal et al. (2016) considered the influences of the varying river stage of river and the clogging layer between river and aquifer, but they did not consider the vertical recharge. Furthermore, the boundary condition Bansal et al. used for treating the clogging layer was erroneous. The questions we try to answer are: 1) Will all these factors (e.g., vertical recharge, river bed clogging layer, varying river stage) affect water table fluctuations and river-aquifer fluxes equally? 2) Is Bansal's solution valid or not for studying groundwater flow in a sloping unconfined aquifer? 3) Is the unsaturated zone process (capillary retention) affect groundwater table significantly or not in a sloping aquifer? In this chapter, we will develop a new analytical model explicitly considering all these factors. The specific tasks to achieve this goal follows. First, we will compare the newly developed analytical solution using a finite element model based on a COMSOL

program. Second, we will study the influences of unsaturated zone process using the coupled unsaturated-saturated flow and transport model of HydroGeoSphere (Therrien et al., 2006). Third, our new analytical solution improves Bansal's boundary condition (Bansal et al. ignored an important term in their boundary condition), and we will check the effects of Bansal's boundary condition by comparing our new analytical solution with the Bansal's solution. Finally, we will investigate the influences of several factors on the aquifer hydrodynamics, such as hydraulic conductivity of the aquifer, hydraulic resistance of the clogging layer, specific yield of the aquifer, infiltration-induced recharge, the variational stage of river, the slope angle and direction of the aquifer (downward or upward).

2.2 Mathematical model

A sloping aquifer with a river on left side and semi-infinite on the other side with recharge infiltrating across the upper surface of the aquifer is schematically shown in Fig. 2-1. The river fully penetrates the aquifer and its stage can vary with time. The aquifer is homogeneous. A thin vertical low-permeability (clogging) layer separates the river from the aquifer. The thicknesses of vertical clogging layer is b, and the hydraulic conductivities of the clogging layer is k. The clogging layer consists of fine sediments such as clay, silt, and fine sand rich materials and its permeability is assumed to be much smaller (at least one order of magnitude smaller) than that of the aquifer. The sloping aquifer bed can be downward or upward from left to right. In this study, downward slope angles are positive while upward slopes are negative. The origin of the coordinate system is at the intercept of the clogging layer with the base of the aquifer. The x-axis is horizontal, increasing to the right, and the z-axis is upward vertical. The unconfined

aquifer is assumed to extend infinitely along the *y*-axis (or the direction perpendicular to the *xz* plane). The vertical recharge can vary with time, but is assumed to be uniform along the *x* axis. The horizontal length of aquifer is infinite on one side (right side in Fig. 2-1). The sloping angle is θ.

We should point out that this conceptual model of a river-aquifer system is consistent with many previous investigations concerning a horizontal aquifer (Ram et al., 1994; Liang and Zhang, 2012; Moutsopoulos, 2013). However, it is different from some recent investigations of a river-aquifer system that honors the importance of bank storage in supplying baseflow. For instance, Rhodes et al. (2017) showed that the river is well connected to bank storage zones on each side of the river, but poorly connected from the broader alluvial aquifer when studying the Brazos River near College Station, Texas.

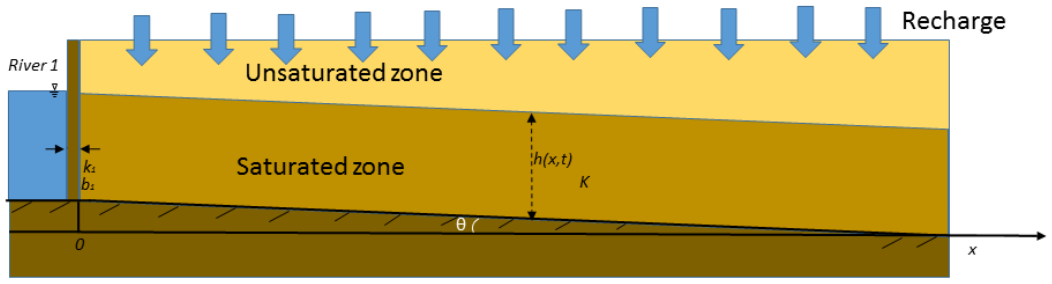

Fig. 2-1 The diagram of the sloping aquifer adjoining with one river with a vertical clogging layer.

Nevertheless, based on the extended Dupuit-Forchheimer assumption or the Boussinesq assumption (1877), the streamlines are considered parallel to the sloping impermeable bed. The modified Darcy's law for such a sloping aquifer is (Chapman, 1980):

$$q(x,t) = -Kh\left(\frac{\partial h}{\partial x} - tan\theta\right)cos^2\theta \tag{2-1}$$

where q is the discharge over the entire unconfined aquifer per unit width; K is the hydraulic conductivity along the bedding (sloping) direction; x is horizontal coordinate; $h=h(x, t)$ is water table height measured in the vertical direction from the sloping impervious base. The modified Darcy's law is derived in Appendix D. Be aware that $h(x, t)$ here is not the hydraulic head as it is not measured against a fixed horizontal reference, rather, it is measured against a sloping base. It is also obvious that if the sloping angle drops to zero, Eq. (2-1) then becomes the standard Darcy's law for horizontal flow in an unconfined aquifer. According to the mass-balance principle, the equation of groundwater flow for a sloping aquifer without any vertical recharge can be expressed as following:

$$\frac{\partial q}{\partial x} + S_y\frac{\partial(h-xtan\theta)}{\partial t} = 0 \tag{2-2}$$

where S_y is specific yield of the aquifer. Substituting Eq. (2-1) into Eq. (2-2) and adding a time-dependent infiltration-induced recharge of $W(t)$, one has

$$\frac{W(t)}{Kcos^2\theta} + \frac{\partial}{\partial x}\left(h\frac{\partial h}{\partial x}\right) - tan\theta\frac{\partial h}{\partial x} = \frac{S_y}{Kcos^2\theta}\frac{\partial h}{\partial t} \tag{2-3}$$

Eq. (2-3) is the governing equation of flow in an unconfined sloping aquifer with recharge, and it may be regarded as the modified Boussinesq equation for a sloping aquifer. The nonlinear nature of Eq. (2-3) is difficult to solve analytically except for a few special cases, similar to the problem of dealing with the Boussinesq equation for an unconfined aquifer with a horizontal base. However, after linearization of Eq. (2-3), we will show that a robust analytical model can be obtained. To proceed, we replace the term

h associated with $\partial h/\partial x$ in the first bracket of the left side of Eq. (2-3) by a prescribed average saturated depth h_a as below.

$$\frac{W(t)}{Kh_a cos^2\theta} + \frac{\partial^2 h}{\partial x^2} - \frac{tan\theta}{h_a}\frac{\partial h}{\partial x} = \frac{S_y}{Kh_a cos^2\theta}\frac{\partial h}{\partial t} \quad (2\text{-}4)$$

The flow rate includes a linearized parameter h_a is follows.

$$q(x,t) = -K\left(h_a\frac{\partial h}{\partial x} - htan\theta\right)cos^2\theta \quad (2\text{-}5)$$

Rivers commonly have dynamic stages because of rainfall, snowmelt, base flow (Mahoney and Rood, 1998) and human activities like periodic dam releases and sedimentary changes (Chen et al., 2001). A rigorous approach for dealing with a river-aquifer system is to incorporate coupled open-channel flow in the river channel and groundwater flow in the aquifer with water flux exchange between the rivers and aquifer. Such a fully coupled approach is beyond the scope of this investigation and will be pursued later. To simplify the problem, the river stage is assumed to vary with time, following a prescribed function. As suggested by Teloglou and Bansal (2012) and others, an exponential function using to describe the river stage will be chosen here as an example. A hydrograph after the pass of a flood wave consists of a rising limb, followed by a falling limb until it reaches the baseflow recession. The base flow recession curves are often described as an exponentially decayed function of time, and the rising branch of a hydrograph may also be approximated by an exponential function of time (Teloglou and Bansal, 2012). We need to point out that other types of river stage functions can also be used if they are shown to match the river stage measurements. Nevertheless, the time-independent river stage is given by the following Eq. (2-6), where $h_s(t)$ is the time-

varying stages for river, h_f is the final stage value for river, h_i is the initial stage for river at t=0; λ is the rate of change used for the exponential functions for river.

$$h_s(t) = h_f - (h_f - h_i)e^{-\lambda t} \quad (2\text{-}6)$$

The following Eq. (2-7a) is the initial water table height, designated as h_i. Such an initial condition has been used in many previous investigations such as Bansal (2016) and others. However, despite its wide use in previous studies, caution must be taken for its use in a sloping aquifer because of a few considerations. First, the use of this initial condition is primarily for the sake of simplifying the analytical model, not because it is commonly seen in real settings. In fact, it is very unlikely to see a uniform water table height above the impermeable base in a sloping aquifer unless there is some sources of water supply (either from recharge or a constant-head boundary in an upper elevation) to sustain the down-gradient flow along the sloping bed. A non-uniform distribution of the water table height cross the domain of interest is mostly like to occur in a real-world setting. Such an issue will be specifically studied in Chapter 4.

Moutsopoulos (2013) developed a linear approximation method for Robin boundary condition, and assumed that the head loss in the vertical clogging layer is much less than the water table height, thus one has $h(x = 0^+, t) + h_s(t) \approx 2h(x = 0^+, t)$ in the vertical clogging layer. The Robin boundary condition is also called as the third boundary condition. It describes head-dependent flux and it is usually used to study a leakage process, such as vertical leakage through basal sediments. Based on this approximation and modified Darcy's law for a sloping aquifer, the boundary condition at interface between the vertical clogging layer and aquifer is obtained in Eq. (2-7b). The right side of

Eq. (2-7b) represents the flow rates in the clogging layer. The left side of Eq. (2-7b) represents the flow rate at the interface between the clogging layer and aquifer. Bansal et al. (2016) used a similar method to deal with the boundary condition of the vertical clogging layer. But they ignored the term of –tan(θ) on the left side, which is included in the left bracket of Eq. (2-7b). This term is important in a sloping aquifer and it reflects the driving force associated with the sloping bed. In section 2.3.2, we will rigorously investigate whether this term can be ignored in an unconfined sloping aquifer or not. Eq. (2-7c) represents the condition that the water table heights do not vary with the horizontal distance in a very long distance from the left boundary L.

$$h(x, t = 0) = h_i \tag{2-7a}$$

$$-Kh(x = 0^+, t)[(\frac{\partial h}{\partial x})_{x=0} - tan\theta] = -kh(x = 0^+, t)\frac{h(x=0^+,t)-h_s(t)}{b} \tag{2-7b}$$

$$\frac{\partial h}{\partial x}_{x=L} = 0 \tag{2-7c}$$

Defining the following dimensionless terms, $h_D = \frac{h-h_i}{h_f-h_i}$, $x_D = \frac{x}{L}$, $t_D = \frac{Kh_a cos^2\theta t}{S_y L^2}$, $\alpha = \frac{Ltan\theta}{h_a}$, $W(t_D) = \frac{L^2 W(t)}{(h_f-h_i)Kh_a cos^2\theta}$, $R = \frac{Kb}{kL}$, $\lambda_D = \frac{S_y L^2 \lambda}{K\mathrm{h_a} cos^2\theta}$, $m = \frac{Kbtan\theta}{k(h_f-h_i)}$, the dimensionless forms of Eq. (2-4) and Eqs. (2-7a) to (2-7c) are presented as below.

$$\frac{\partial^2 h_D}{\partial {x_D}^2} - \alpha\frac{\partial h_D}{\partial x_D} + W(t_D) = \frac{\partial h_D}{\partial t_D} \tag{2-8}$$

$$h_D(x_D, t_D = 0) = 0 \tag{2-9a}$$

$$R(\frac{\partial h_D}{\partial x_D})_{x_D=0} = h_D(x_D = 0^+, t_D) + e^{-\lambda_D t_D} - 1 + m \tag{2-9b}$$

$$(\frac{\partial h}{\partial x_D})_{x_D=1} = 0 \tag{2-9c}$$

Define a new parameter $\varphi = h_D e^{-\frac{\alpha x_D}{2}}$, above four equations are changed to

$$\frac{\partial^2 \varphi}{\partial {x_D}^2} - \frac{\alpha^2 \varphi}{4} + e^{-\frac{\alpha x_D}{2}} W(t_D) = \frac{\partial \varphi}{\partial t_D} \tag{2-10a}$$

$$\varphi(x_D, t_D = 0) = 0 \tag{2-10b}$$

$$[R\frac{\partial \varphi}{\partial x_D} + \left(\frac{R\alpha}{2} - 1\right)\varphi]|_{x_D=0} = e^{-\lambda_D t_D} - 1 + m \tag{2-10c}$$

$$(\frac{\partial \varphi}{\partial x_D} + \frac{\alpha}{2}\varphi)|_{x_D=1} = 0 \tag{2-10d}$$

The partial different equation (PDE) Eq. (2-10a) can be transformed into an ordinary different equation (ODE) by eliminating the *x* terms using an Integral transform method. The Integral transform of $\varphi(x_D, t_D)$ is defined as Eq. (2-11a) and the corresponding inversion formula is defined as Eq. (2-11b).

$$\bar{\varphi}(\omega_n, t_D) = \int_0^1 \varphi(x_D, t_D)\, K(\omega_n, x_D) dx_D \tag{2-11a}$$

$$\varphi(x_D, t_D) = \sum_{n=0}^{\infty} K(\omega_n, x_D)\, \bar{\varphi}(\omega_n, t_D) \tag{2-11b}$$

where $K(\omega_n, x_D)$ and ω_n are transform kernel and eigenvalue, respectively, the overbar means the variable in frequency-domain hereinafter. The kernel $K(\omega_n, x_D)$ is the normalized eigenfunction of the following eigenvalue problem.

$$\frac{d^2 k}{d{x_D}^2} + \omega_n^2 k = 0 \tag{2-12a}$$

$$\left[\frac{\partial k}{\partial x_D} + \left(\frac{\alpha}{2} - \frac{1}{R}\right)k\right]|_{x_D=0} = 0 \tag{2-13a}$$

$$(\frac{\partial k}{\partial x_D} + \frac{\alpha}{2}k)|_{x_D=1} = 0 \tag{2-13b}$$

The kernel $K(\omega_n, x_D)$ is defined as

$$K(\omega_n, x_D) = A_n k(\omega_n, x_D) = A_n[\omega_n \cos(\omega_n x_D) + \left(\frac{1}{R} - \frac{\alpha}{2}\right) \sin(\omega_n x_D)] \tag{2-14}$$

where

$$A_n = \frac{\sqrt{2}}{\sqrt{\left[\omega_n^2 + (\frac{1}{R} - \frac{\alpha}{2})^2\right](1 + \frac{\frac{\alpha}{2}}{\omega_n^2 + \frac{1}{4}\alpha^2}) + \frac{1}{R} - \frac{\alpha}{2}}} \tag{2-15}$$

Taking integral transform on Eq. (2-10a) leads to

$$\int_0^1 K(\omega_n, x_D) e^{-\frac{\alpha x_D}{2}} W(t_D)\, dx_D + \int_0^1 K(\omega_n, x_D) \frac{\partial^2 \varphi}{\partial {x_D}^2} dx_D = \int_0^1 K(\omega_n, x_D) \frac{\partial \varphi}{\partial t_D} dx_D +$$

$$\alpha^2/4 \int_0^1 K(\omega_n, x_D) \varphi(x_D, t_D)\, dx_D \tag{2-16}$$

Based on Green's function theorem, the left side of Eq. (2-16) can be written as:

$$\int_0^1 K(\omega_n, x_D) e^{-\frac{\alpha x_D}{2}} W(t_D)\, dx_D + \int_0^1 K(\omega_n, x_D) \frac{\partial^2 \varphi}{\partial {x_D}^2} dx_D =$$

$$\int_0^1 K(\omega_n, x_D) e^{-\frac{\alpha x_D}{2}} W(t_D)\, dx_D - \omega_n^2 \bar{\varphi} - \frac{K_{x_D=0}\left(e^{-\lambda_D t_D} - 1 + m\right)}{R} \tag{2-17}$$

Substituting Eqs. (2-11a), (2-13a), (2-13b) and (2-17) into Eq. (2-16), defining $\beta_n = \omega_n^2 + \alpha^2/4$, one has

$$\frac{\partial \bar{\varphi}}{\partial t_D} + \beta_n \bar{\varphi} = -\frac{K_{x_D=0}\left(e^{-\lambda_D t_D} - 1 + m\right)}{R} + \frac{A_n}{\beta_n} W(t_D) \left\{ e^{-\frac{\alpha}{2}} \left[\beta_n \sin(\omega_n) - \frac{1}{R} \left(\frac{\alpha}{2} \sin(\omega_n) + \right. \right. \right.$$

$$\left. \left. \left. \omega_n \cos(\omega_n) \right) \right] + \frac{\omega_n}{R} \right\} \tag{2-18a}$$

$$\bar{\varphi}(0) = 0 \tag{2-18b}$$

Rearranging Eq. (2-18a) yield as

$$\frac{\partial \bar{\varphi}}{\partial t_D} + \beta_n \bar{\varphi} = B(t_D) \tag{2-19}$$

where

$$B(t_D) = -\frac{K_{x_D=0}\left(e^{-\lambda_D t_D} - 1 + \mathrm{m}\right)}{R} + \frac{A_n}{\beta_n} W(t_D) \left\{ e^{-\frac{\alpha}{2}} \left[\beta_n \sin(\omega_n) - \frac{1}{R} \left(\frac{\alpha}{2} \sin(\omega_n) + \omega_n \cos(\omega_n) \right) \right] + \frac{\omega_n}{R} \right\}$$

The solution of Eq. (2-19) subject to Eq. (2-18b) can be obtained as

$$\bar{\varphi}(\omega_n, t_D) = \exp(-\beta_n t_D) \int_0^{t_D} B(t) \exp(\beta_n t)\, dt \tag{2-20}$$

Defining $\xi_1 = -\frac{1-m}{\beta_n}$,

$\xi_2 = \frac{1}{\beta_n - \lambda_D}$,

$\xi_3 = \frac{1-\mathrm{m}}{\beta_n} - \frac{1}{\beta_n - \lambda_D}$,

$$\xi_4 = \frac{A_n}{\beta_n} \left\{ e^{-\frac{\alpha}{2}} \left[\beta_n \sin(\omega_n) - \frac{1}{R} \left(\frac{\alpha}{2} \sin(\omega_n) + \omega_n \cos(\omega_n) \right) \right] + \frac{\omega_n}{R} \right\},$$

one obtains

$$\bar{\varphi}(\omega_n, t_D) = -\frac{A_n \omega_n}{R} \left[\xi_1 + \xi_2 \exp(-\lambda_D t_D) + \xi_3 \exp(-\beta_n t_D) \right] -$$

$$\xi_4 \exp(-\beta_n t_D) \int_0^{t_D} W(t_D) \exp(\beta_n t)\, dt \tag{2-21}$$

Substituting Eq. (2-21) into Eq. (2-11b), it has

$$\varphi(x_D, t_D) = \sum_{n=0}^{\infty} K(\omega_n, x_D) \left\{ -\frac{A_n \omega_n}{R} \left[\xi_1 + \xi_2 \exp(-\lambda_D t_D) + \xi_3 \exp(-\beta_n t_D) \right] - \right.$$

$$\left. \xi_4 \exp(-\beta_n t_D) \int_0^{t_D} W(t_D) \exp(\beta_n t)\, dt \right\} \tag{2-22}$$

The final solution (in dimensionless form) can be obtained by transformation.

$$h_D(x_D, t_D) = \varphi(x_D, t_D)\exp(\alpha x_D/2) \quad (2\text{-}23)$$

Eq. (2-23) serves as the working equation for computing the water table heights above the impermeable base at any given location and time. When this is obtained, the river-aquifer flux can be computed using the modified Darcy's law for a sloping aquifer (Eq. (2-1)) at the interface of the clogging layer and the aquifer. The MATLAB code to obtain the solution of Eq. (2-23) is presented in Appendix A.

2.3 Results and discussion

2.3.1 Comparison of analytical solution with numerical solutions

In this section, we will check the new analytical solution developed above by comparing with two sets of numerical solutions. The first set of numerical solution concerns a linearized modified Boussinesq equation for a sloping aquifer using a finite-element COMSOL program (Li et al., 2009). The second set of numerical solution concerns the coupled unsaturated and saturated flow process for a sloping aquifer using HydroGeoSphere (Therrien et al., 2006). We use these two sets of numerical solutions to simulate the groundwater table fluctuations and lateral flux along the sloping bed. As a reference, we also include the results of a horizontal aquifer as a special case to illustrate the impact of sloping feature on the overall hydrodynamics of a river-sloping aquifer system. The setting up of the numerical models are as follows.

The thickness of the clogging layer is set as 1 m, and the hydraulic conductivity of the clogging layer is set as 0.248 m/d. The hydraulic conductivity of the aquifer along the sloping bed is set as 2.5 m/d, the specific yield the aquifer material is set as 0.25 and the initial water table height of aquifer is set as 5 m. The vertical recharge is set as zero for the sake of illustration. The chosen parameters of the clogging layers are similar to those used in previous studies (Bansal et al., 2016). However, we should also point out the clogging layer in actual field condition could be much more complex than the simple model used here (Sebok et al., 2015). For instance, the clogging layer could be highly heterogeneous with different thickness and hydraulic conductivity, and they could be even missing in certain locations of the river banks, thus leaving "windows" for preferential flows to occur (Calver, 2001; Leek et al., 2009; Tang et al., 2017). For instance, Calver (2001) and Leek et al. (2009) has stated that the riverbed hydraulic conductivity can vary over several orders of magnitude within a single river reach, and such riverbed heterogeneity imposes significant impact on river-aquifer exchange fluxes. It is our hope that the baseline research established in this study can serve as an important step stone for investigating a complex river-aquifer system with heterogeneous clogging layers and a sloping aquifer base in the near future. Chen (2000) described a measurement method of streambed hydraulic conductivity, and Chen (2004) presented a range of vertical hydraulic conductivity values for the silt and clay bed which was tested in streambed based on the method of Chen (2000). Chen (2004) stated that the values of vertical hydraulic conductivity ranged from 0.8 m/d to 2.9 m/d. Furthermore, he presented two cases for the thickness of the silt/clay layer in streambed. In one case, the thickness of the silt/clay layer was 1.4 m. In the other case, the thickness of the silt/clay

layer was 3.5 m. Sebok et al. (2015) presented the field test values of horizontal hydraulic conductivity and vertical hydraulic conductivity at 40 individual test locations in streambed using slug tests, and the range of field tested horizontal hydraulic conductivity values are from 0.19 m/day to 80.46 m/day. It is seen that the setup of our study conforms to the realistic values of hydrological parameters. The initial and final stages for river are set as 5 and 10 m, respectively, and $\lambda = 0.1\ d^{-1}$. For the coupled unsaturated and saturated flow process in HydroGeoSphere, the unsaturated zone properties are assumed to follow the Van Genuchten (1980) model without loss of generality. Specifically, the so-called alpha and beta values of the aquifer are 12.4 m^{-1} and 2.68, respectively; and the alpha and beta values of the clogging layer are 3.6 m^{-1} and 2.68, respectively. Alpha [L^{-1}] is relative to the inverse of the air-entry pressure head and beta [dimensionless] is the pore-size distribution index. Such values are reflective of the sand-rich materials of aquifer and clay-rich materials of the clogging layer. The porosity of aquifer is 0.41 and the porosity clogging layer is 0.43. The residual saturation value of the aquifer is set as 0.16 and the residual saturation the clogging layer is set as 0.078. The parameters of Van Genuchten model are refer to the classical values from Carsel and Parrish (1988). The alpha and porosity values of the aquifer and the clogging layer are similar to those of loamy sand and loam, respectively. The reason to choose these values is that the hydraulic conductivities of loamy sand and loam in the study of Carsel and Parrish (1988) approximate the assigned values of aquifer and the clogging layer. We choose different beta values of aquifer and the clogging layer in this study. The reason is that when we used the beta values of loamy sand and loam in the study of Carsel and Parrish (1988), the numerical program of HydroGeoSphere could not be convergent for no obvious

reasons. Through a few tests, the beta value (2.68) of sand in the study of Carsel and Parrish (1988) is the best replacement for the numerical program of HydroGeoSphere. The residual saturation value of the clogging layer is similar to the values of loam. The residual saturation value of aquifer is different from that of the clogging layer. In general, residual saturation value (or called the undrainable porosity by some scholars) is regarded as close to the difference of the total porosity and the specific yield (or called drainable porosity by some scholars).

The design of COMSOL program is briefly illustrated as follows. For the purpose of comparison, we generate three sets of hypothetical aquifers here: a horizontal aquifer as a reference of comparison, a sloping aquifer with a 5° sloping angle, and a sloping aquifer with a 10° sloping angle. The horizontal length of the aquifer is 1000 m. We need point out that 1000 m is long enough in this study. In this chapter, we focus on studying water table heights from x=0 m to x=150 m, because this is the region that the water table varies mostly. We set up a similar COMSOL model with a horizontal length of 2000 m. The results show that water table heights and river-aquifer fluxes are identical between the horizontal lengths of 1000 m and 2000 m, meaning that the use of 1000 m here is suffix for approximating a semi-infinite extent. The horizontal grid space is 0.1 m. An analysis of grid convergence was carried out in three cases of COMSOL model, and it showed that the grid spacing did not affect the results of water table heights and river-aquifer fluxes. It means the grid spacing dependence is not a concern in the simulations of COMSOL model. The actual values of parameter are calculated by Eq. (2-7) for three types of aquifers.

The design of the model developed within HydroGeoSphere is briefly outlined as follows. We generate three sets of hypothetical aquifers: a horizontal aquifer as a reference of comparison, a sloping aquifer with a 5° sloping angle, and sloping aquifer with a 10° sloping angle. The horizontal length of the aquifer is 1000 m. The horizontal grid space in the clogging layer is 0.1 m, the horizontal grid space in the aquifer from x=0 m to x=200m is 0.5 m and the horizontal grid space in the aquifer from x=200 m to x=1000 m is 2 m. The vertical grid space for both the aquifer and clogging layers is set at 0.25 m. For the same reason, we only study the water table height from x=0 m to x=150 m and the river-aquifer flux at x=0 m. The horizontal grid space setting (2 m) from x=200 m to x=1000 m does not affect our results in this study. The river edge is located at x=0 m and the clogging layer is located from x=0 m to x=1m. The initial water table heights of the river, the clogging layer and the aquifer are all 5 m. The specified heads of river are set as the sums of base elevations and the stages of river with a time step of 0.1 day. The base elevations of river are different for three aquifers. The values are calculated by $\tan(\theta)$ times the length of aquifer. The specified head of aquifer at x=1001 m is set as 5 m and the base elevation is set as 0 m. Similarly, an analysis of grid convergence is carried out in three cases of HydroGeoSphere model, and it shows that the grid spacing does not affect the results of water table heights and river-aquifer fluxes.

An important step to obtain the approximate analytical solution of transient flow in a river-aquifer system is to linearize h using h_a in the Boussinesq equation, where h_a is the spatially averaged thickness of the unconfined aquifer. Liang and Zhang (2012) investigated how to determine the value of h_a for a horizontal aquifer, and they recommended to use the average value of the initial heads at the left and right boundaries.

We adopt the suggestion of Liang and Zhang (2012) for the determination of h_a , and obtain h_a =5 m which is the average of the initial heads at the left and right boundary. The value of h_a is used in the analytical model and COMSOL simulation. The objective is to validate the new analytical solution for a rapidly rising river stage.

Fig. 2-2 describes the water table heights at x=0 m, x=50 m and x=100 m in a period of t=0 to 50 d, and Fig. 2-3 describes the water table height distribution at t=10, 30 and t=50 d. The results are obtained from analytical solution, and separate numerical simulations by COMSOL and numerical simulation by HydroGeoSphere. From these two figures, we find that the results of analytical solution fit very well with the results of COMSOL solution. As the analytical solution and the COMSOL numerical solution both deal with the same linearized modified Boussinesq equation, the excellent agreement of both solutions provides evidence that the developed new analytical solution is reliable. The maximum difference of water table heights between the results of two methods is 11 mm. The average difference in water table heights between the results of two methods is 7.1 mm. Such minor differences between analytical solution and COMSOL solution stems from the numerical errors that are probably associated with the time step used in the COMSOL simulation. The following results are discussed: 1) water table heights at x=0, 20, 50, 80, 100 and 150 m from 0.1 day to 50 days with a time step of 0.1 days; 2) water table heights at t=10, 20, 30, 40 and 50 d from 0 m to 150 m.

When the time is from 30th day to 50th day, the discrepancy of water table between the analytical model and the HydroGeoSphere model is small but noticeable for the horizontal aquifer case. The results of HydroGeoSphere agree with the results of analytical solution very well for a sloping aquifer with a 5° sloping angle. When the slope

angle increases from 0º to 10º, the discrepancy between the analytical solution and the HydroGeoSphere solution slightly increases in a range from x=70 m to x=150 m.

Fig. 2-4 shows the river-aquifer flux at the interface of vertical clogging layer and aquifer. Similarly, the results of analytical solution fit greatly with the results of COMSOL model. When the sloping angle increases from 0º to 10º, the discrepancy between the analytical solution and the HydroGeoSphere solution slightly increases in a range from 0.1 day to 25 day.

2.3.2 Comparison of analytical solution with the Bansal's (2016) solution

In section 2.2.2, we mentioned that Bansal et al. (2016) used a similar method to deal with the boundary condition of a vertical clogging layer in a sloping aquifer and ignored an important term of –tan(θ) which is included in the equation of boundary condition for the clogging layer in this study. The analytical solution of Bansal (2016) is called the Bansal's solution hereinafter. One objective of our analytical solution is an improvement to study the river-aquifer system with a clogging layer in a sloping aquifer. This section compares the results of our new analytical solution and the Bansal's solution to check whether the "–tan(θ)" term can be ignored or not. The setting of model is the same as in section 2.3.1.

After obtaining the analytical and the numerical solutions for 0°, 5° and 10°, Fig. 2-5 describes the water table heights with time at x=0, 50 and 100 m, Fig. 2-6 describes the water table height distribution at t=10, 30 and 50 d, Fig. 2-7 describes river-aquifer fluxes a the logging layer-aquifer interface. The solid line A represents the results of our solution, the dashed line B represents the results of the Bansal's solution. The results of

our analytical solution fits greatly with the results of Bansal's solution for a horizontal aquifer. When the sloping angle increases from 0º to 10º, the discrepancy between our analytical solution and the Bansal's solution increases significantly. In a range of x=0 m to =150 m of the sloping aquifers, the discrepancy between our analytical solution and the Bansal's solution decreases when moving away from the river. The boundary condition of Eq. (7b) represents water-balance at the interface between aquifer and clogging layer. The neglect of the "–tan(θ)" term will overestimate water table height and river-aquifer flux.

2.3.3 Analysis of parameter impacts on the river-aquifer system

In this section, we will investigate the influences of water table fluctuation and river-aquifer flux in the presence of a sloping bed with different hydraulic parameters. Based on Eq. (2-8) to Eq. (2-9c), it is easy to see that hydraulic parameters b, k, K, S_y affect hydrodynamics of the river-aquifer system. River stage is described by Eq. (2-6) with λ=0.1 d^{-1} and h_i=5 m and h_f=10 m. Consistent with the previous discussion, the base model has K=2.5 m/d, S_y=0.25, L=1000 m, k=0.248 m/d and b_1 =1 m. In the first set of analyses, the value of b/k is doubled from 4.03 d to 8.06 d, while holding the other parameters constant. In the second set of analyses, the value of K is doubled from 2.5 m/d to 5 m/d while holding the other parameters constant. In the third set of analyses, the S_y value is increased from 0.25 to 0.35 while holding the other parameters constant.

Fig 2-8 and Fig 2-9 presents the water table heights between at t=10 d and t=30 d respectively. Fig 2-10 displays river-aquifer fluxes for three types of aquifers. A few observations are evident. First, when the value of hydraulic resistance of the clogging

layer, b/k, is doubled, the river-aquifer flux decreases and the hydraulic gradient in aquifer decreases. The flow rates in aquifers also decrease, and the water table heights decline. Second, when the value of K is doubled, the flow rates in aquifers increase significantly, and the river-aquifer fluxes increase remarkably. The water table heights increase in a range of x=50 m to x=100 m for 0° and 5°. The sloping beds increase the flow rates in aquifer, thus the flow rates in a sloping aquifer with a 10° sloping angle are significantly greater than the other two types of aquifer. When the S_y value increases from 0.25 to 0.35, the unsaturated zone could uphold much more water, thus the variational rate of water table height versus time slows down.

2.3.4 Upward sloping bed

When studying river-aquifer interaction, the direction of slope matters greatly. The purpose of this section is to investigate the groundwater flow in an unconfined sloping aquifer with an upward sloping angle and the presence of a dynamic river stage at the left. The setting of this section is exactly the same as in previous sections except that the impermeable base of the unconfined aquifer has an upward slope. Fig. 2-11 displays water table heights at t=10, 30 and 50 d for sloping aquifers with 5° and 10° upward sloping angles, with a rising river. The initial and final stages for river are set as 5 m and 10 m, respectively, and $\lambda = 0.1\ d^{-1}$. The water table heights for such sloping cases are higher than their counterparts of a horizontal aquifer, as evidence in Fig. 2-3. Fig. 2-12 displays river-aquifer fluxes for 5° and 10° sloping aquifers with a rising river. The solid line represents downward sloping aquifer (as a reference of comparison). The dashed line represents upward sloping aquifer. For the upward sloping aquifer, the direction of river-

aquifer fluxes is from right to left at the beginning, because the initial hydraulic gradient drives water flow to the left (as the initial water table profile is assumed to be parallel with the sloping base). As the stage of river increases rapidly after a few days, the direction of river-aquifer fluxes reverses its direction.

Fig. 2-13 presents water table heights at t=10, 30 and 50 d for sloping aquifers with upward 5° and 10° sloping angles with a constant river stage of 5 m. The water table heights increase with time in regions near the left river for the upward sloping aquifers, and decrease with time for the downward sloping aquifers. Fig. 2-14 displays river-aquifer fluxes for the upward 5° and 10° sloping aquifers with a constant river stage at 5 m. The flow rates for both downward and upward sloping aquifers increase with time. The flow directions for the downward sloping aquifers are towards the right and the flow directions for the upward sloping aquifers are towards the left.

2.3.5 Responses of recharge to groundwater table and river-aquifer fluxes

In this section, we study the influences of infiltrated recharge on water table height and river-aquifer fluxes for downward sloping aquifers. The analytical solution developed in section 2.2.2 considered the factor of recharge to groundwater on the top. For the sake of illustration, we will use a sequence of piecewise functions here. Specifically, during a period from t_1 to t_n, where n is a positive integer number representing the number of piecewise steps, the recharge change from W_1 to W_n. The model setup is exactly the same as in section 2.3.1 except that recharge is included here.

As an example, we simulate two recharge events, and each event lasts 1 day. The values of recharge are 20 mm/day on the 10^{th} day and 40 mm/day on the 20^{th} day, and

zeros for the rest time. We have to point out that such sporadic recharge events could be used to represent the extreme but short precipitation events in arid and semi-arid regions, but may not be representative of precipitation events in humid regions in which longer-term, sustained recharge will occur. Fig. 2-15, Fig 2-16 and Fig. 2-17 present water table heights change with time at x=0, 50 and x=100 m for three types of aquifers. The figures show that the sloping angles hardly affect the response of water table heights. The responses of recharge to water table heights at x=0 m is slightly less than the responses of recharge to water table heights at x=100 m. This is consistent with the phenomenon in Fig. 2-18. When the aquifers obtain recharge on the top, the river-aquifer fluxes will slightly decrease and the region close to the river will obtain less recharge from the river. However, when the recharge rate increases, the responses to water table heights increase too. The discrepancy in water table heights for different spatial distance from the river will be evident, when the aquifers obtain more recharge on the top. Once again, the relatively minor impact from the recharge is mostly because the short term recharge events which do not bring in sufficient amount of the water into the unconfined aquifer to alter the hydrodynamics. The story could be very different if long-term sustainable recharge events occur over the time of interest.

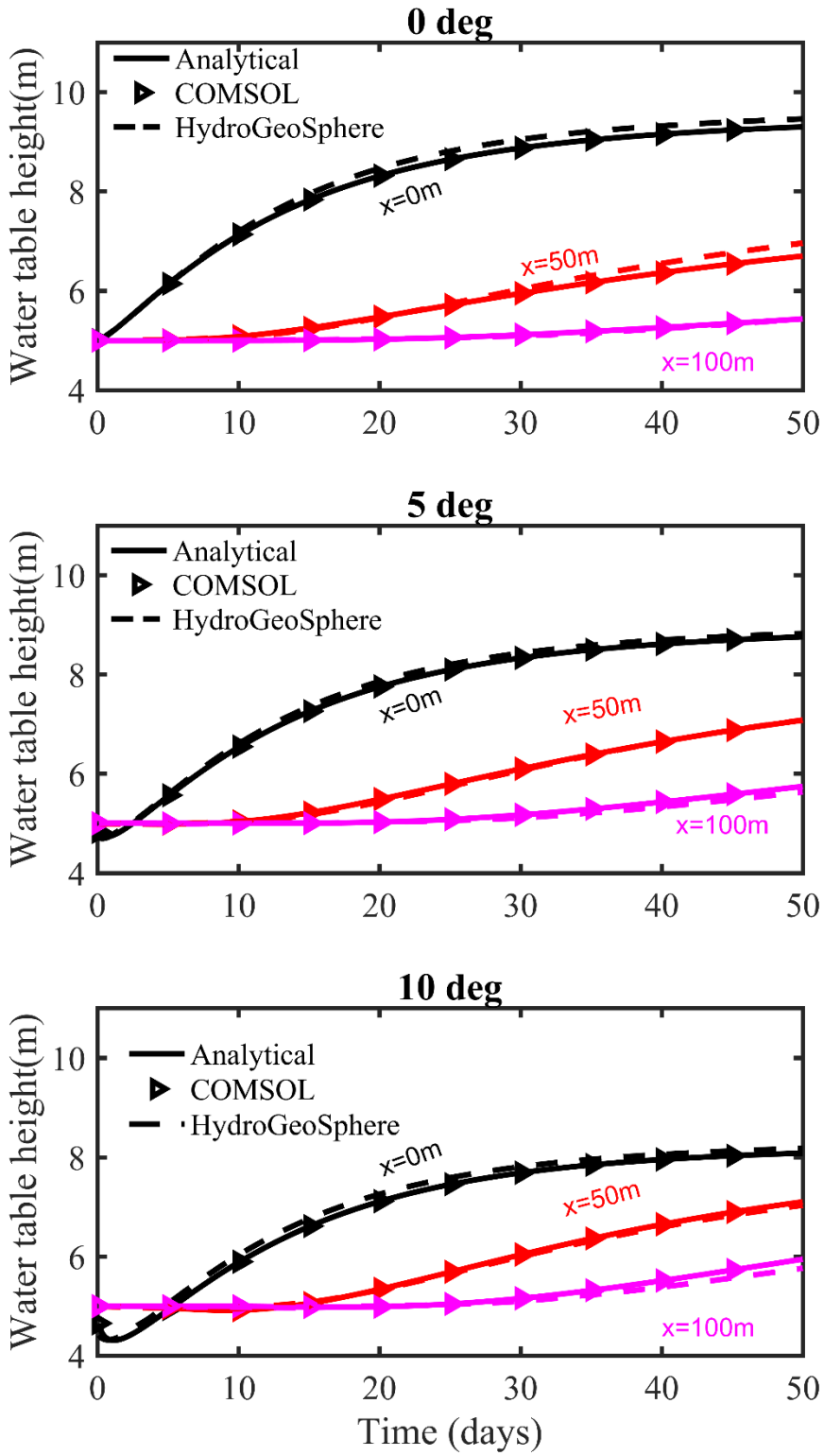

Fig. 2-2 Comparison of water table heights with time at *x*=0, 50 and 100 m in a horizontal aquifer, a 5° sloping aquifer, and a 10° sloping aquifer among analytical solution, numerical solutions of COMSOL and HydroGeoSphere.

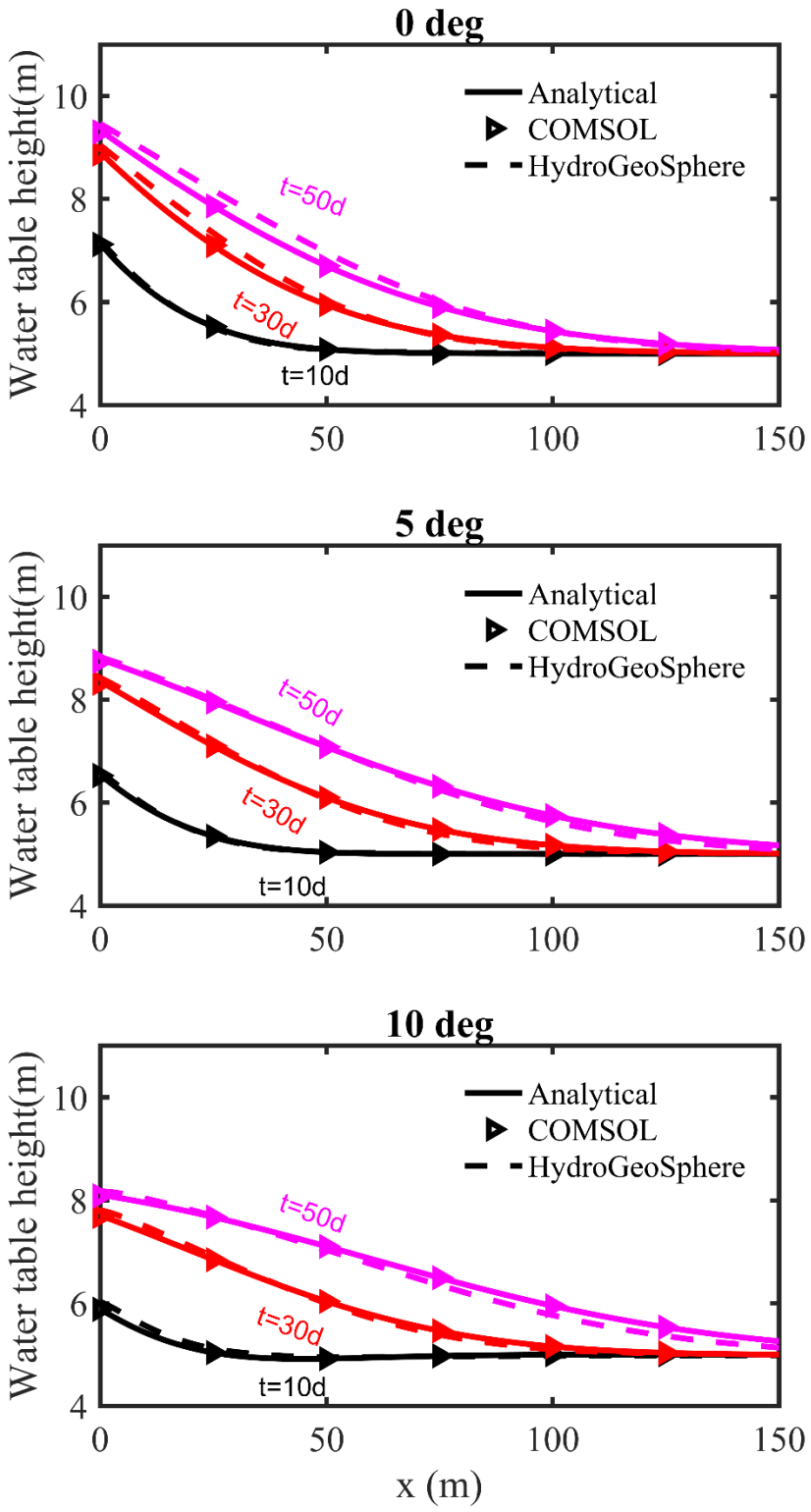

Fig. 2-3 Comparison of water table heights above the impermeable bed at *t*=10, 30 and 50 d for a horizontal aquifer, a 5° sloping aquifer, and a 10° sloping aquifer among analytical solution, numerical solutions of COMSOL and HydroGeoSphere.

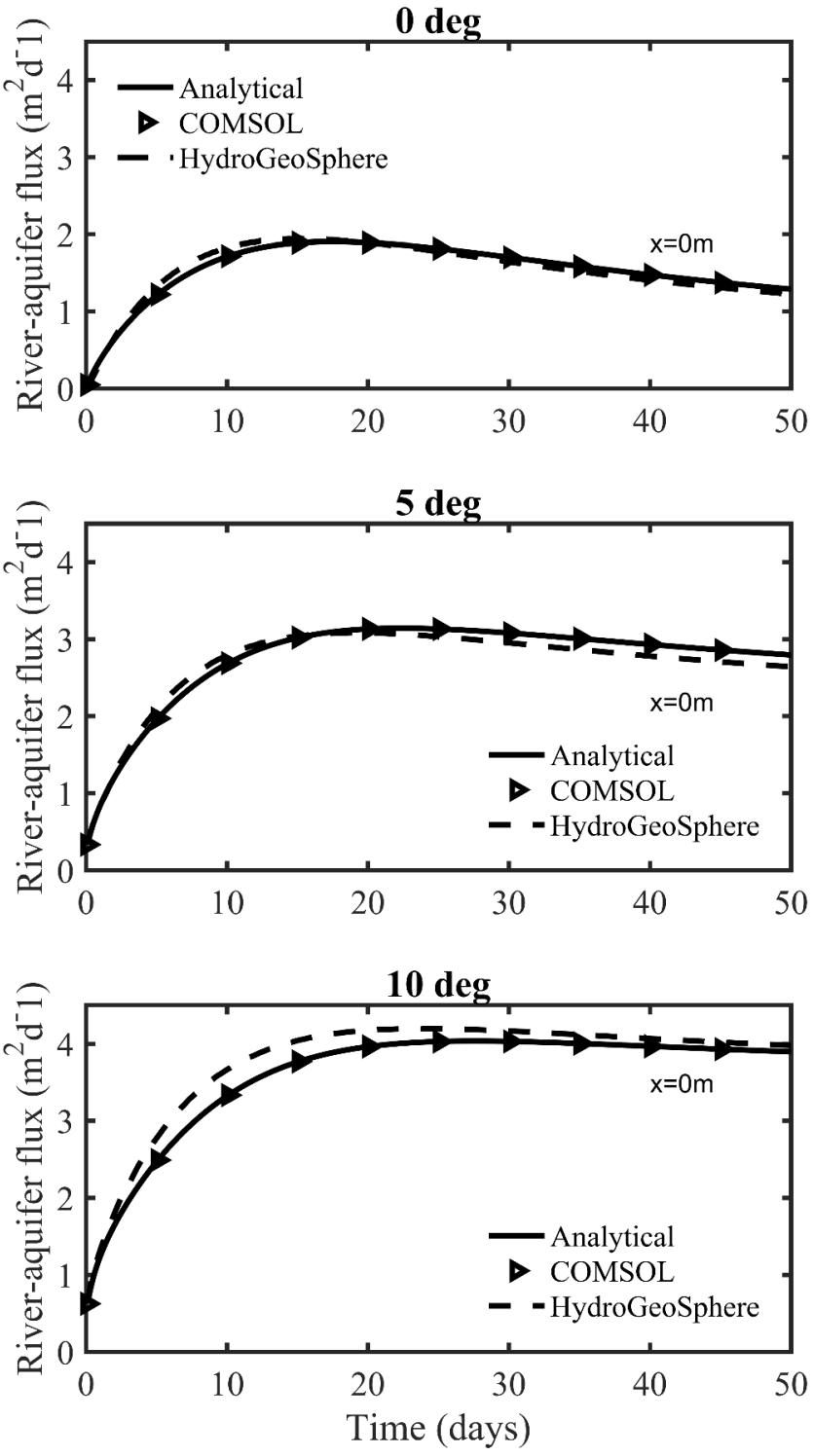

Fig. 2-4 Comparison of river-aquifer fluxes at the vertical clogging layer in a horizontal aquifer, a 5° sloping aquifer, and a 10° sloping aquifer among analytical solution, numerical solutions of COMSOL and HydroGeoSphere.

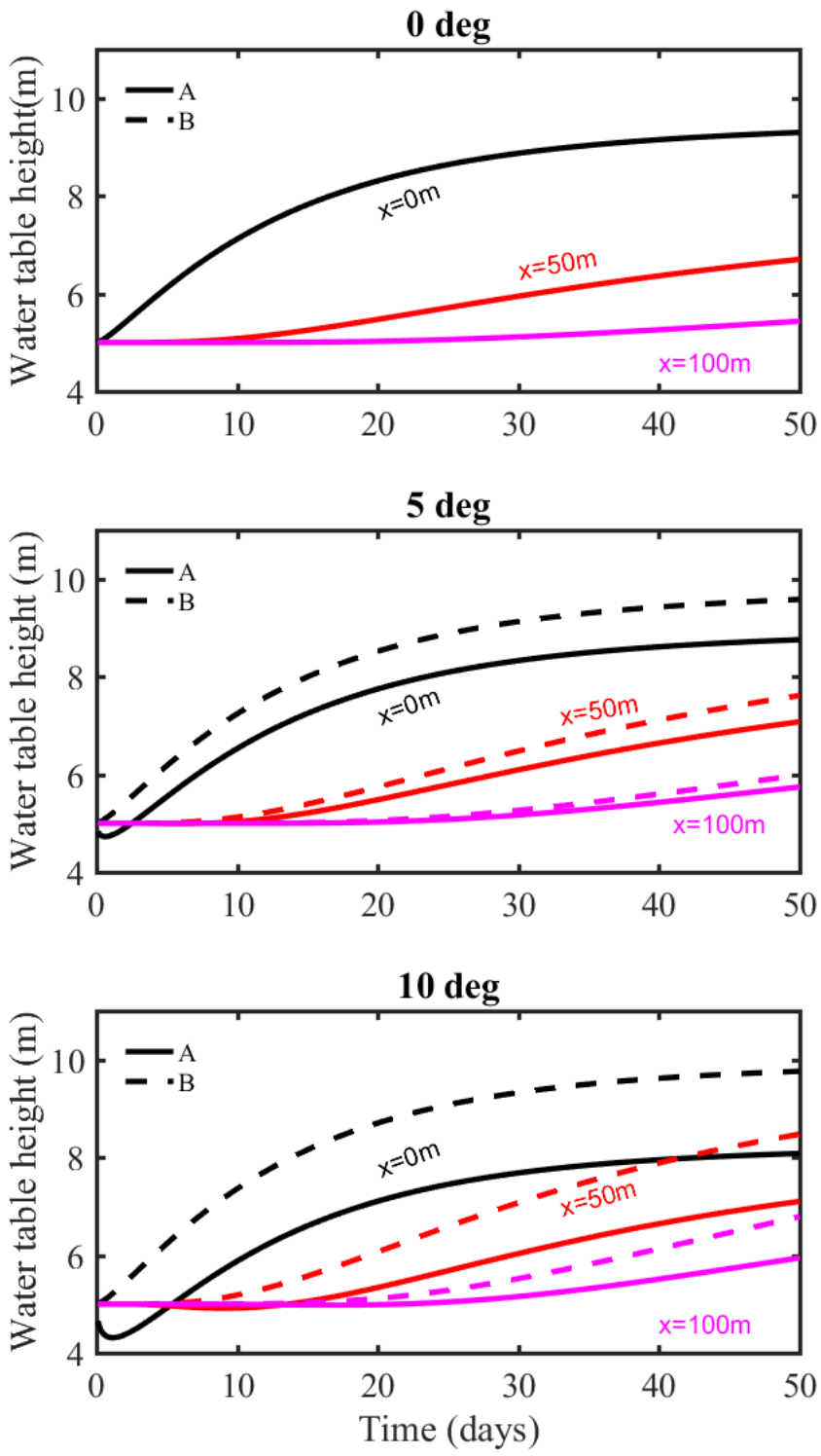

Fig. 2-5 Comparison of water table heights with time at *x*=0, 50 and 100 m in a horizontal aquifer, a 5° sloping aquifer, and a 10° sloping aquifer between our analytical solution (A) and the Bansal's solution (B).

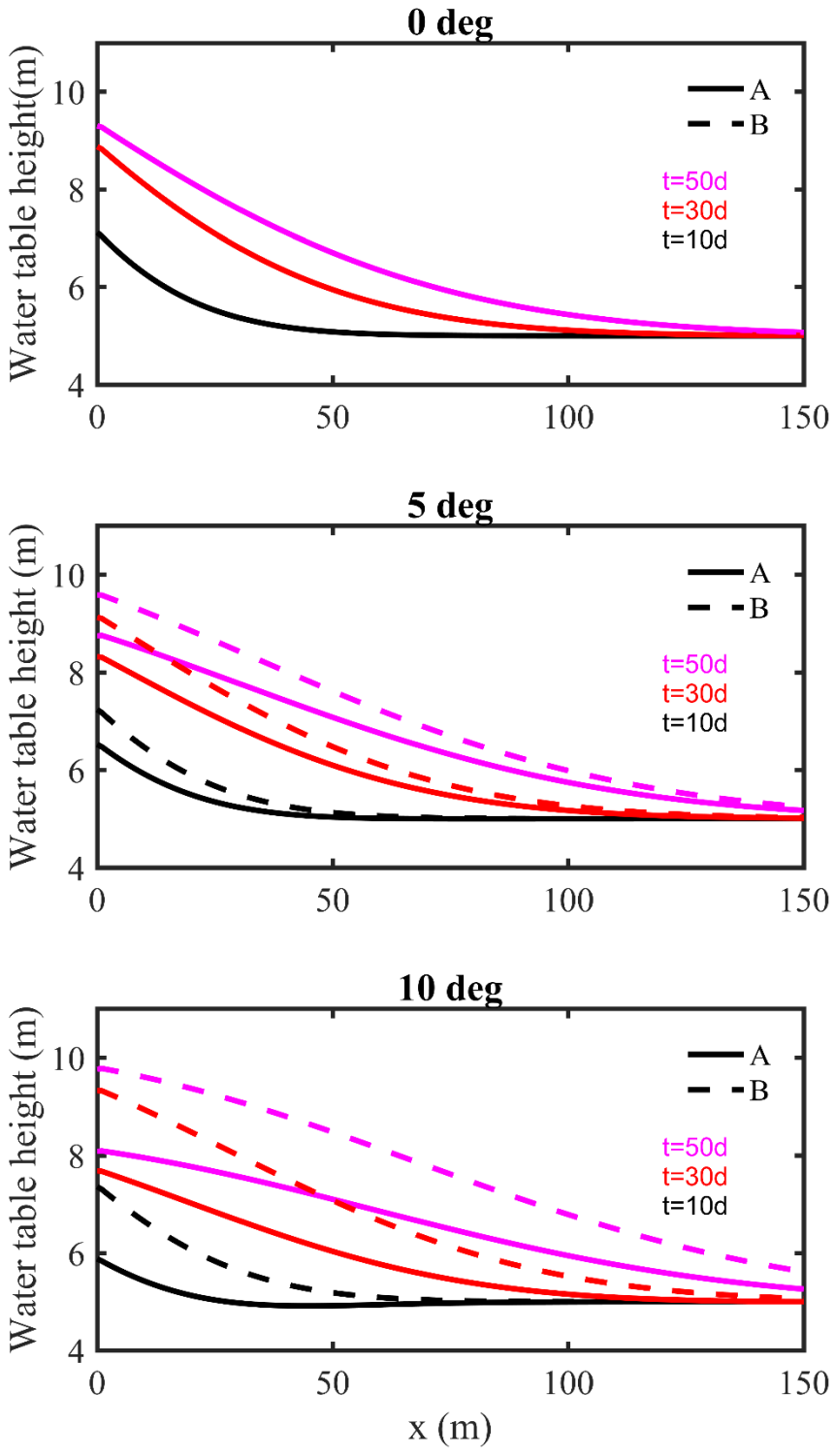

Fig. 2-6 Comparison of water table heights above he impermeable bed at *t*=10, 30 and 50 d for a horizontal aquifer, a 5° sloping aquifer, and a 10° sloping aquifer between our analytical solution (A) and the Bansal's solution (B).

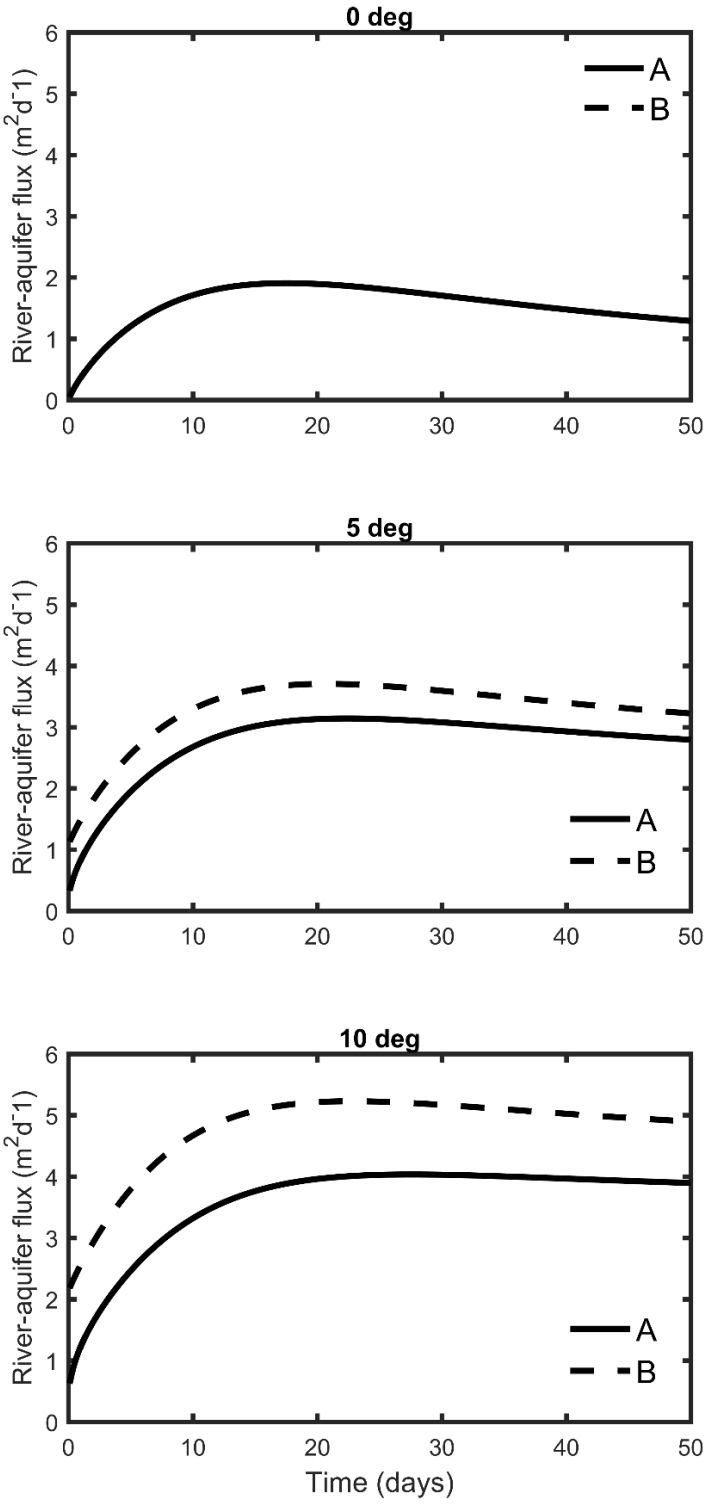

Fig. 2-7 Comparison of river-aquifer fluxes at the left and right rivers in a horizontal aquifer, a 5° sloping aquifer, and a 10° sloping aquifer between our analytical solution (A) and the Bansal's solution (B)..

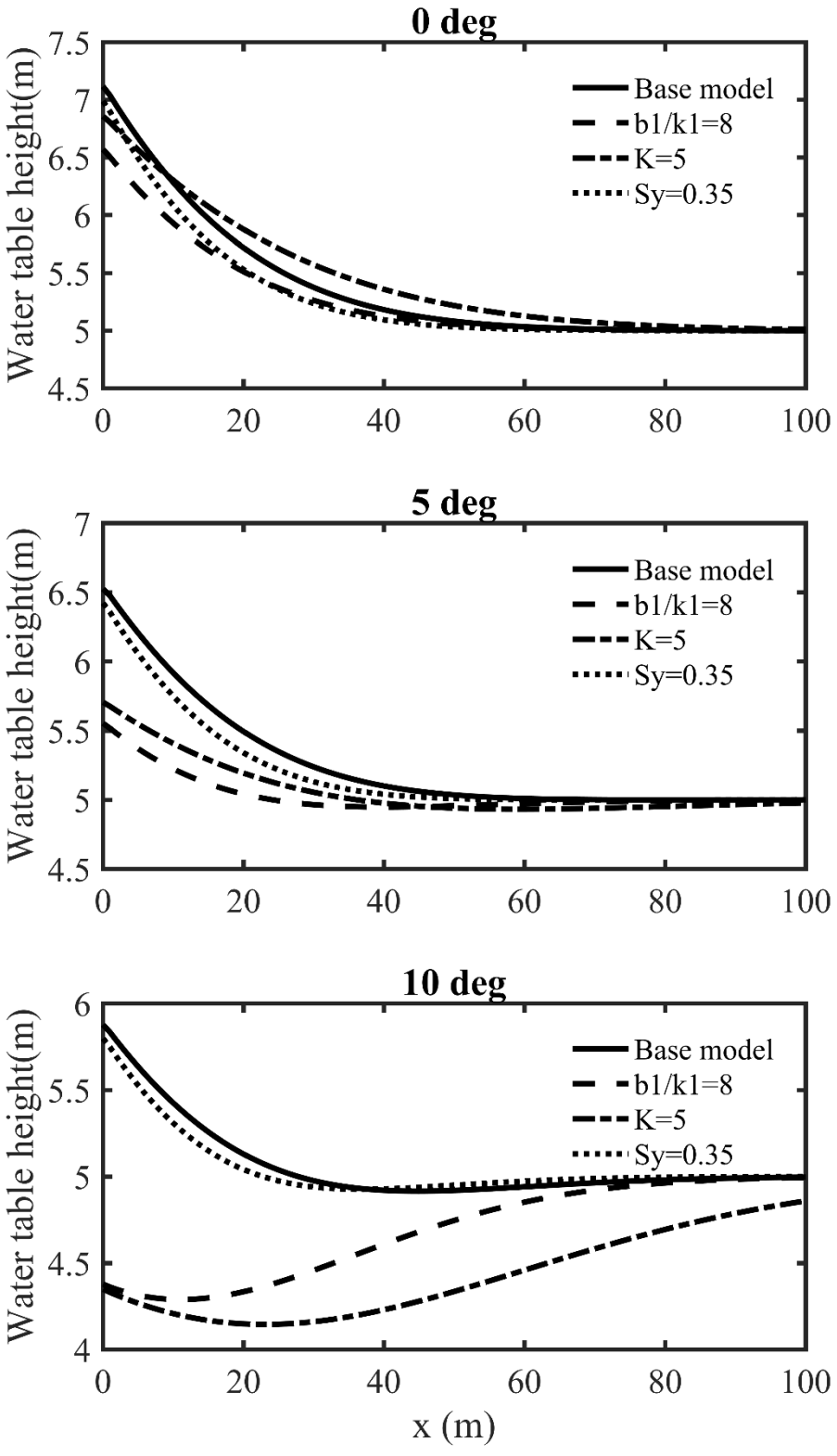

Fig. 2-8 Analysis of parameter impacts on water table heights above the impermeable bed in a horizontal aquifer, a 5° sloping aquifer, and a 10° sloping aquifer at *t*=10 d.

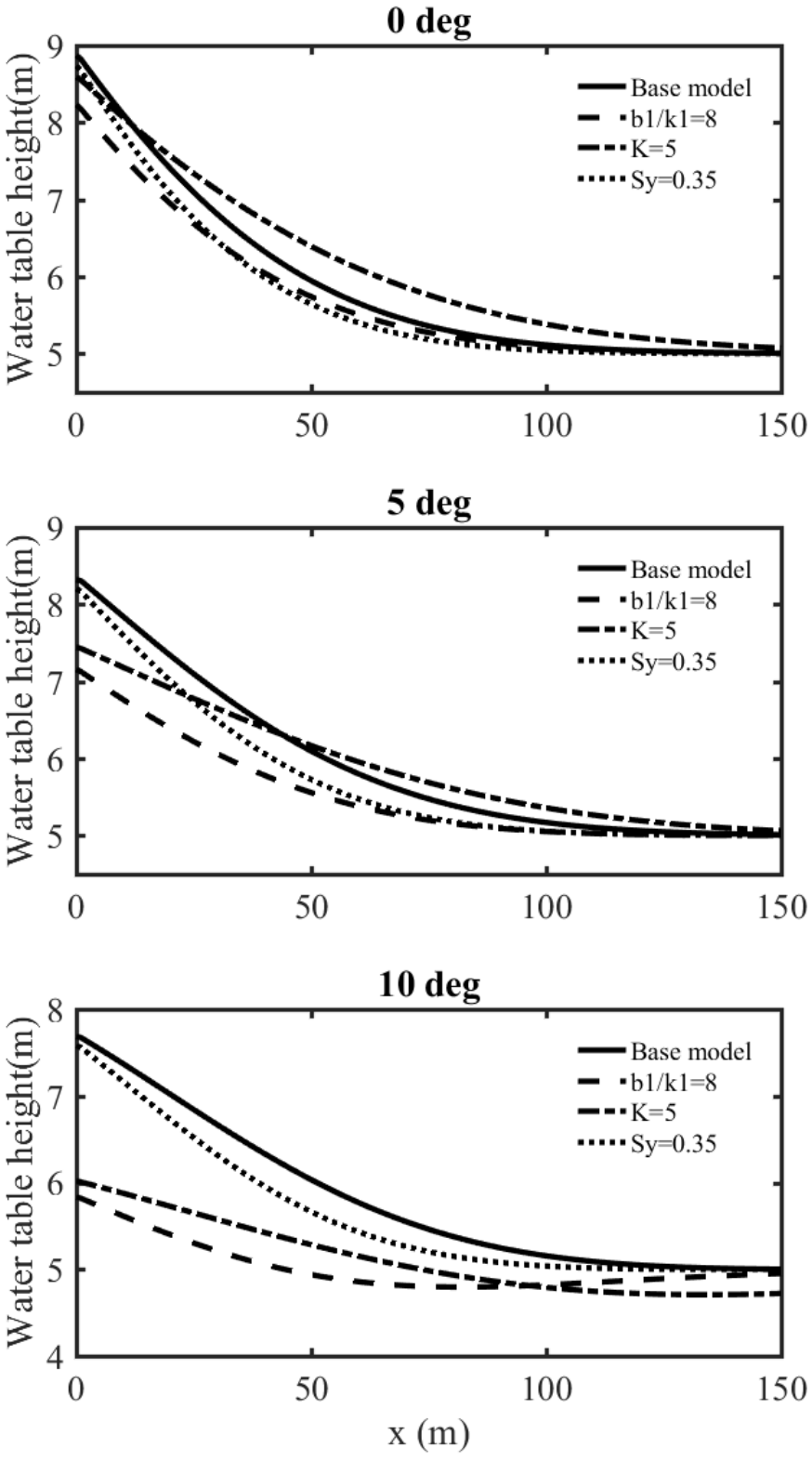

Fig. 2-9 Analysis of parameter impacts on water table heights above the impermeable bed in a horizontal aquifer, a 5° sloping aquifer, and a 10° sloping aquifer at *t*=30 d.

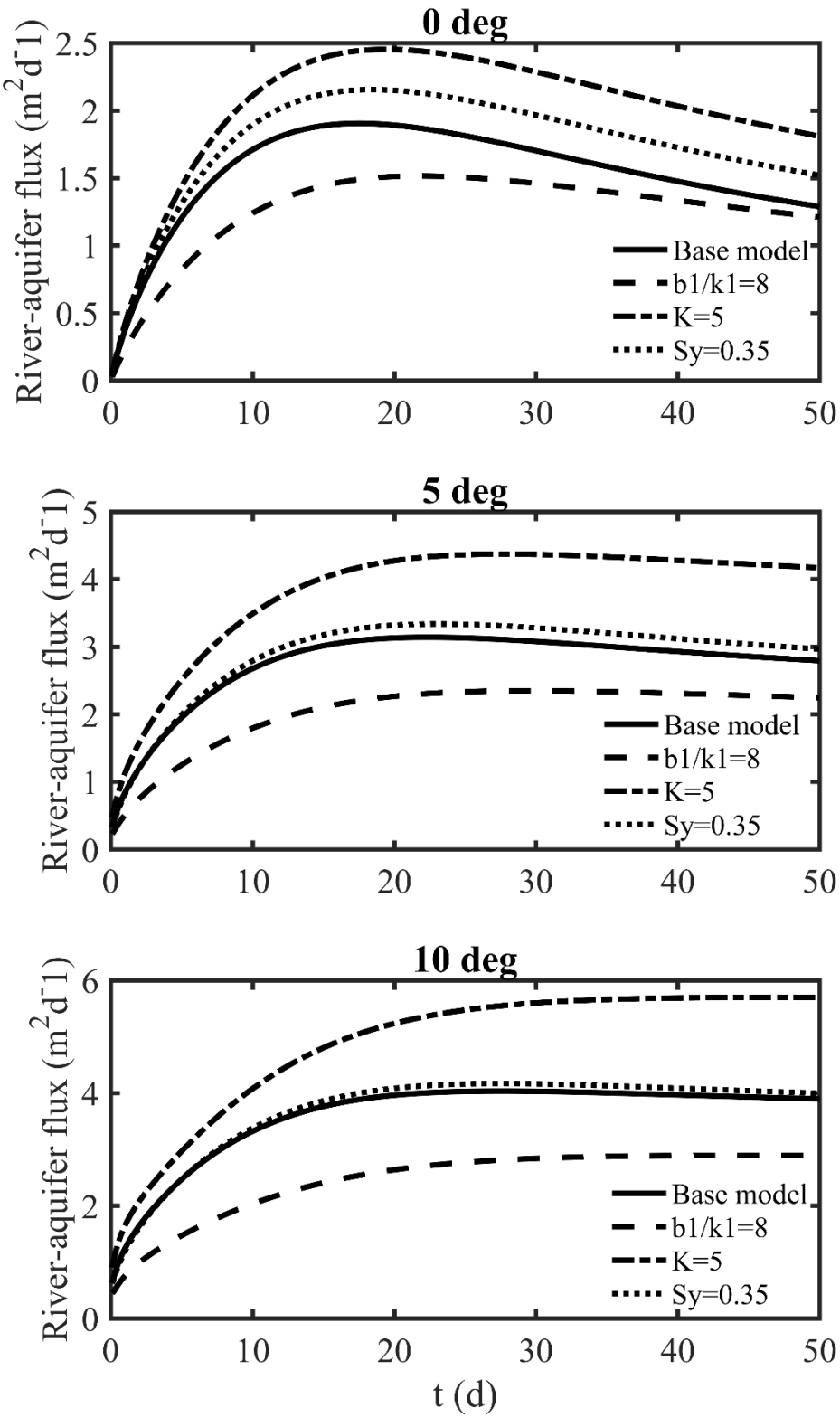

Fig. 2-10 Analysis of parameter impacts on river-aquifer fluxes at the left and right rivers in a horizontal aquifer, a 5° sloping aquifer, and a 10° sloping aquifer.

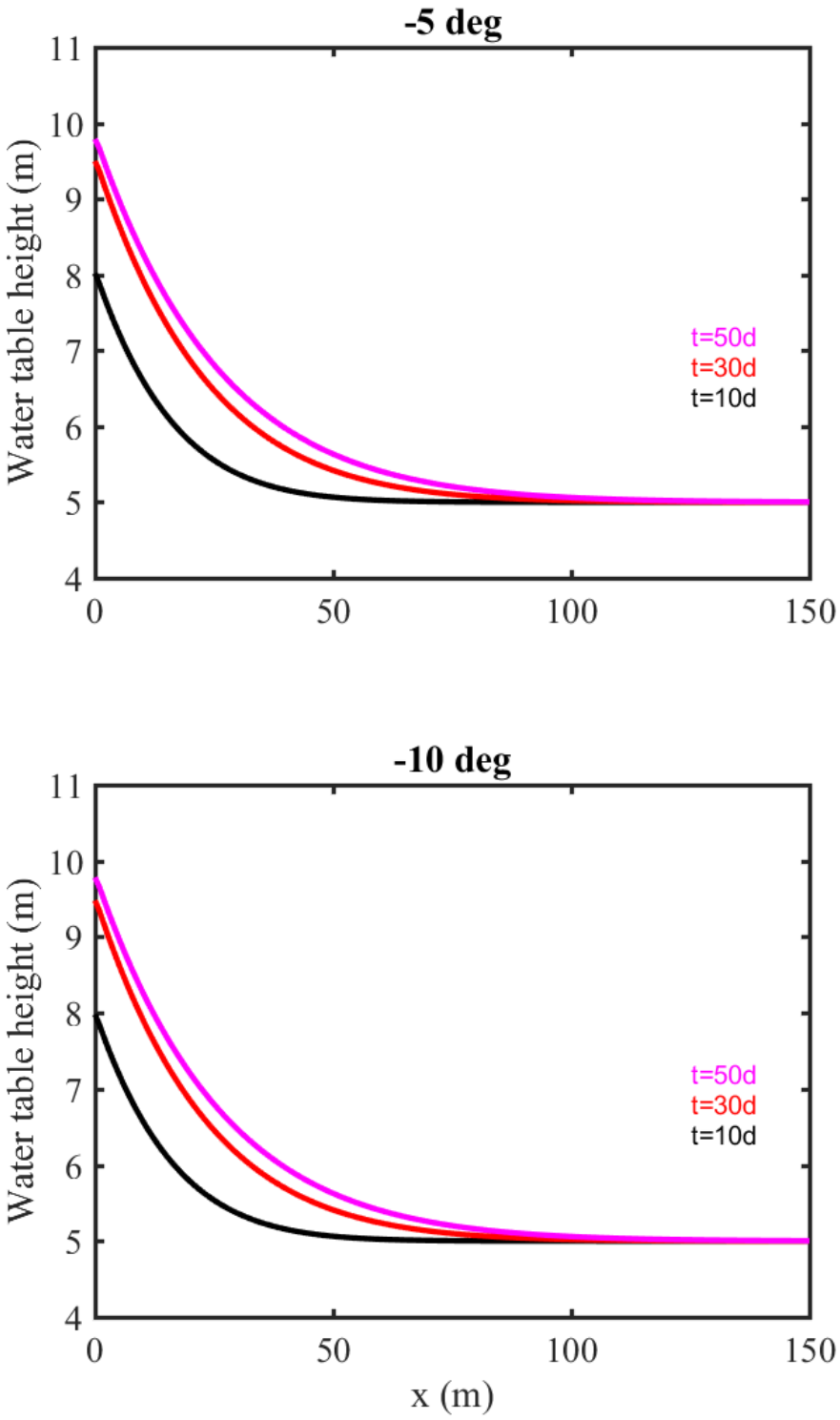

Fig. 2-11 Comparison of water table heights above the impermeable bed *t*=10, 30 and 50 d in a 5° upward sloping aquifer, and a 10° upward sloping aquifer with a rising stage of river.

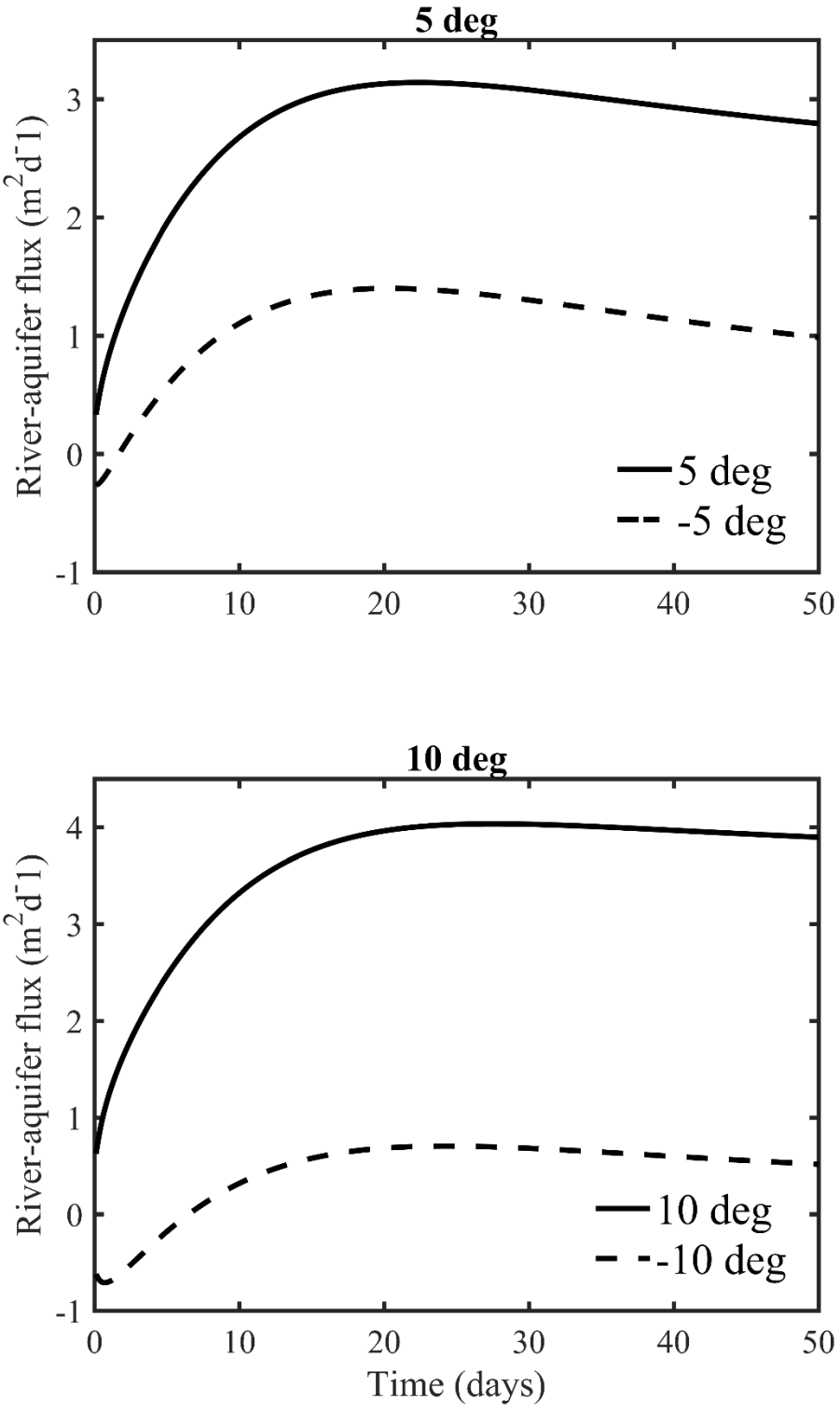

Fig. 2-12 Comparison of river-aquifer fluxes at the vertical clogging layer in a 5° upward sloping aquifer, a 5° downward sloping aquifer, a 10° upward sloping aquifer and a 10° downward sloping aquifer with a rising stage of river.

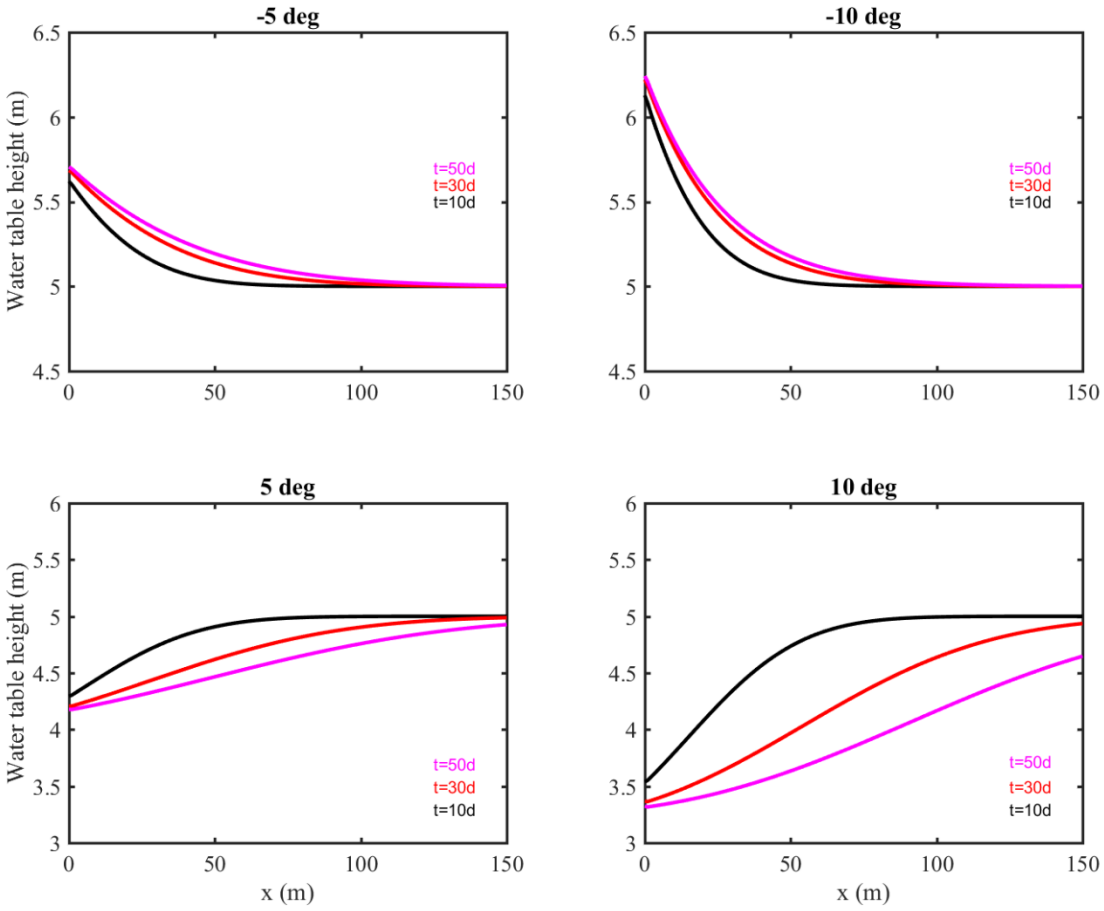

Fig. 2-13 Comparison of water table heights above the impermeable bed at *t*=10, 30 and 50 d in a 5° upward sloping aquifer, a 5° downward sloping aquifer, a 10° upward sloping aquifer, and a 10° downward sloping aquifer with a constant stage of river.

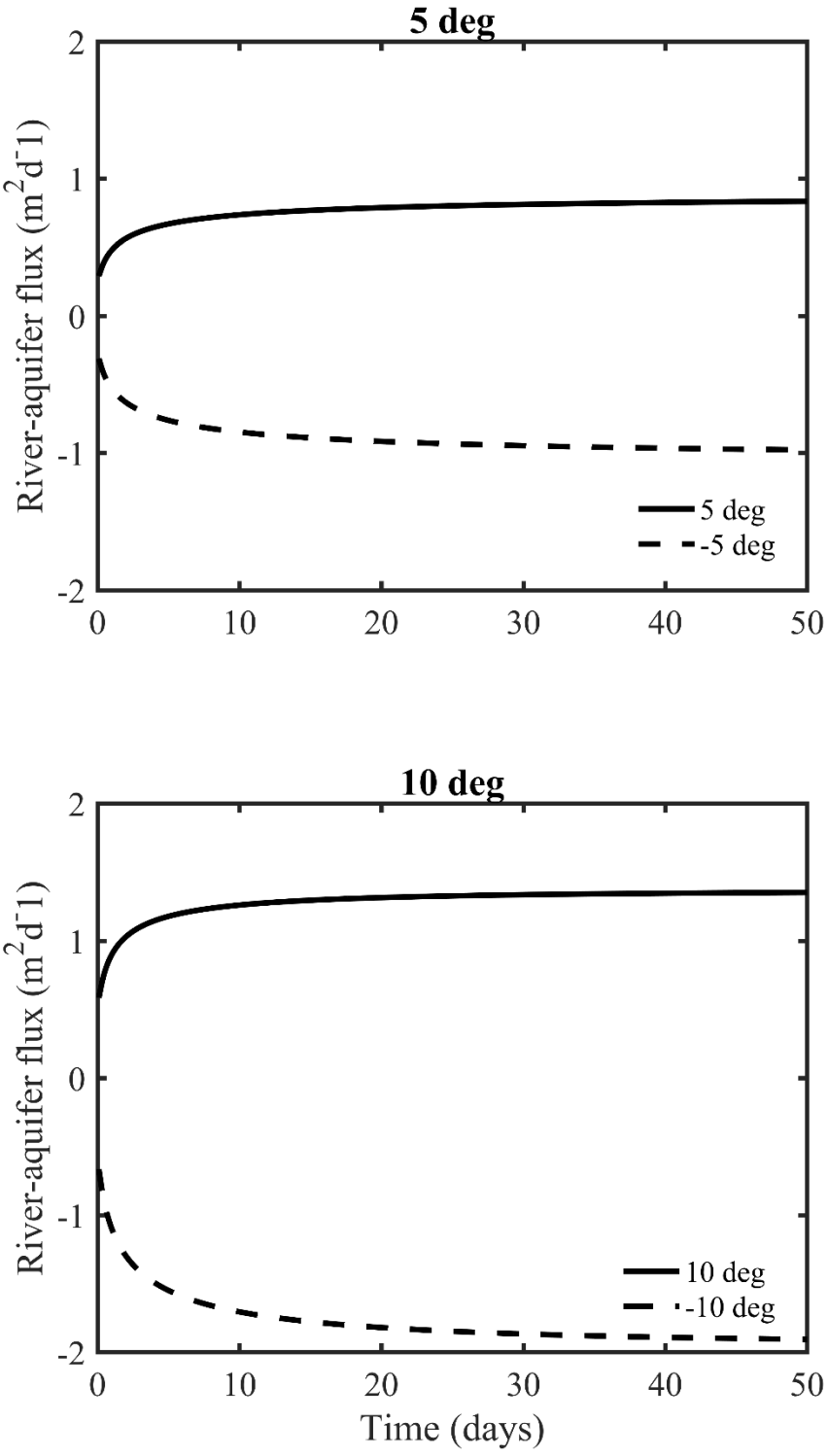

Fig. 2-14 Comparison of River-aquifer fluxes at the vertical clogging layer in a 5° upward sloping aquifer, a 5° downward sloping aquifer, a 10° upward sloping aquifer and a 10° downward sloping aquifer with a constant stage of river.

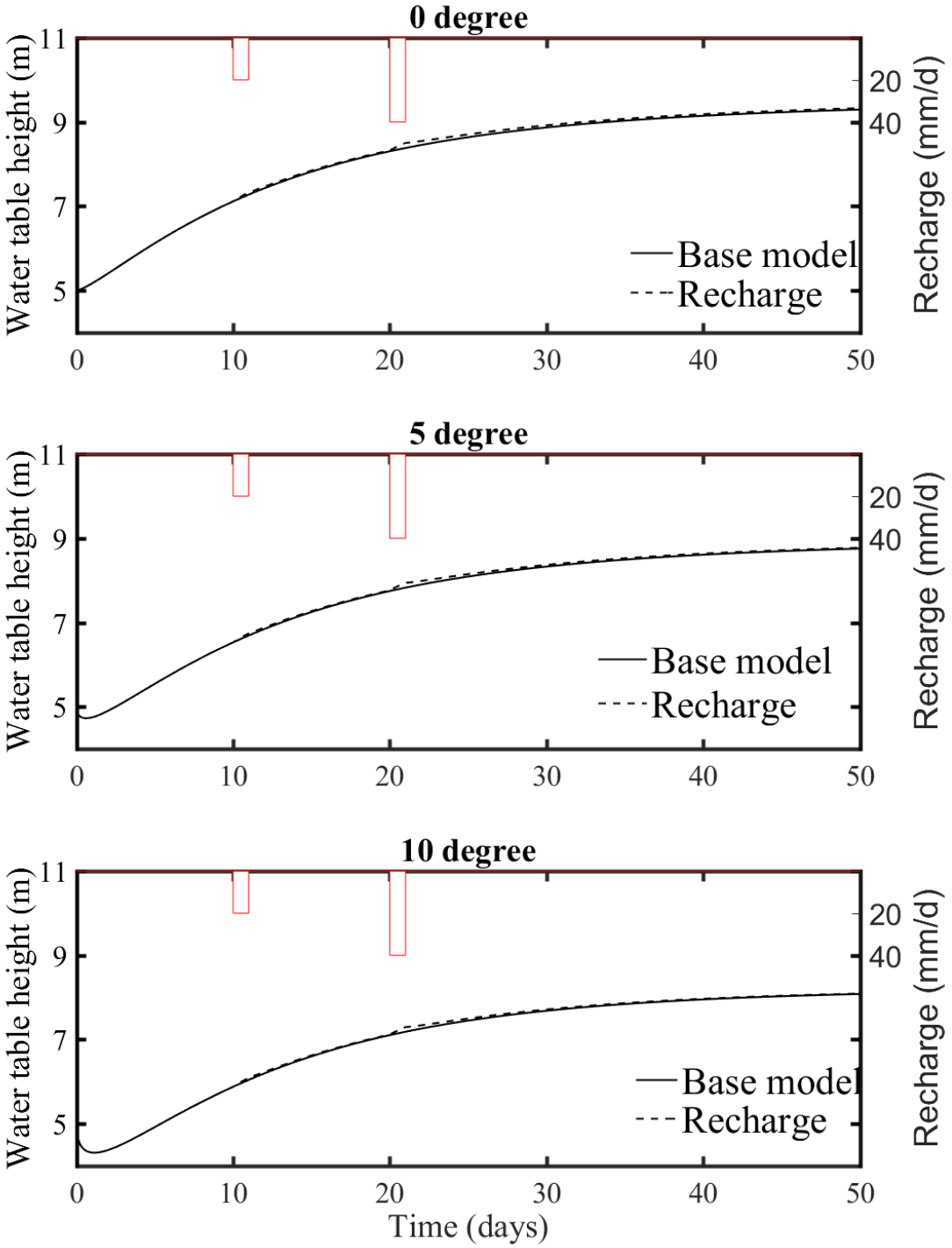

Fig. 2-15 Impact of infiltrated recharge on water table heights above the impermeable base at *x*=0 m in a horizontal aquifer, a 5° sloping aquifer, and a 10° sloping aquifer.

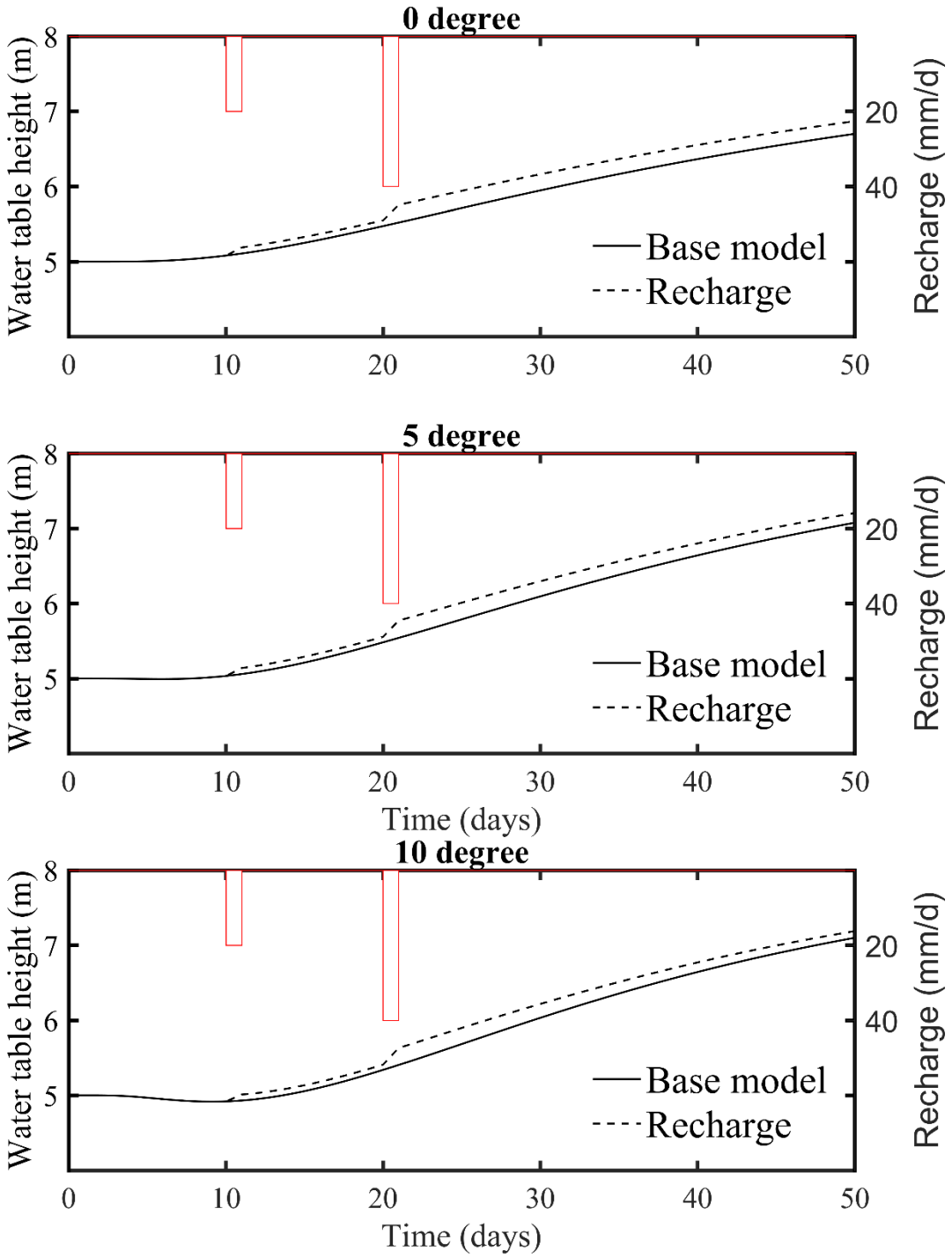

Fig. 2-16 Impact of infiltrated recharge on water table heights above the impermeable base at *x*=50 m in a horizontal aquifer, a 5° sloping aquifer, and a 10° sloping aquifer.

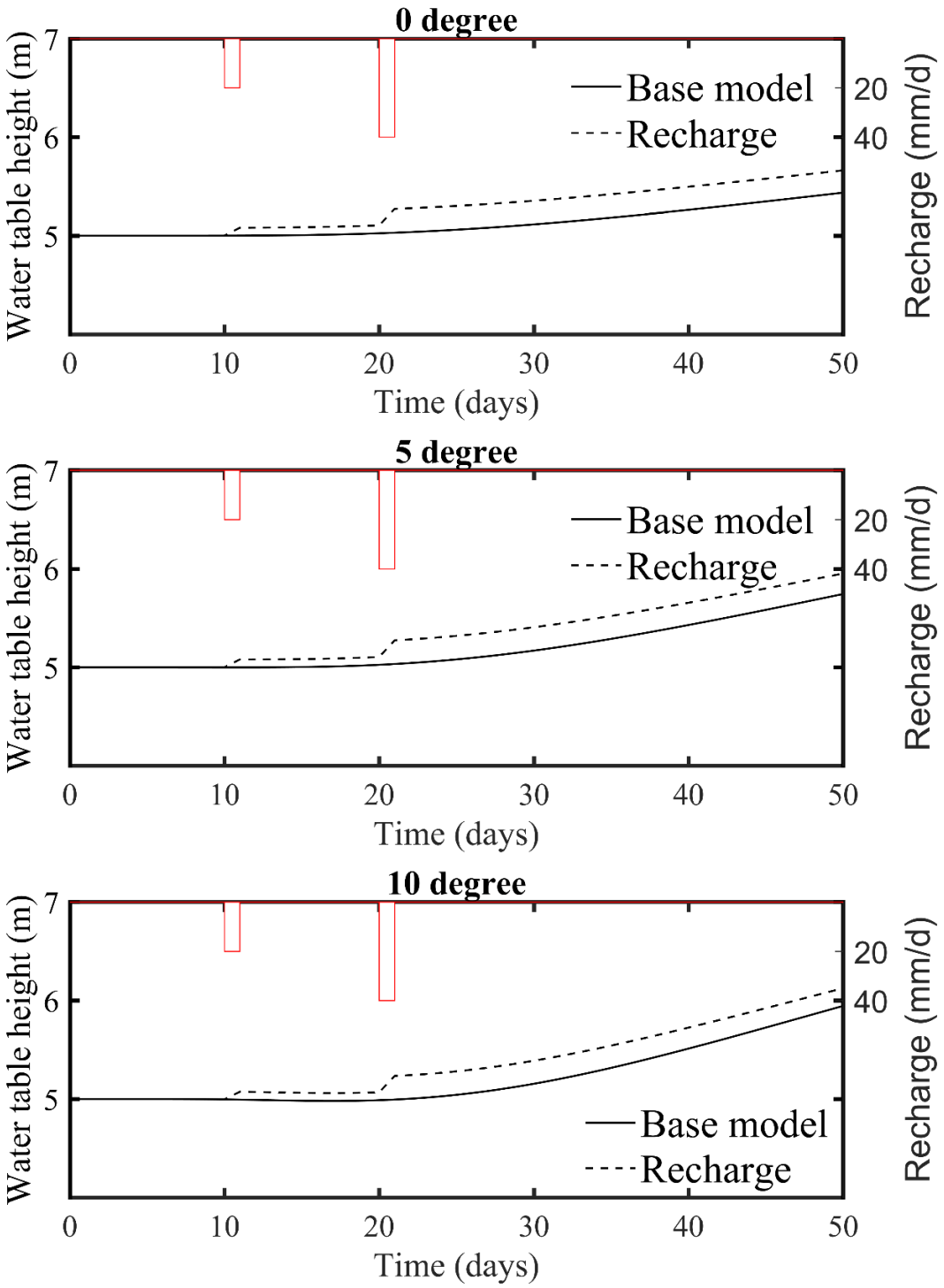

Fig. 2-17 Impact of infiltrated recharge on water table heights above the impermeable base at x=100 m in a horizontal aquifer, a 5° sloping aquifer, and a 10° sloping aquifer.

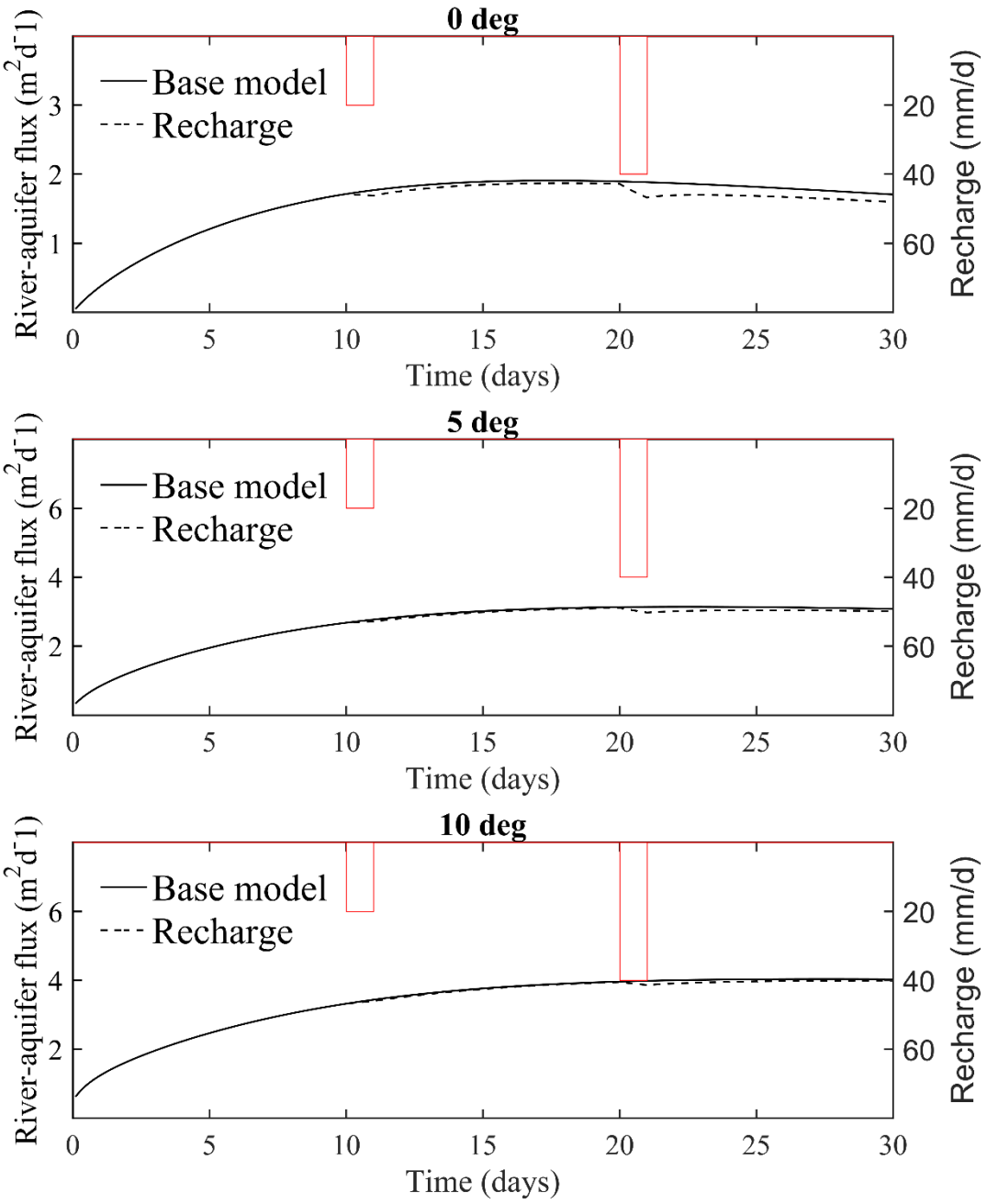

Fig. 2-18 Impact of infiltrated recharges on river-aquifer fluxes at the river in a horizontal aquifer, a 5° sloping aquifer, and a 10° sloping aquifer.

2.4 Conclusions

In this chapter, an unconfined sloping aquifer bounded by a river with a low permeability vertical clogging layer is considered. Special attention has been paid to the impact of sloping feature on the water table variation and the river-aquifer flux. An approximate analytical solution is developed based on the linearized Boussinesq equation to study groundwater flow in such a sloping aquifer. The solution could deal with the time-dependent river stage and time-dependent vertical infiltrated recharge. The analytical solution is compared with numerical solutions of COMSOL and HydroGeoSphere. The results of numerical solution based on the same linearized modified Boussinesq equation as the analytical solution using the finite element method by COMSOL fit very well with the results of analytical solution. The numerical model of HydroGeoSphere couples the saturated process and the unsaturated process. Our analytical solution does not specifically consider the unsaturated process, as commonly done in most analytical model of unconfined flow, instead, simplifying the unconfined flow process into a water table boundary with the use of the specific yield concept. The unsaturated process and the linearized approximation cause a few discrepancies between our analytical solution and numerical solution of HydroGeoSphere.

We have compared our solution with the Bansal's solution. Bansal et al. (2016) developed an analytical solution for the river-aquifer system with the presence of a sloping aquifer. They ignored an important term of boundary condition in their study without explanation. Bansal et al. (2016) verified their solution by numerical method, but the numerical method is based on the linearized modified Boussinesq equation, which also ignored that same term in the treatment of boundary condition. The results of

comparison between our solution and Bansal's solution display that the Bansal's solution overestimates the water table heights and river-aquifer flux.

We have compared the downward sloping bed case and the upward sloping bed case. The features of two cases are similar. However, the flow directions coming from the sloping bed driving forces are opposite for these two cases. The sloping bed provides an additional flow driving force, in addition to the gradient of water table heights above the impermeable base of the aquifer.

We have also compared the response of sporadic (short-term) recharge events on the top to groundwater table and river-aquifer flux. The results display that the sloping angle affect the responses of such recharge events barely. The recharge on the top will increase the groundwater table and decrease the flux recharged from river.

CHAPTER 3

TRANSIENT GROUNDWATER FLOW IN A SLOPING AQUIFER WITH TWO PARALLEL RIVERS

3.1 Introduction

Chapter 2 discusses the interaction of one river with a sloping aquifer. This chapter concerns the interaction of two rivers with a sloping aquifer. There are a number of reasons to necessitate the study of this chapter. First, because of the nonlinear nature of flow in an unconfined sloping aquifer, the presence of two rivers cannot be regarded as a simple superposition of one river. It is also unclear if the analytical model developed under a linearization process of the modified Boussinesq equation for an unconfined sloping aquifer is good approximation or not of the nonlinear flow process there. Second, it is also interest to see the interference of river-aquifer interactions with the presence of two rivers in the sloping aquifer framework. Third, the study of unconfined flow in a sloping aquifer bounded by two rivers whose stages can independently vary with time has received much less attention in comparison with the single river-aquifer system. Thus much needed knowledge gap has to be filled. Fourth, the interaction of two rivers with a sloping aquifer could be very different from that in a horizontal aquifer, as the rivers located on the down-gradient and up-gradient sides of the sloping aquifer could play drastically different roles in terms affecting the evolution of water table profile and the river-aquifer fluxes. Fifth, the two river-aquifer scenarios may be seen in a few actual field settings. One example is to study transmitting water between two parallel rivers through a sloping unconfined aquifer. The other example is to study influence of seawater

tidal fluctuation in a coastal sloping aquifer in a peninsula setting (Sedghi and Zhan, 2016).

An unconfined sloping aquifer between two parallel rivers was studied by Upadhyaya and Chauhan (2002), but with a large room for advancement. For instance, Upadhyaya and Chauhan (2002) did not consider the influences of clogging layers between rivers and aquifer and the various stages of rivers. The authors also only obtained a steady-state solution rather than a transient state solution for the sloping aquifer. Such issues will be resolved in this chapter. By including two clogging layers at the river-aquifer interface and considering flow transiency, the newly developed model can deal with a much broad range of problems. In this section, we will develop a general analytical model to deal with the unconfined sloping aquifer with two rivers. The vertical clogging layers, variable infiltrated recharge, variable river stages and the sloping angle are concerned. Based on the numerical model of HydroGeoSphere which is capable of handling coupled saturated and unsaturated flow processes, we can investigate the influences of unsaturated flow process on the hydrodynamics of unconfined aquifer, specifically the evolution of the water table height and the river-aquifer fluxes.

3.2 Mathematical model

A schematic sloping aquifer between two parallel rivers with water infiltrated recharge is presented in Fig. 3-1. Similarly, both rivers fully penetrate the aquifer. The two rivers are located in two sides of the homogeneous aquifer in the x direction with two thin clogging layers between aquifer and rivers respectively. The thicknesses of the left and right clogging layers are b_1 and b_2, respectively; the hydraulic conductivities of the left and right clogging layers are k_1 and k_2, respectively. The aquifer is downward sloping

from left to right. Similar to section 2.2, the origin of the coordinate system is at the intercept of the left clogging layer with the base of the aquifer, the *x*-axis is horizontal, pointing to the right, and the positive direction of *z*-axis is upward vertical. The two river stages can vary with time independently, and the vertical recharge can also vary with time. The horizontal distance between two rivers is L and the sloping angle is θ. A river-aquifer system with a horizontal base is a standard model in many textbooks (Bear, 1972; Fetter, 1999; Domenico and Schwartz, 1998) and is used as a reference of comparison. In contrast to the river-aquifer with a horizontal base, a river-aquifer system with a sloping base has not been fully understood with many unanswered questions, which will be addressed in this study. A minor point to note is that the two parallel rivers here may be replaced with some other surface water features such as two parallel canals or drains, if they operate similarly as rivers. The system studied here is also applicable for a coastal sloping aquifer bounded on both sides by oceans whose water level can fluctuate with time. This scenario can be seen in peninsula settings or long-strip islands (Sedghi and Zhan, 2016).

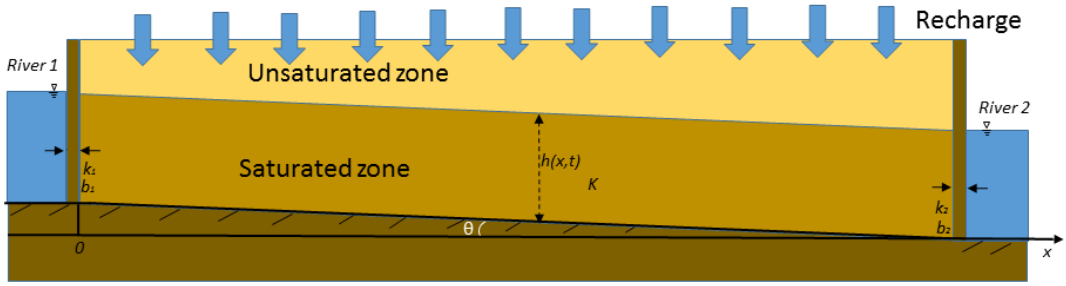

Fig. 3-1 The diagram of the sloping aquifer adjoining with two rivers by thin sedimentary layers.

The details of the modified Darcy's law, the linearized Boussinesq equation and the corresponding assumptions for a sloping aquifer were discussed in Eqs. (2-1) to (2-5) in

section 2.2 and will not be repeated here. The method and procedure are similar to section 2.2 except the boundary condition of river 2. However, the procedure of analytical model is necessary to be intact and strict for a check. We need to present the details for the sake of completeness.

The time-independent river stages are also described by the suggested exponential functions of Teloglou and Bansal (2012), which are given by the following Eqs. (3-1a) and (3-1b), where $h_{s_1}(t)$ and $h_{s_2}(\mathrm{t})$ are the time-varying stages for rivers 1 (left river) and river 2 (right river), respectively; h_{f_1} and h_{f_2} are the final stage values for rivers 1 and 2, respectively; h_i is the initial (identical) stage for rivers 1 and 2 at t=0; λ_1 and λ_2 are the rates of change used for the exponential functions for rivers 1 and 2, respectively.

$$h_{s_1}(t) = h_{f_1} - (h_{f_1} - h_i)e^{-\lambda_1 \mathrm{t}} \tag{3-1a}$$

$$h_{s_2}(t) = h_{f_2} - (h_{f_2} - h_i)e^{-\lambda_2 \mathrm{t}} \tag{3-1b}$$

The initial condition is the same as that in chapter 2 (Eq. (3-2a)). Based on the modified Darcy's law used in sloping aquifers and a linear approximation of the Robin boundary condition by Moutsopoulos (2013), a mass balance principle can be used at the interface of the clogging layer and the aquifer, and the associated boundary conditions are obtained in Eqs. (3-2b) and (3-2c). The right sides of Eqs. (3-2b) and (3-2c) represent the flow rates in the clogging layers. The left sides of Eqs. (3-2b) and (3-2c) represent the flow rates at the interface between the clogging layers and aquifer.

$$h(x, t = 0) = h_i \tag{3-2a}$$

$$-Kh(x = 0^+, t)[(\frac{\partial h}{\partial x})_{x=0} - tan\theta] = -k_1 h(x = 0^+, t)\frac{h(x=0^+,t) - h_{s_1}(t)}{b_1} \tag{3-2b}$$

$$-Kh(x=L^{-},t)[(\frac{\partial h}{\partial x})_{x=L}-tan\theta]=k_2h(x=L^{-},t)\frac{h(x=L^{-},t)-h_{s_2}(t)}{b_2} \quad (3\text{-}2c)$$

Defining the following dimensionless terms, $h_D=\frac{h-h_i}{h_{f_1}-h_i}$, $x_D=\frac{x}{L}$, $t_D=\frac{Kh_acos^2\theta t}{S_yL^2}$, $\alpha=\frac{Ltan\theta}{h_a}$, $W(t_D)=\frac{LW(t)}{Kh_acos^2\theta}$, $R_1=\frac{Kb_1}{k_1L}$, $R_2=\frac{Kb_2}{k_2L}$, $\mu=\frac{h_{f_2}-h_i}{h_{f_1}-h_i}$, $\lambda_{1D}=\frac{S_yL^2\lambda_1}{Kh_acos^2\theta}$, $\lambda_{2D}=\frac{S_yL^2\lambda_2}{Kh_acos^2\theta}$, $m_1=\frac{Kb_1tan\theta}{k_1(h_{f_1}-h_i)}$, $m_2=\frac{Kb_2tan\theta}{k_2(h_{f_1}-h_i)}$, the dimensionless forms of Eq. (2-4) and Eqs. (3-2a) to (3-2c) are presented as below.

$$\frac{\partial^2h_D}{\partial x_D{}^2}-\alpha\frac{\partial h_D}{\partial x_D}+W(t_D)=\frac{\partial h_D}{\partial t_D} \quad (3\text{-}3)$$

$$h_D(x_D,t_D=0)=0 \quad (3\text{-}4a)$$

$$R_1(\frac{\partial h_D}{\partial x_D})_{x_D=0}=h_D(x_D=0^{+},t_D)+e^{-\lambda_{1D}t_D}-1+m_1 \quad (3\text{-}4b)$$

$$R_2(\frac{\partial h_D}{\partial x_D})_{x_D=1}=-h_D(x_D=1^{-},t_D)-\mu e^{-\lambda_{2D}t_D}+\mu+m_2 \quad (3\text{-}4c)$$

Similar to section 2.2, we define a new parameter $\varphi=h_De^{-\frac{\alpha x_D}{2}}$, above four equations are changed to

$$\frac{\partial^2\varphi}{\partial x_D{}^2}-\frac{\alpha^2\varphi}{4}+e^{-\frac{\alpha x_D}{2}}W(t_D)=\frac{\partial\varphi}{\partial t_D} \quad (3\text{-}5a)$$

$$\varphi(x_D,t_D=0)=0 \quad (3\text{-}5b)$$

$$\left[R_1\frac{\partial\varphi}{\partial x_D}+(R_1\alpha/2-1)\varphi\right]|_{x_D=0}=e^{-\lambda_{1D}t_D}-1+m_1 \quad (3\text{-}5c)$$

$$\left[R_2\frac{\partial\varphi}{\partial x_D}+(R_2\alpha/2+1)\varphi\right]|_{x_D=1}=e^{-\frac{\alpha}{2}}[-\mu\left(e^{-\lambda_{2D}t_D}-1\right)+m_2] \quad (3\text{-}5d)$$

The PDE of Eq. (3-5a) can be transformed into an ordinary different equation by eliminating the *x* terms using an Integral transform method. The Integral transform of

$\varphi(x_D, t_D)$ is defined as Eq. (3-6a) and the corresponding inversion formula is defined as Eq. (3-6b).

$$\bar{\varphi}(\omega_n, t_D) = \int_0^1 \varphi(x_D, t_D)\, K(\omega_n, x_D) dx_D \tag{3-6a}$$

$$\varphi(x_D, t_D) = \sum_{n=0}^{\infty} K(\omega_n, x_D)\, \bar{\varphi}(\omega_n, t_D) \tag{3-6b}$$

where $K(\omega_n, x_D)$ and ω_n are transform kernel and eigenvalue, respectively. The kernel $K(\omega_n, x_D)$ is a normalized eigenfunction of the following eigenvalue problem.

$$\frac{d^2k}{dx_D{}^2} + \omega_n^2 k = 0 \tag{3-7a}$$

$$\left[\frac{\partial k}{\partial x_D} + \left(\frac{\alpha}{2} - \frac{1}{R_1}\right) k\right]|_{x_D=0} = 0 \tag{3-8a}$$

$$\left[\frac{\partial k}{\partial x_D} + \left(\frac{\alpha}{2} + \frac{1}{R_2}\right) k\right]|_{x_D=1} = 0 \tag{3-8b}$$

The kernel $K(\omega_n, x_D)$ is defined as

$$K(\omega_n, x_D) = A_n k(\omega_n, x_D) = A_n[\omega_n \cos(\omega_n x_D) + \left(\frac{1}{R_1} - \frac{\alpha}{2}\right) \sin(\omega_n x_D)] \tag{3-9}$$

where

$$A_n = \frac{\sqrt{2}}{\sqrt{\left[\omega_n^2 + (\alpha/2 - 1/R_1)^2\right]\left[1 + \frac{\frac{\alpha}{2} + \frac{1}{R_2}}{\omega_n^2 + (\alpha/2 + 1/R_2)^2}\right] + \frac{1}{R_1} - \frac{\alpha}{2}}} \tag{3-10}$$

Be aware that Eq. (3-10) of A_n is different from Eq. (2-15). Taking integral transform on Eq. (3-5a) leads to

$$\int_0^1 K(\omega_n, x_D) e^{-\frac{\alpha x_D}{2}} W(t_D)\, dx_D + \int_0^1 K(\omega_n, x_D) \frac{\partial^2 \varphi}{\partial x_D{}^2} dx_D = \int_0^1 K(\omega_n, x_D) \frac{\partial \varphi}{\partial t_D} dx_D + \alpha^2/4 \int_0^1 K(\omega_n, x_D) \varphi(x_D, t_D)\, dx_D \tag{3-11}$$

Based on Green's function theorem, the left side of Eq. (3-11) can be written as:

$$\int_0^1 K(\omega_n, x_D) e^{-\frac{\alpha x_D}{2}} W(t_D)\, dx_D + \int_0^1 K(\omega_n, x_D) \frac{\partial^2 \varphi}{\partial {x_D}^2} dx_D =$$

$$\int_0^1 K(\omega_n, x_D) e^{-\frac{\alpha x_D}{2}} W(t_D)\, dx_D - \omega_n^2 \bar{\varphi} + \frac{K_{x_D=1}\left(\mu - \mu e^{-\lambda_{2D} t_D} + m_2\right)}{R_2 \exp(\alpha/2)} - \frac{K_{x_D=0}\left(e^{-\lambda_{1D} t_D} - 1 + m_1\right)}{R_1} \tag{3-12}$$

Substituting Eqs. (3-6a), (3-8a), (3-8b) and (3-12) into Eq. (3-11), and defining $\beta_n = \omega_n^2 + \alpha^2/4$, one has

$$\frac{\partial \bar{\varphi}}{\partial t_D} + \beta_n \bar{\varphi} = \frac{K_{x_D=1}\left(\mu - \mu e^{-\lambda_{2D} t_D} + m_2\right)}{R_2 \exp(\alpha/2)} - \frac{K_{x_D=0}\left(e^{-\lambda_{1D} t_D} - 1 + m_1\right)}{R_1} +$$

$$\frac{A_n}{\beta_n} W(t_D) \left\{ e^{-\frac{\alpha}{2}} \left[\beta_n \sin(\omega_n) - \frac{1}{R_1} \left(\frac{\alpha}{2} \sin(\omega_n) + \omega_n \cos(\omega_n) \right) \right] + \frac{\omega_n}{R_1} \right\} \tag{3-13a}$$

$$\bar{\varphi}(0) = 0 \tag{3-13b}$$

Rearranging Eq. (3-13a) yield as

$$\frac{\partial \bar{\varphi}}{\partial t_D} + \beta_n \bar{\varphi} = B(t_D) \tag{3-14}$$

where

$$B(t_D) = \frac{K_{x_D=1}\left(\mu - \mu e^{-\lambda_{2D} t_D} + m_2\right)}{R_2 \exp(\alpha/2)} - \frac{K_{x_D=0}\left(e^{-\lambda_{1D} t_D} - 1 + m_1\right)}{R_1} + \frac{A_n}{\beta_n} W(t_D) \left\{ e^{-\frac{\alpha}{2}} \left[\beta_n \sin(\omega_n) - \right.\right.$$

$$\left.\left. \frac{1}{R_1} \left(\frac{\alpha}{2} \sin(\omega_n) + \omega_n \cos(\omega_n) \right) \right] + \frac{\omega_n}{R_1} \right\}$$

The solution of Eq. (3-14) subject to Eq. (3-13b) can be straightway obtained as

$$\bar{\varphi}(\omega_n, t_D) = \exp(-\beta_n t_D) \int_0^{t_D} B(t) \exp(\beta_n t)\, dt \tag{3-15}$$

Defining $\xi_1 = A_n \frac{\omega_n R_2 \exp(\alpha/2)(1-m_1) + (\mu + m_2) R_1 \left[\omega_n \cos(\omega_n) + \left(\frac{1}{R_1} - \frac{\alpha}{2} \right) \sin(\omega_n) \right]}{R_1 R_2 \beta_n \exp(\alpha/2)}$,

$$\xi_2 = A_n \frac{\omega_n/R_1}{\beta_n - \lambda_{1D}},$$

$$\xi_3 = A_n \frac{\mu\left[\omega_n \cos(\omega_n) + \left(\frac{1}{R_1} - \frac{\alpha}{2}\right)\sin(\omega_n)\right]}{(\beta_n - \lambda_{2D})R_2 \exp(\alpha/2)},$$

$$\xi_4 =$$

$$A_n \frac{R_2[\lambda_{1D} + m_1(\beta_n - \lambda_{1D})]\omega_n(\beta_n - \lambda_{2D})\exp\left(\frac{\alpha}{2}\right) + R_1[\mu\lambda_{2D} - m_2(\beta_n - \lambda_{2D})](\beta_n - \lambda_{1D})\left[\omega_n \cos(\omega_n) + \left(\frac{1}{R_1} - \frac{\alpha}{2}\right)\sin(\omega_n)\right]}{\beta_n R_1 R_2 (\beta_n - \lambda_{1D})(\beta_n - \lambda_{2D})\exp(\alpha/2)}$$

,

$$\xi_5 = \frac{A_n}{\beta_n}\left\{e^{-\frac{\alpha}{2}}\left[\beta_n \sin(\omega_n) - \frac{1}{R_1}\left(\frac{\alpha}{2}\sin(\omega_n) + \omega_n \cos(\omega_n)\right)\right] + \frac{\omega_n}{R_1}\right\},$$

one obtains

$$\bar{\varphi}(\omega_n, t_D) = \xi_1 - \xi_2 \exp(-\lambda_{1D} t_D) - \xi_3 \exp(-\lambda_{2D} t_D) + \xi_4 \exp(-\beta_n t_D) -$$

$$\xi_5 \exp(-\beta_n t_D) \int_0^{t_D} W(t_D) \exp(\beta_n t)\, dt \qquad (3\text{-}16)$$

Substituting Eq. (3-16) into Eq. (3-6b) leads to

$$\varphi(x_D, t_D) = \sum_{n=0}^{\infty} K(\omega_n, x_D)[\, \xi_1 - \xi_2 \exp(-\lambda_{1D} t_D) - \xi_3 \exp(-\lambda_{2D} t_D) +$$

$$\xi_4 \exp(-\beta_n t_D) - \xi_5 \exp(-\beta_n t_D) \int_0^{t_D} W(t) \exp(\beta_n t)\, dt] \qquad (3\text{-}17)$$

The final solution (in dimensionless form) can be obtained as

$$h_D(x_D, t_D) = \varphi(x_D, t_D) \exp(\alpha x_D/2) \qquad (3\text{-}18)$$

Eq. (3-18) serves as the working equation for computing the water table heights above the impermeable base at any given location and time. When this is obtained, the river-aquifer flux can be computed using the modified Darcy's law for a sloping aquifer (Eq. (2-1)) at the interface of the two clogging layers and the aquifer. If allowing the distance between the two rivers to be infinitely large and the hydraulic conductivity of the right

vertical clogging layer to be identical with *K* of aquifer, the system investigated here degenerated to the single river chase of chapter 2. The MATLAB code to obtain the solution of Eq. (3-18) is presented in Appendix B.

3.3 Results and Discussion

3.3.1 Comparison of analytical solution with numerical solutions

In this section, the new analytical solution developed above will be compared with COMSOL program and HydroGeoSphere. Similarly, we also present the results for a horizontal aquifer, a sloping aquifer with 5º sloping angle and a sloping aquifer with 10º sloping angle. The setting up of the numerical models are as follows.

The thickness of two clogging layers are both set as 1 m, and the hydraulic conductivities of those clogging layers are identical and set as 0.248 m/d. The hydrological parameters of material and the initial head in the aquifer are same as that set in section 2.3.1. The vertical recharge is set as zero for the sake of illustration. The initial and final stages for river 1 are set as 5 and 10 m, respectively, and $\lambda_1 = 0.1\ d^{-1}$. The constant stage of 5 m is set for river 2 over the entire time of interest (or $\lambda_2 = 0\ d^{-1}$). We need to point out the reason to set only one rising or declining river here and after. Though we obtain the water table heights and river-aquifer fluxes under two fluctuant rivers, it is difficult to separate the influences by the fluctuations of the stages.

The hydrological parameters for unsaturated zone in HydroGeoSphere are same as that set in section 2.3.1. Discussion of these parameters have been presented in chapter 2 and will not repeat here.

The design of COMSOL program is briefly illustrated as follows. The horizontal length of the aquifer is 100 m. Once again, the use of a relatively small aquifer length here is for the purpose of visual inspection, and the conclusions hold when aquifer lengths are longer (such as 1000 m or even longer). The horizontal grid space is 0.01 m. The boundary conditions of river 1 and river 2 are set by Eq. (3-2b) and Eq. (3-2c). The actual values of parameters are calculated by Eqs. (3-2b) and (3-2c) for three aquifers.

The design of HydroGeoSphere is briefly outlined as follows. The horizontal length of the aquifer is 100 m. The horizontal lengths of the clogging layers are both 1 m. The horizontal grid space in the clogging layers is 0.1 m, and the horizontal grid space in the aquifer is 0.5 m. The vertical grid space for both the aquifer and clogging layers is set at 0.25 m. River 1 is located at x=0 m and river 2 is located at x=102 m. The base elevations, specific heads of two rivers with time are similar to section 2.3.1.

An analysis of grid convergence was carried out in three cases of COMSOL model and HydroGeoSphere, and it showed that the grid spacing did not affect the results of water table heights and river-aquifer fluxes.

Be aware that we did not use the method of Liang and Zhang (2012) to set the linearized parameter h_a. We use the average value of initial heads and final heads at the left and right boundaries and have h_a =6.25 m in the analytical model and COMSOL simulation. The reason is that the stage of river 1 increase rapidly and the average

thickness of aquifer increase remarkably in this case. If we use the average value of initial heads at the left and right boundaries as h_a, the solution may be underestimated. Here we find the average thickness value of aquifer may cause remarkable discrepancies between analytical solution and HydroGeoSphere, when the stage of river rise or decline in a high range. It implies researchers should consider the issue of accuracy in analytical solution for a great range of river stage.

Fig. 3-2 and Fig. 3-3 compare the water table heights by analytical solution, COMSOL program and HydroGeoSphere. The two figures show that the results of COMSOL agree with the results of analytical solution very well. The results of HydroGeoSphere also fit well with the results of analytical solution for t=10 d. But when the time is around 30 days and the horizontal distance to river 1 is around 60 meters, the discrepancy of water table between the analytical model and the HydroGeoSphere model is relatively large. This could be because of a few reasons. First, the HydroGeoSphere model does not involves any linearization process, and the analytical model does. Second, the HydroGeoSphere model considered the coupled unsaturated and saturated flow process while the analytical model only concerns the saturated flow process. When the sloping angle increases from 0^o to 10^o, the discrepancy between the analytical solution and the HydroGeoSphere solution increase as well. More remarkable, such a discrepancy at 30^{th} day is larger than that at 50^{th} day in a range from x=40 m to x=80 m. Fig. 3-4 displays the river-aquifer fluxes at the river 1 and river 2, where Q_1 and Q_2 represent the river-aquifer flux (per unit width) at the left and right rivers. Similar observations as those observed in Figs. 3-2 and 3-3 are also seen here. First, the results of the analytical model fit greatly with the results of COMSOL model. Second, when the sloping angle

increases, the discrepancy between the analytical model and the HydroGeoSphere model increases. Third, the discrepancy of fluxes between the analytical model and the HydroGeoSphere model for river 1 (at x=0 m) is considerably larger than that at river 2, due to the fact the water stage at river 1 changes rapidly with time while the water stage at river 2 remains the same all the time.

To quantify the differences between analytical and numerical solutions, a dimensionless index called the relative percentage difference (RPD) is defined as follows:

$$\text{RPD} = \frac{h_{num} - h_{ana}}{h_{num}} * 100\% \quad (24)$$

where h_{ana} is the water table height computed using the newly developed analytical solution, and h_{num} is the water table height computed with either COMSOL or HydroGeoSphere. The ranges of RPD values are shown in Table 1. Similar RPD is also calculated for the river-aquifer fluxes for both rivers 1 and 2 and the results are also summarized in Table 1. The data calculated for RPD values include: 1) water table heights at x=0, 20, 50, 80 and 100 m from 0.1 day to 50 days with a time step of 0.1 days; 2) water table heights at t=10, 20, 30, 40 and 50 d from 0 m to 100 m; 3) river-aquifer fluxes at river 1 and river 2 from 0.1 days to 50 days with a time step of 0.1 days.

A few observations can be seen from Table 1. First, the RPD values for the pair of analytical and COMSOL models for three different sloping angles are less than 0.1%. Second, the variational range of RPD for the river-aquifer flux is greater than that for the water table height. Third, the range of RPDs for both water table heights and river-aquifer flux increases when the sloping angle increases. Fourth, the RPD for the pair of the

analytical and COMSOL models are universally smaller than that for the pair of the analytical and HydroGeoSphere models. Specifically, when the sloping angle is 10º, the RPD of water table height for the pair of the analytical and HydroGeoSphere models ranges from -5.07% to 2.71%, while the RPD of river-aquifer flux for the same pair ranges from -14.05% to 12.71%. This finding indicates that the potential errors associated with the analytical solution which involves a linearization process of the nonlinear Boussinesq equation and omits the unsaturated zone flow process may become considerably large to disqualify the use of such an analytical model, particularly when the river-aquifer flux is of the primary concern. On the other hand, the analytical model serves as a reasonably good approximation to compute both the water table height and river-aquifer flux when the sloping angle is less than is 10º. In fact, a careful inspection of the flow field generated by the HydroGeoSphere model suggests that flow does not always follow the direction of the sloping bed, as assumed in the analytical model, particularly in the regions close to two rivers. Such a deviation of flow direction from the "assumed" sloping bed direction becomes worse when the sloping angle becomes greater. In fact, the direction of flow near river 1 changes gradually from horizontal to the sloping direction, while the direction of flow near river 2 changes gradually from the sloping direction to horizontal. Although the scales for such flow transitions to occur are relatively small as compared to the entire flow distance, they do become larger when the sloping angle increases. An interesting point to note is that when the water stage of river 1 rises with a slower rate (with a smaller λ_1 value), the corresponding RPDs for the pair of the analytical and HydroGeoSphere models get smaller (results not shown in Table 1).

Table 1. Range of Relative Percentage Difference (RPD) between analytical and numerical solutions in three aquifers.

Sloping angles	COMSOL RPD (%)		HydroGeoSphere RPD (%)	
	Water table height	River-aquifer flux	Water table height	River-aquifer flux
0º	-0.043 to 0.018	-0.040 to 0.025	-3.20 to 1.56	-2.39 to 16.79
5º	-0.068 to 0.098	-0.060 to 0.086	-4.67 to 1.57	-5.65 to 10.08
10º	-0.078 to 0.061	-0.051 to 0.046	-5.07 to 2.71	-14.05 to 12.71

3.3.2 Analysis of parameter impacts on the river-aquifer system

We will study the influences of hydraulic parameters on the water table heights and river-aquifer fluxes again for the case of a sloping aquifer connecting with two rivers. Similarly, b_1/k_1, b_2/k_2, K, S_y affect the hydrodynamics of the river-aquifer system independently. Without loss of generality, we allow the hydraulic resistances of two clogging layers, b_1/k_1, b_2/k_2, to be identical in the following analysis. Different hydraulic resistances of these two clogging layers can be used, not will not change the primary findings. The corresponding hydraulic parameters of aquifer and clogging layers for base model and matched models are same as that in section 2.3.3 and will not be repeated here.

Fig. 3-5, Fig. 3-6 and Fig. 3-7 show water table heights and river-aquifer fluxes for aquifers with three different sloping angles of 0°, 5° and 10°, where Q_1 and Q_2 represent the river-aquifer flux (per unit width) at the left and right rivers, respectively. The stage

of river 1 is described by Eq. (3-1a) with λ_1=0.1 d^{-1} and h_i=5 m and h_{f1}=10 m. The stage of river 2 remains constant at 5 m.

A few interesting observations can be made from Fig. 3-5 and Fig. 3-6. First, for the special case of a horizontal aquifer (or a sloping angle of 0°), the water table heights declines from left to right over the entire domain of interest. This is caused by a rapidly rising river stage on the left. However, for the case of a sloping aquifer, the water table height declines first from left to right, and then rise again, generating a convex shape. Furthermore, the convex shape of the water table height become more visible when the sloping angle becomes larger. Similar convex shape has also been observed in Fig. 3-3. The appearance of convex shape of water table height is a unique feature of a sloping aquifer and it is impossible to occur in a horizontal aquifer when evaporation is omitted. This is due to the fact that the water table height is measured against the sloping bed, not a fixed horizontal reference plane. This observation can be understood as follows. For the problem investigated here, flow is always from left to right when the left river stage rises and the right river stage remains the same when vertical recharge/evaporation is absent, thus the hydraulic head declines continuously over the entire domain. For a horizontal aquifer, the slope of the water table height represents the hydraulic gradient itself when the Dupuit (or horizontal flow) assumption is invoked, thus the water table height must decline with distance from left to right. However, for a sloping aquifer case, the hydraulic gradient consists of two contributions: 1) the gradient of water table height; 2) the slope of the bed. Therefore, when the slope of the bed becomes greater than the magnitude of the hydraulic gradient, the gradient of water table height can reverse its direction to become opposite of the sloping direction. In another word, when the slope is dipping

from left to right, the water table height can actually increase from left to right. This is exactly what happens for regions close to the right river in Figs. 3-3, 3-5 and 3-6.

Second, we also see from Figs. 3-3, 3-5 and 3-6 that the convex shape of the water table height for a sloping aquifer becomes less visible when time gets longer. This is because the river stage at the left increases with time, so the overall hydraulic gradient increases with time as well. The increase of hydraulic gradient will make it less likely for the slope of bed to surpass the hydraulic gradient, thus reducing the likelihood of reverse water table height gradient, leading to a less visible convex shape of the water table height. If the left river rises sufficiently high and the hydraulic gradient becomes sufficiently large, then the slope of bed probably will never surpass the hydraulic gradient, and the convex shape of the water table height will disappear entirely.

The river-aquifer fluxes shown in Fig. 3-7 also has a few interesting points to note. First, for the special case of a horizontal aquifer, rise of the left river stage will result in a rapid increase of river-aquifer flux there (Q_1) at the beginning, due to a significant hydraulic gradient over the clogging layer. However, as the rate of river stage rise slows down (because of the exponential function of Eq. (3-1a)), the hydraulic gradient over the clogging layer at the left river declines, resulting in the drop of the river-aquifer flux Q_1 after reaching a maximum value. The river-aquifer flux at the right (Q_2), however, increases from zero at the beginning over the time interval of discussion in Fig. 3-7. The increase of Q_2 over the time interval of interest is also evident in Figs. 3-5 and 3-6, as one can see that the water table gradient (which equal to the hydraulic gradient for a horizontal aquifer) near the right river becomes larger when time is longer.

Second, when the aquifer becomes sloping instead of horizontal, the river-aquifer flux is aided with the help of the sloping bed, beside the rise of left river. The contribution of such a sloping bed to Q_1 will lead to a less dramatic increase of Q_1 with time at the early stage and also a less dramatic decrease of Q_1 with time at the late stage after reaching its peak value. When the sloping angle becomes greater enough (for instance, 10°), the decline trend of Q_1 with time may disappear completely. The variational feature of Q_2 is a little more complex for the sloping cases. It appears that Q_2 typically experiences an increase period first, followed by a relatively flat or stable flux during the intermediate stage, and then a slightly greater rate of increase at late stage. The variational trend of Q_2 is understandable if considering the following factors. First, as the initial water table height is arbitrarily set to be 5 m over the entire domain, the hydraulic gradient driven by the sloping angle will immediately initiate flow from left to right and results in a rise of water table heights near the right river at the early times, as also observed in Fig. 3-5 for at time of 10 days. This will induce a relatively rapid increase of river-aquifer flux at the right river. The change of water table heights near the right river will eventually slow down, leading to a relatively flat segment of Q_2-time distribution at the intermediate times. At later time, the rise of river stage at the left will propagate through the aquifer and reach the right river, resulting a relatively steady increase of Q_2 at later times.

Besides above observations, it is also worthwhile to see the influences of different parameters on the shape of the water table height and river-aquifer fluxes. First, from Figs. 3-5, 3-6 and 3-7, one can see that for the special case of a horizontal aquifer (or a sloping angle of 0°), increasing the value of b_1/k_1 or b_2/k_2 reduces the water table height over most portion of the aquifer. This is because increasing the hydraulic resistance of the

two clogging layers will reduce the river-aquifer fluxes, thus reduce the water table height. Specifically, the reduction of water table heights decreases from the left to right. One can clearly see from Fig. 3-7 that the river-aquifer flux decreases remarkablely at x=0 m. For the two sloping aquifers (with sloping angles of 5° and 10°), it is easy to see from Figs. 3-5 and 3-6 that the water table height drops in most part of aquifer, and only rises in a narrow region near river 2.

The increase of K value augments the flow rate in the aquifer, and consequently the river-aquifer fluxes increase significantly in all three aquifers. The river-aquifer flux increases more when the sloping angle becomes greater. The discharge to river 2 for the 10° sloping bed shows remarkable fluctuations over the 30 days period. Such a discharge declines gently from 8^{th} day to 15^{th} day, and then rises from 16^{th} day.

The influence of specific yield is relatively minor when compared to other hydrological parameters when the recharge/evaporation is absent. When the specific yield increases, the capacity of aquifer releasing or storing water due to water table dropping or rising becomes stronger, thus the variation of water table heights becomes less dramatic.

3.3.3 Different characters of horizontal and sloping aquifers

Fig. 3-8 presents water table heights distributions for the same three sloping angles discussed in section 3.3.2, but with a constant river stage on the left river and a rising river stage on the right river. Specifically, the stage of left river (river 1) is set at 5 m above the aquifer, and the stage of right river (river 2) is described by Eq. (3-1b) with λ_2=0.1 d^{-1}, h_i=5 m, and h_{f2}=10 m. When the aquifer is horizontal, the rise of river stage on the right river leads to a flow condition that is exactly the same as that generated by a rise

of river stage on the left (provided that the rise of river stage follow the same function) except that the flow direction is reversed. However, when the aquifer is sloping, then the flow condition generated by a rise of river stage on the right river is considerably different from that generated by a rise of river stage on the left, even the rise of river stage follow exactly the same function.

A few interesting observations can be made about Fig. 3-8 and Fig. 3-9. First, when a sloping bed is presented and the initial water table heights are 5 m over the entire domain, if the right river stages start to rise following the exponential function of Eq. (3-1b), the water table heights close to the right river will start to rise rapidly as well at the early time. Interesting enough, the water table heights near the left river actually will drop below the initial 5 m because it cannot sustain the flow driven by the sloping angle. Consequently, an uprising curve of water table height distribution from left to right will be seen. The greater the sloping angle, the more dramatic uprising curve will be seen for the water table height distribution. Second, for the horizontal aquifer case, the river-aquifer flux at the left river (Q_1) starts at 0 and then becomes negative (meaning that flow is from right to left), due to the rise of river stage on the right. However, for the sloping aquifer cases, a finite positive Q_1 exists because of the driving force of the sloping angle when the initial water table heights are the same (5 m). At the early times, as the water table heights near the left river will drop quite rapidly (as seen in Fig. 3-8), a greater hydraulic gradient is generated near the left river, resulting a raid rise of Q_1 at early times. Such a rise of Q_1 cannot sustain too long as the rise of river stage at the right river will offset the sloping driving flow, leading to a relatively stable Q_1 for the rest of times. Third, the river-aquifer flux at the right river (Q_2) shows some interesting features.

Similar to Q_1 at the beginning, the initial flow is driven by the sloping angle, so Q_2 will have the same positive value as Q_1 at t=0. When time is greater than zero, the water table heights near the right river will start to rise. Such a water table rise plus the rise of water stage on the right river will substantially offset the sloping driven flow, resulting a rapid decline of Q_2 and eventually a reversal of flow direction, i.e., Q_2 will change from positive to negative at a particular moment during the early stage flow. After that, the continuous rise of right river stage and the rise of water table heights near the right river will allow Q_2 to reach its maximum in magnitude. After that moment, as both the rise of right river stage and the rise of water table heights slows down with time, the magnitude of Q_2 will start to drop. However, if the sloping angle is greater enough (such as 10°), the sloping driven flow is so strong that the rise of right river stage and the rise of water table heights near the right river is not greater enough to offset the sloping driven flow, thus Q_2 will remain positive (meaning that flow is from left to right) for a considerable period of time, as evident in Fig. 3-9 (the bottom figure).

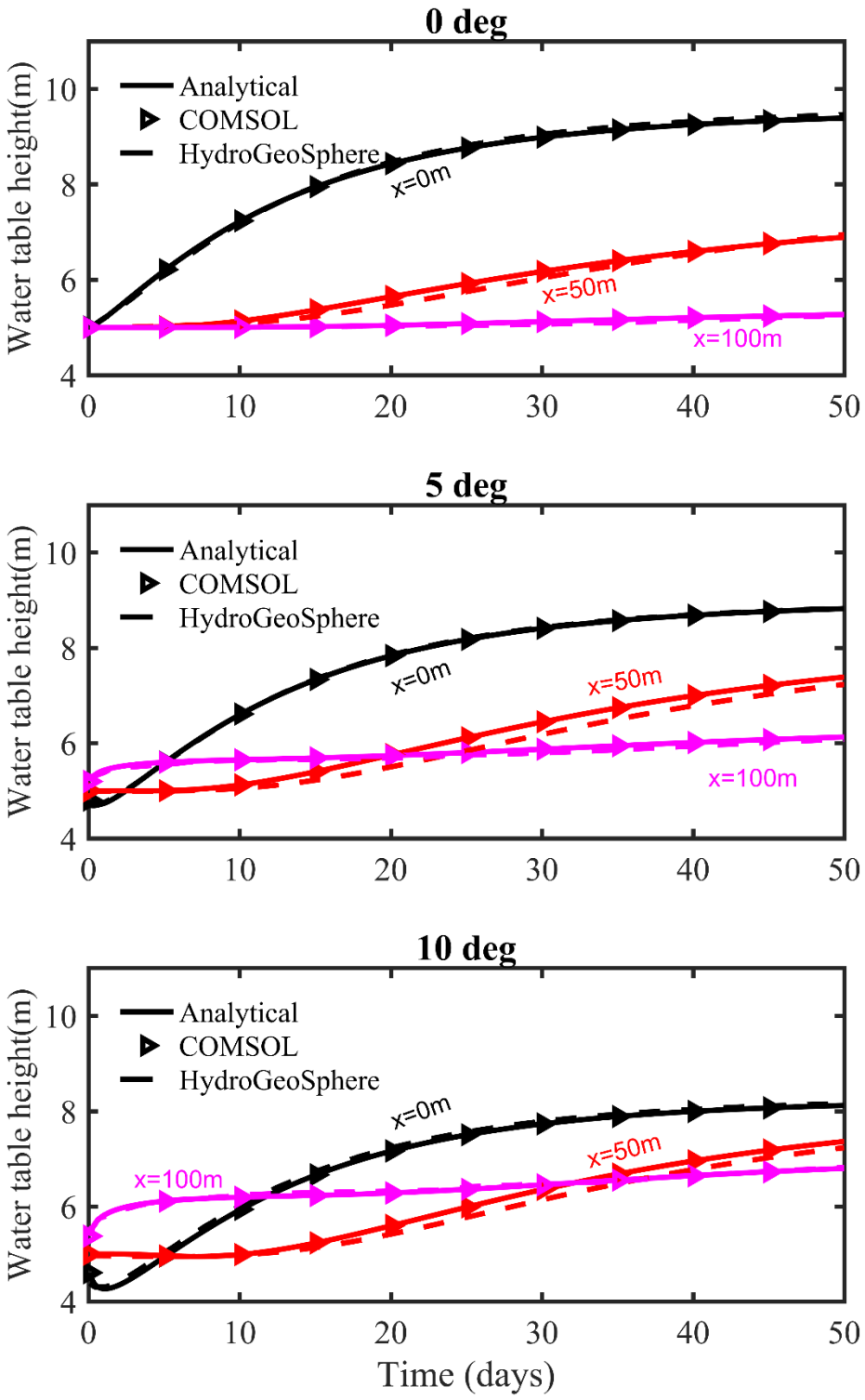

Fig. 3-2 Comparison of water table heights with time at *x*=0, 50 and 100 m in a horizontal aquifer, a 5° sloping aquifer, and a 10° sloping aquifer among analytical solution, numerical solutions of COMSOL and HydroGeoSphere.

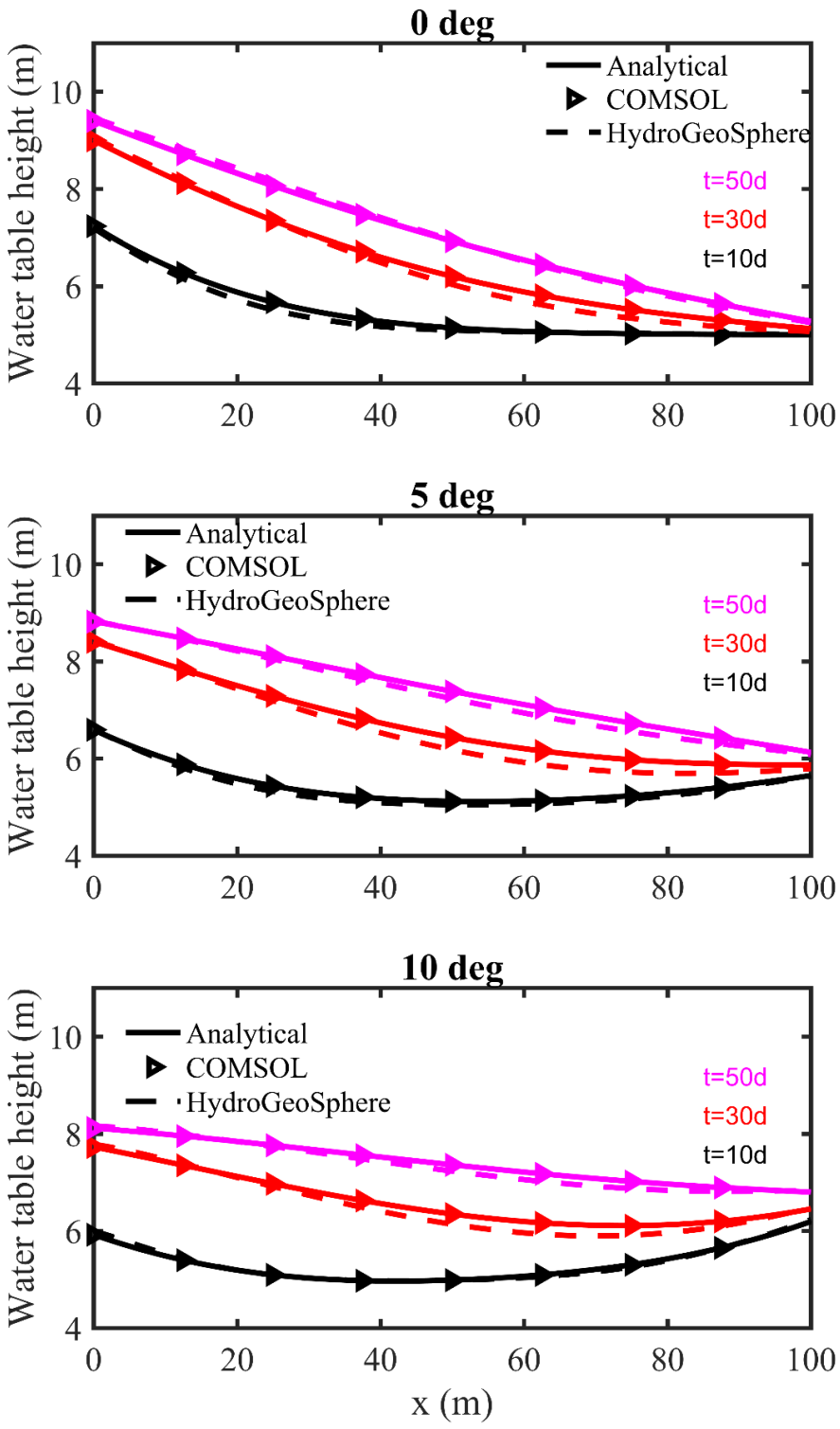

Fig. 3-3 Comparison of water table heights above he impermeable bed at *t*=10, 30 and 50 d for a horizontal aquifer, a 5° sloping aquifer, and a 10° sloping aquifer among analytical solution, numerical solutions of COMSOL and HydroGeoSphere.

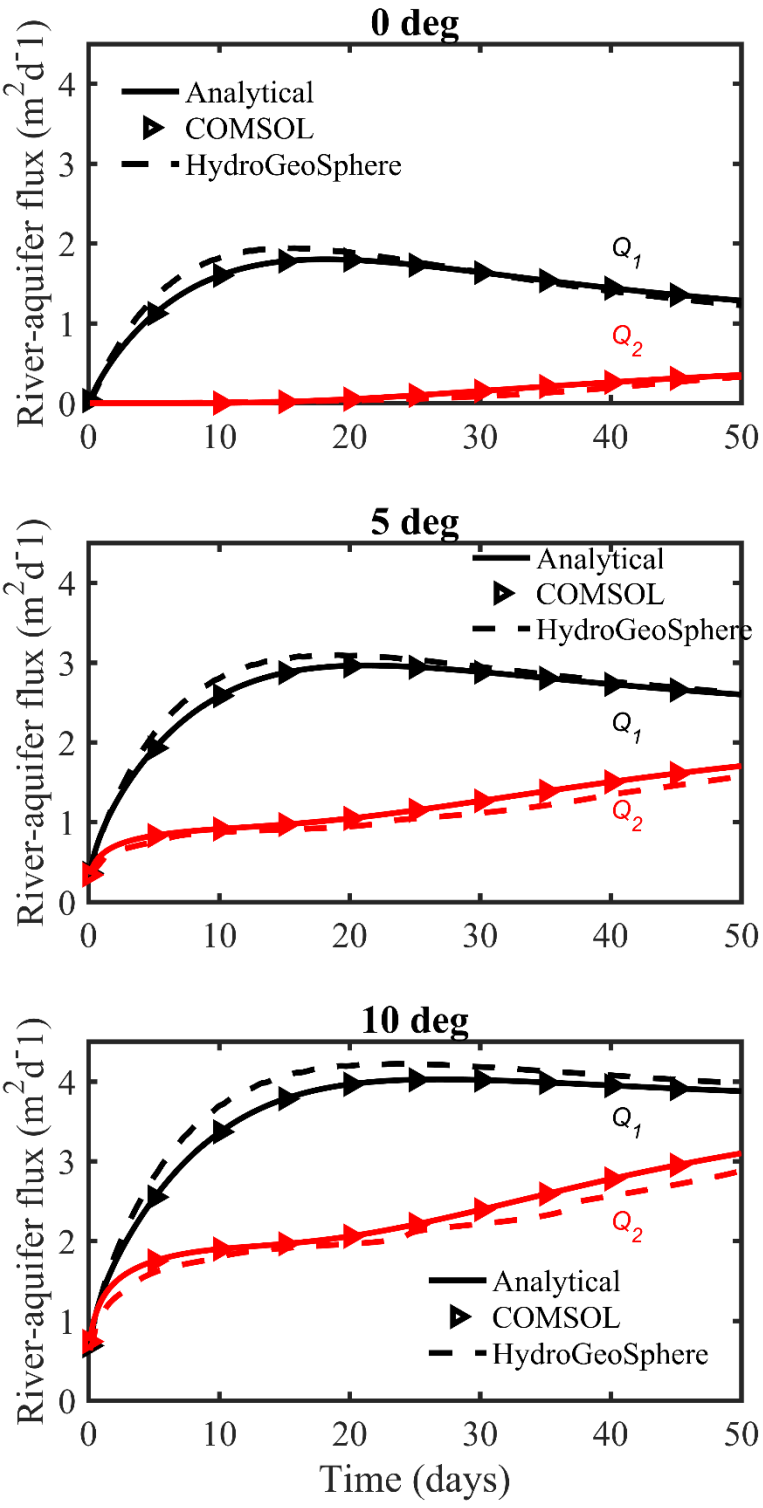

Fig. 3-4 Comparison of river-aquifer fluxes at the left and right rivers in a horizontal aquifer, a 5° sloping aquifer, and a 10° sloping aquifer among analytical solution, numerical solutions of COMSOL and HydroGeoSphere.

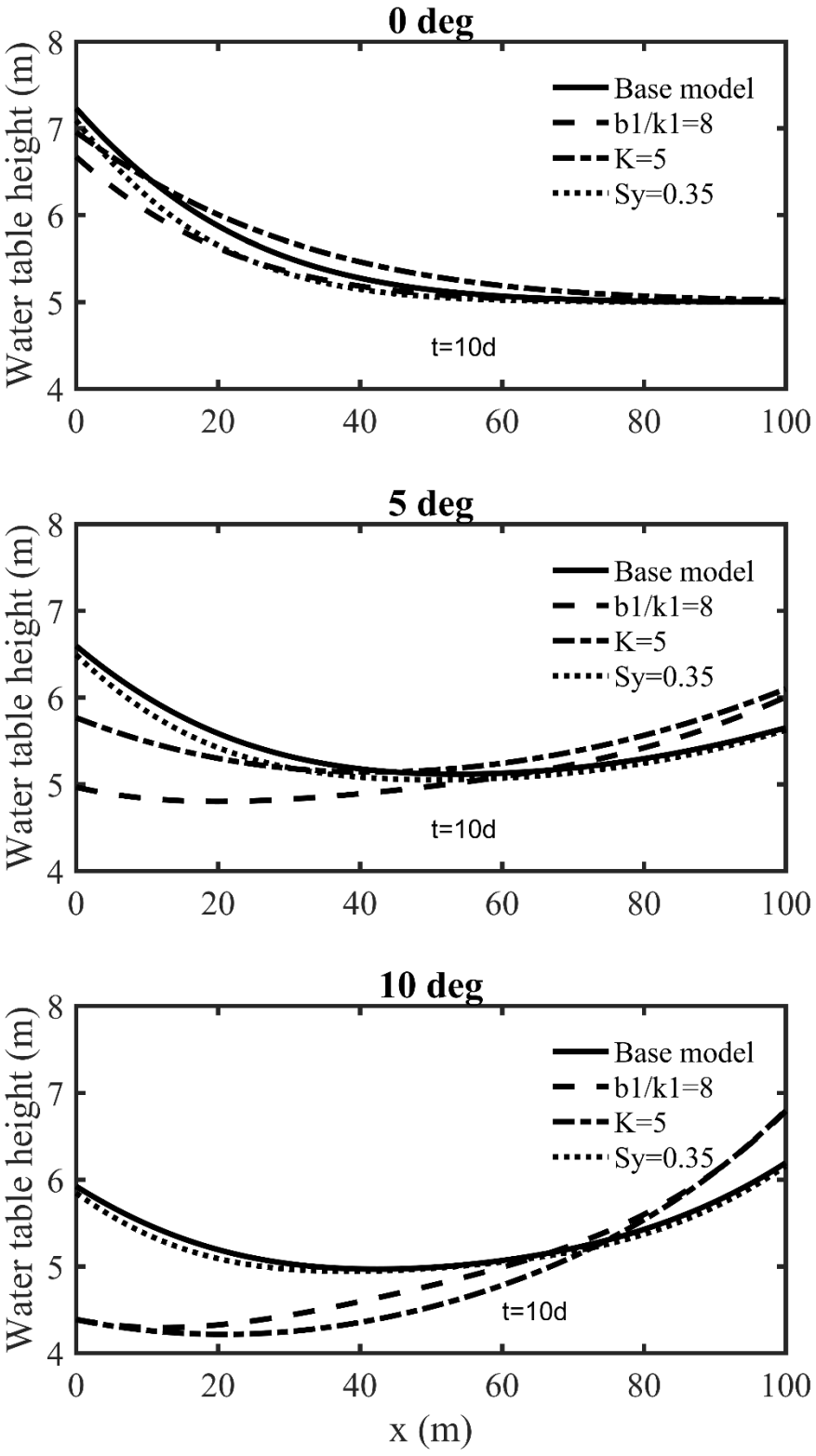

Fig. 3-5 Analysis of parameter impacts on water table heights above the impermeable bed in a horizontal aquifer, a 5° sloping aquifer, and a 10° sloping aquifer at *t*=10 d.

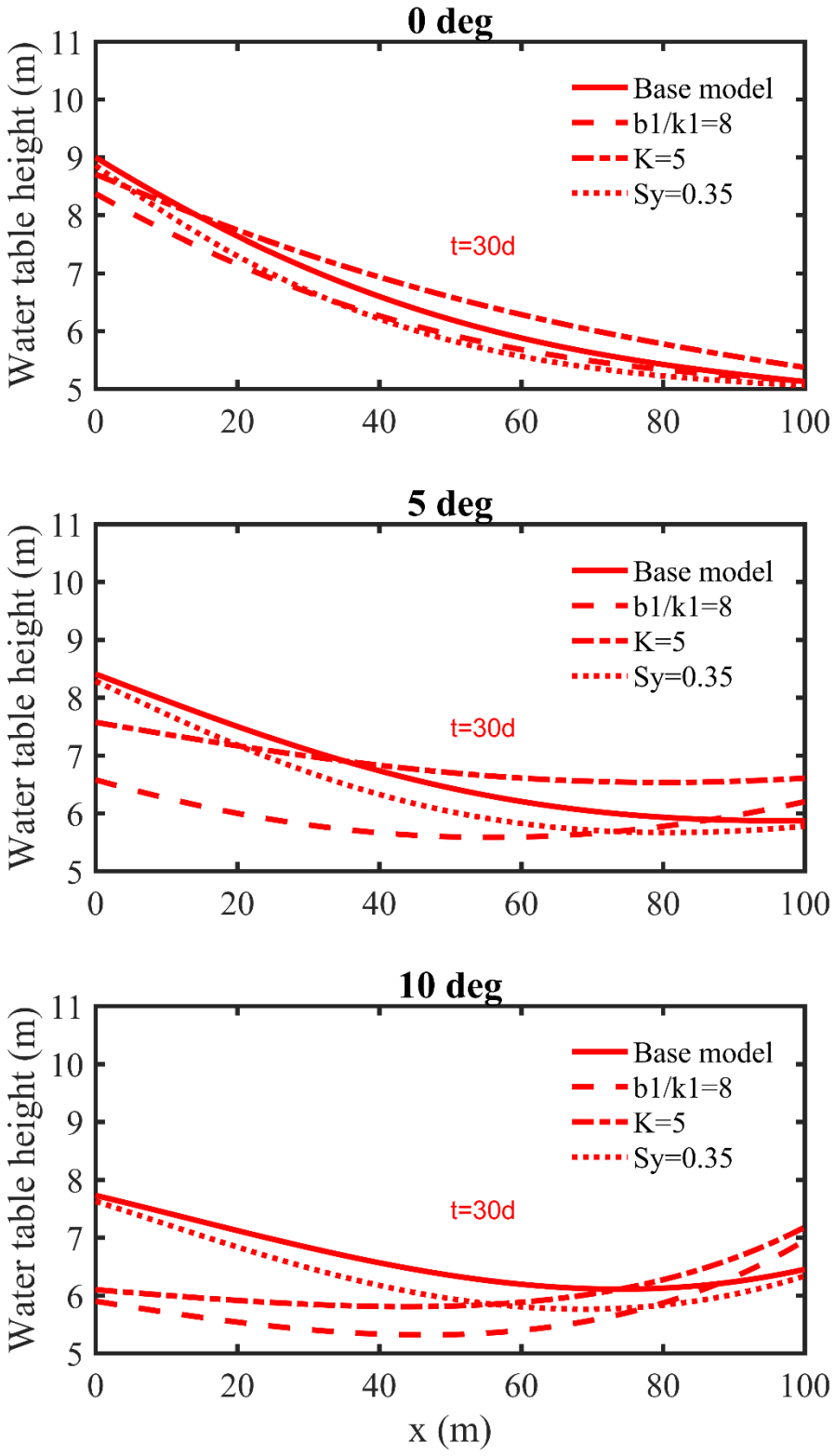

Fig. 3-6 Analysis of parameter impacts on water table heights above the impermeable bed in a horizontal aquifer, a 5° sloping aquifer, and a 10° sloping aquifer at *t*=30 d.

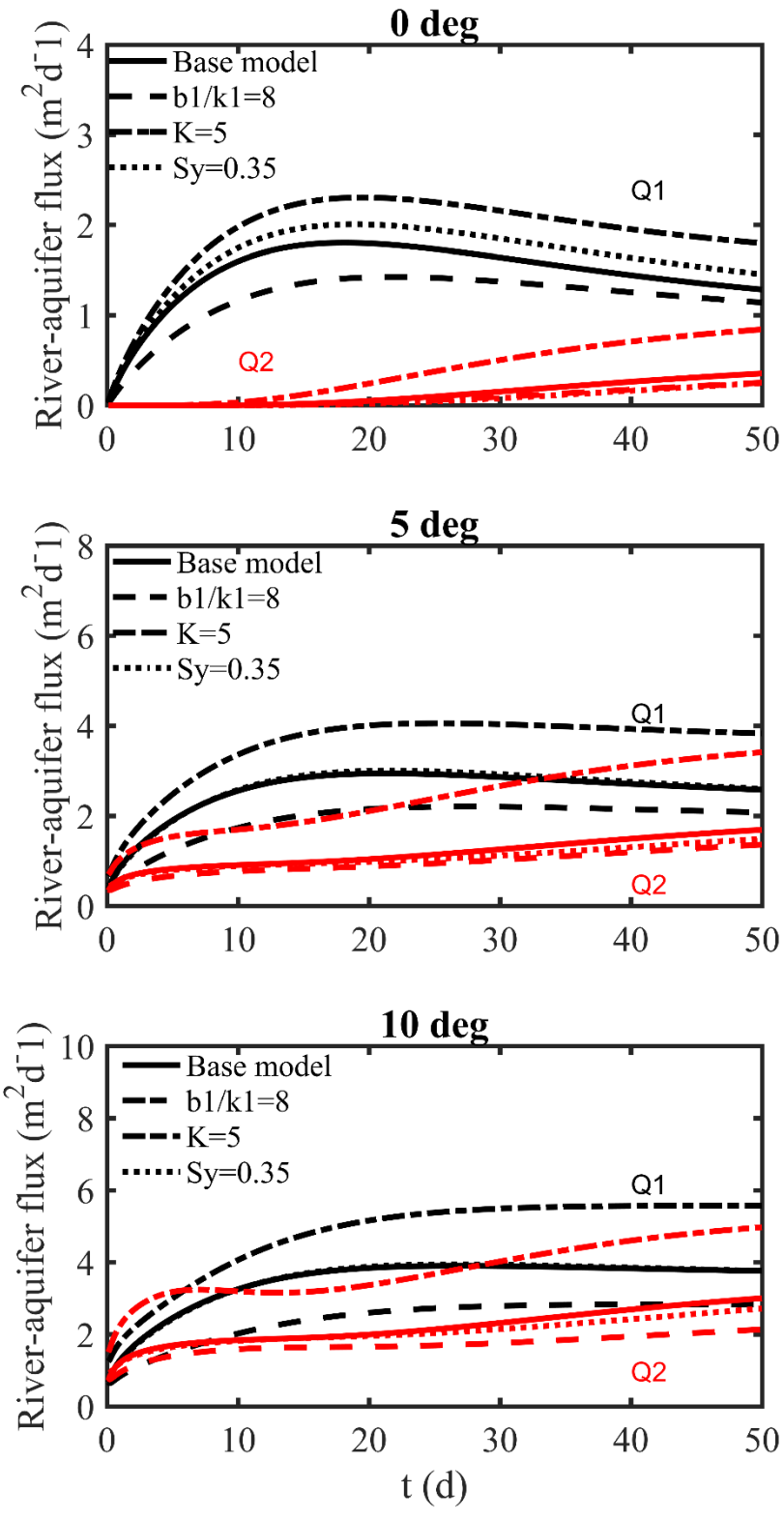

Fig. 3-7 Analysis of parameter impacts on river-aquifer fluxes at the left and right rivers in a horizontal aquifer, a 5° sloping aquifer, and a 10° sloping aquifer.

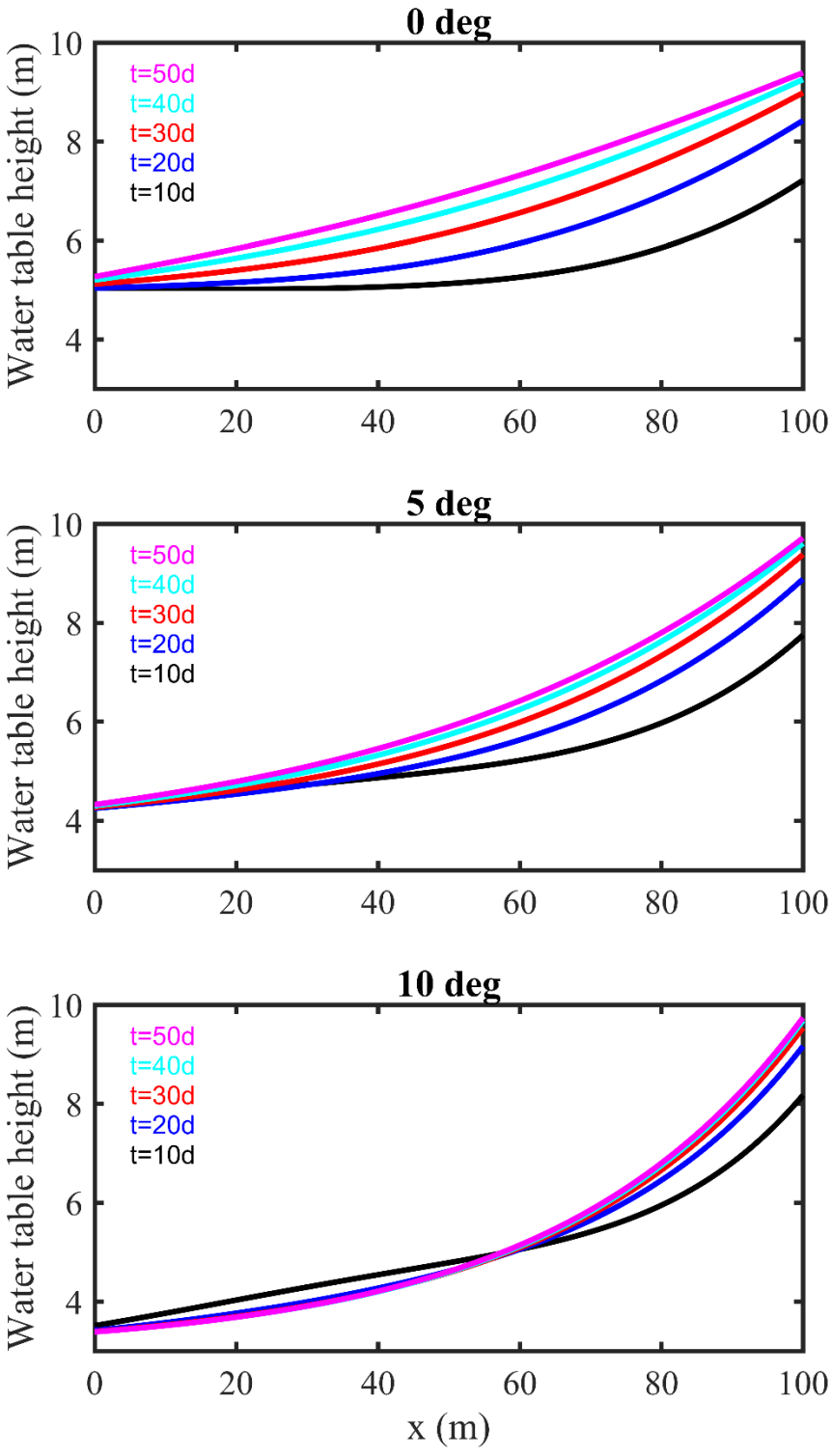

Fig. 3-8 Comparison of water table heights above the impermeable bed at *t*=10, 20, 30, 40 and 50 d in a horizontal aquifer, a 5° sloping aquifer, and a 10° sloping aquifer with a constant stage of left river (river 1) and a rising stage of right river (river 2).

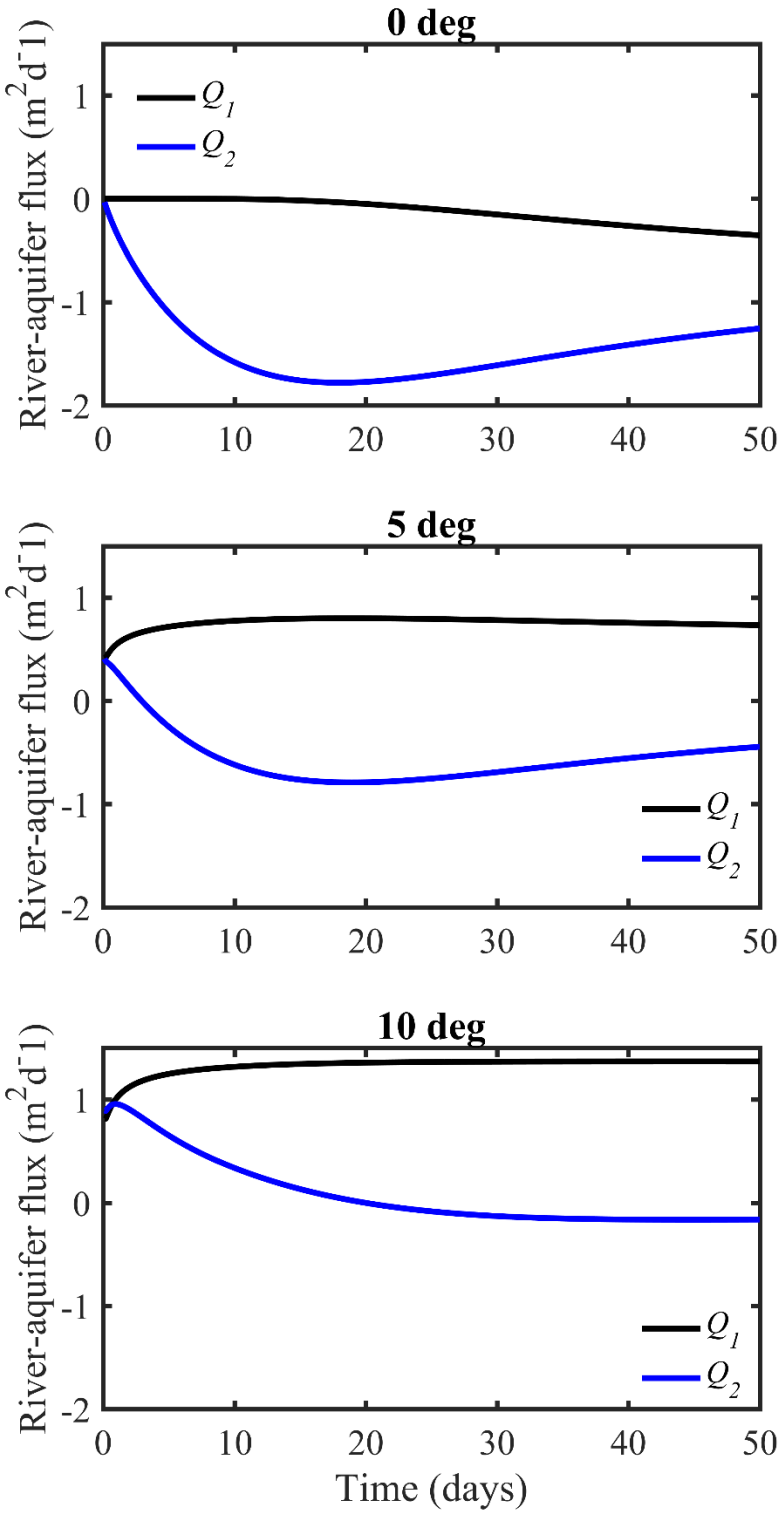

Fig. 3-9 Comparison of river-aquifer fluxes at the left and right rivers in a horizontal aquifer, a 5° sloping aquifer, and a 10° sloping aquifer with a constant stage of left river (river 1) and a rising stage of right river (river 2).

3.3.4 Responses of recharge to groundwater table and river-aquifer fluxes

In this section, we will investigate the influences of infiltrated recharge (or recharge for simplicity), $W(t)$, on water table height and river-aquifer flux for sloping aquifers with different sloping angles of 0°, 5°, and 10°. The analytical model developed in this study allow the recharge to change with time using any prescribed functions. The model setup is exactly the same as in section 3.31 with the recharges of 20 mm/day on the 10^{th} day and 40 mm/day on the 20^{th} day. Fig. 3-10 and Fig. 3-11 present the responses of water table heights at x=20, 50 and 80 m, and river-aquifer fluxes for three different aquifers with sloping angles of 0°, 5°, and 10°. The results without recharge events (the base model) are also included as references in Fig. 3-10 and Fig. 3-11. A few observations can be made from Fig. 3-10 and Fig. 3-11.

First, in general, the two recharge events have relatively minor impacts on both the water table heights and river-aquifer fluxes. They will generate a minor and temporary jump of water table heights during the recharge period, but will not affect the overall water table distribution. Such a temporary jump of water table heights will result in a small (but noticeable) and temporary drop of the river-aquifer flux at the left river (Q_1) and a small and noticeable temporary increase of the river-aquifer flux at the right river (Q_2). Second, the impact of recharge on the overall behavior of water table heights and river-aquifer fluxes appears to be less sensitive to the sloping angle. This is very different from what has been seen in sections 3.3.1 and 3.3.2, in which the degree of sloping affects the hydrodynamic behavior quite significantly. Third, the impacts of the first recharge event (20 mm/day on the 10^{th} day) are barely noticeable in Fig. 3-10 and Fig. 3-11, as compared to the stronger recharge event of 40 mm/day. This also implies that

sporadic and relatively low strength recharge event will play a much minor role in the system investigated here. However, long-term and sustainable recharge events will affect both water table profile and river-aquifer fluxes to much greater extent.

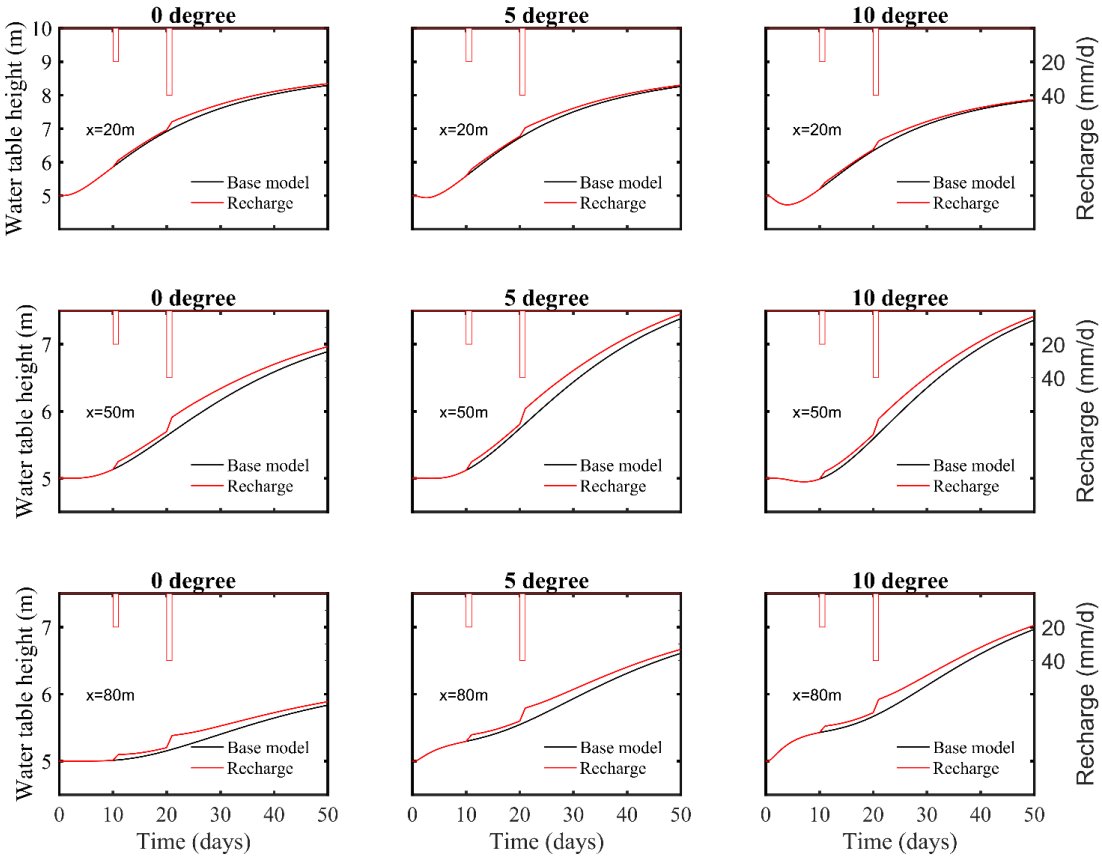

Fig. 3-10 Impact of infiltrated recharge on water table heights above the impermeable base at x=50 m in a horizontal aquifer, a 5° sloping aquifer, and a 10° sloping aquifer.

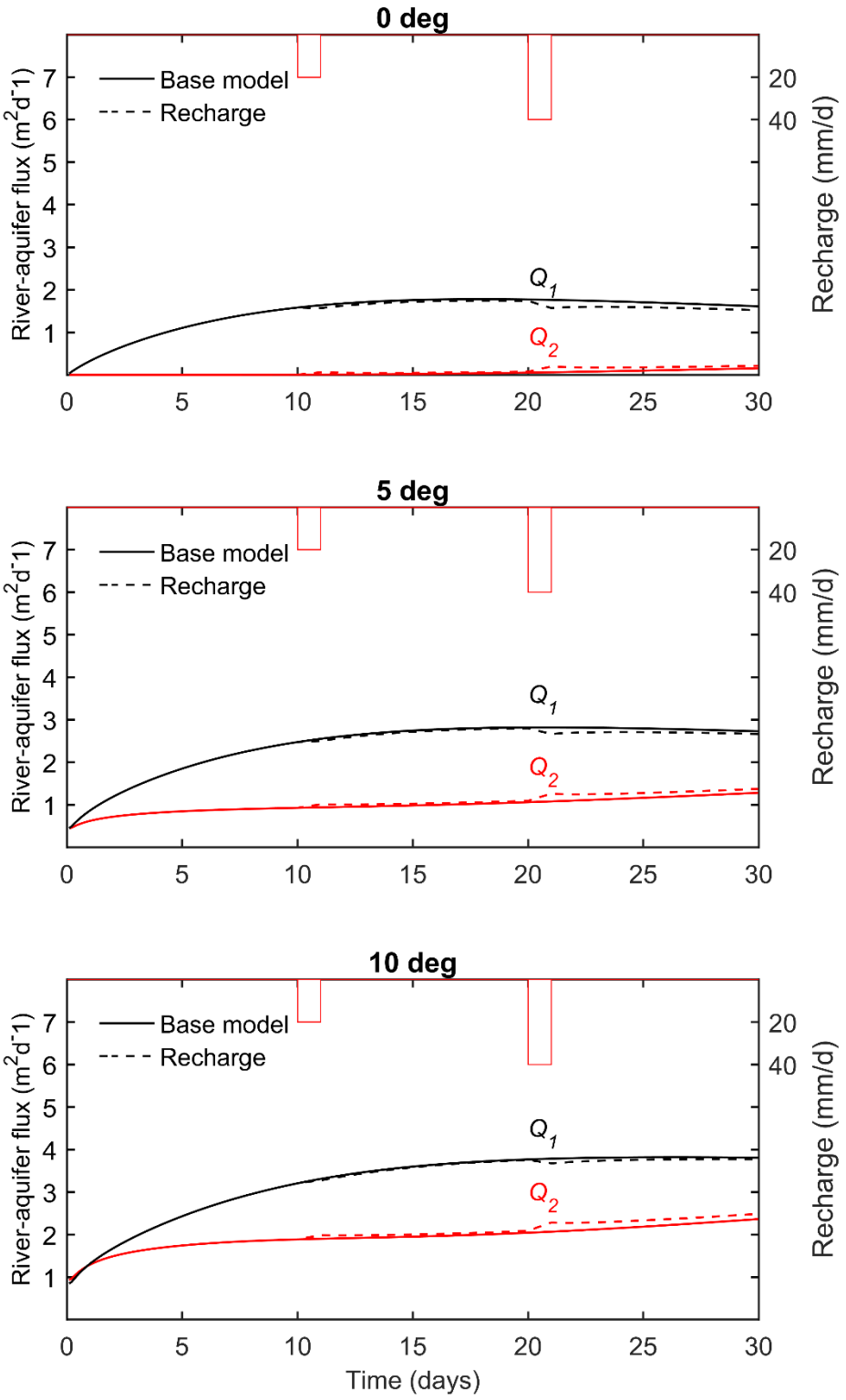

Fig. 3-11 Impact of infiltrated recharges on river-aquifer fluxes at the left and right rivers in a horizontal aquifer, a 5° sloping aquifer, and a 10° sloping aquifer.

3.4 Conclusions

In this chapter, groundwater flow in an unconfined sloping aquifer bounded by two parallel rivers with the presence of two less permeable river beds (or clogging layers) is studied in some great details. The analytical solution is first compared with a finite-element program of COMSOL for various cases, also based on the same linearized modified Boussinesq equation as the analytical solution. We conclude the analytical solution agrees very well with the COMSOL solution, thus provides evidence for the reliability of the new analytical solutions. After this test, the analytical solution is compared with a full scale numerical model using HydroGeoSphere which considers the coupled unsaturated and saturated flow process. Such a comparison is aimed at checking the robustness of the linearization of the Boussinesq equation modified for a sloping aquifer and also the problem of neglecting the unsaturated flow process. Out results show that the linearized analytical solution can serve as a reliable and reasonably well approximation if the sloping angle is less than 10°.

The flow character of a sloping aquifer is quite different from that of a horizontal aquifer. The variations of river stages (either on the left or right boundary of the aquifer) will cause much more variations of water table heights and river-aquifer fluxes in a sloping aquifer. In particular, the water table profile in a sloping aquifer shows some unique features that has never been seen in a horizontal aquifer. For instance, the water table profile may evolve from a straight line parallel with the sloping bed at the beginning to a convex shape, even without any recharge/evaporation.

Different hydraulic parameters may cause different influences on water table evolution and river-aquifer fluxes in a sloping aquifer, and such influences are more

complex in a sloping aquifer than those observed in a horizontal aquifer. The increased hydraulic conductivity of aquifer will increase river-aquifer fluxes, and it will increase the water table heights near the down-slope river and decrease the water table height on up-slope river. The impact from increased hydraulic conductivity gets stronger when the sloping angle becomes larger.

The increased hydraulic resistance (or the inverse of hydraulic conductance) of the clogging layer will suppress the river-aquifer fluxes and water table evolution.

Sporadic recharge events only create short-term minor jump on the water table profile, and in general does not affect the overall evolution of water table profile and river-aquifer fluxes. The influence of sporadic recharge events also does not appear to be sensitive to the sloping angle of aquifer. However, such a conclusion may not hold for long-term recharge events with significant amount of recharge.

CHAPTER 4

A NEW METHOD OF TRANSIENT GROUNDWATER FLOW IN A SLOPING AQUIFER

4.1 Introduction

In chapters 2 and 3, we have investigated transient groundwater flow in a sloping aquifer with a fully penetrating river in presence of a vertical clogging layer. We have studied the water table heights fluctuation and river-aquifer flux with a constant stage in section 2.3.4. The results show that the initial condition used is probably unsustainable (albeit it is convenient for the analytical modeling), as the water table heights change rapidly at the beginning of time. In a real river-aquifer environment, when the stage of river does not fluctuate, and there no precipitation over a long period of time and without human activity, it is impossible to have the initial condition as that used in chapters 2 and 3 (i.e. a constant water table height above the impermeable base of a sloping aquifer). For such a case, the water table usually approximates its steady state. This implies that the general setting of initial condition in chapters 2 and 3 is too ideal to deal with the realistic problem. Now the question is: what is the realistic initial condition to use in a sloping unconfined aquifer? In this chapter, we will develop a new method to investigate resolve the initial condition issue and also discuss its application. A key of this new method is to simulate a river stage variation that includes two phases: 1) a phase with a relatively long time of nearly stable river stage to allow the system of investigated reaches its pseudo-steady state; 2) a rapidly rising phase to simulate the rise of the river. A third phase that describes the declining of the river stage can also add into the analysis after the second

phase, if necessary. The third phase can be straightforwardly handled on the basis of the first and second phases.

4.2 Mathematical model

The coordinate system and the basic model is the same as that in section 2.2. We study a sloping aquifer with a river on one side and semi-infinite on the other side with water infiltrated recharge in Fig. 2-1.

First, to mimic the time-series of river stages, we need to search for a suitable function to describe it. Based on a trial-and-error process for fitting the realistic water stage data collected by U.S. Geological Survey (USGS) at a number of sites (with details given below), we find that sigmoid functions are suitable candidates to describe the stage of river. The sigmoid function is usually used in artificial neural networks in hydrology (Imrie et al., 2000). Other functions of river stages used in previous investigations include harmonic functions and exponential functions (Teloglou and Bansal, 2012; Van Der Valk, 2005). Although these two types of functions can describe the stage of river in a few special cases, they are incapable of describing the phase 1 and phase 2 outlined above in the introduction, thus are not recommended for this study. Nevertheless, the river stage in this chapter consists of the summations of a sequence of sigmoid functions

$$h_s(t) = h_f - (h_f - h_i)\left(\sum_{k=1}^{n} \frac{p_k}{(1+\exp(a_k(t-c_k)))}\right) \quad (4\text{-}1)$$

where $h_s(\mathrm{t})$ is the time-varying stage for river, h_f is the highest stage value of river in the studied period, h_i is the initial stage for river. In Eq. (4-1), a_k [T^{-1}], p_k [dimensionless] and c_k [T] are all fitting parameters. The parameter n is a number relate to the stage of river. The range of a basic sigmoid function $f(x) = 1/(1+\exp(-x))$ is from 0 to 1. By

adjusting the values of a_k, p_k and c_k, Eq. (4-1) can simulate a wide range of possible river stages encountered in real-world setting. For instance, Fig. 4-1 and Fig. 4-2 present two comparisons between the fitted curves by Eq. (4-1) and real stages for a river and a lake. The locations of lake and river are Clear Lake in Lakeport, CA (USGS database, site numbers of 11450000) and Braden River in Lakewood Ranch, FL (USGS database, site numbers of 02300033), respectively. The period of 0 day to 72 days is corresponding to the date of 10/18/2012 to 12/29/2012 in Fig. 4-1. The period of 0 day to 23 days is corresponding to the date of 05/02/2018 to 05/25/2018 in Fig. 4-2. It is easy to see that Eq. (4-1) can describe the stage of surface water greatly. The curve function of Fig. 4-1 is $h_s = 1.731 - 1.341 * \{0.516/[1 + \exp\big(0.603(t - 45)\big)] + 0.5/[1 + \exp(t - 66)]\}$. The determination of coefficient R^2 for the fitting using above function is 0.997. The curve function of Fig. 4-2 is $h_s = 6.197 - 3 * \{\frac{0.167}{[1+\exp(t-12)]} + \frac{0.833}{[1+\exp\big(5(t-17.8)\big)]} + 0.377/[1 + \exp\big(-9(t - 19.5)\big)] + 0.355/[1 + \exp\big(-5(t - 2)\big)]\}$. The determination of coefficient R^2 for the fitting using above function is 0.961. The values of R^2 for both cases are close to 1.0, suggesting the satisfactory of fitting.

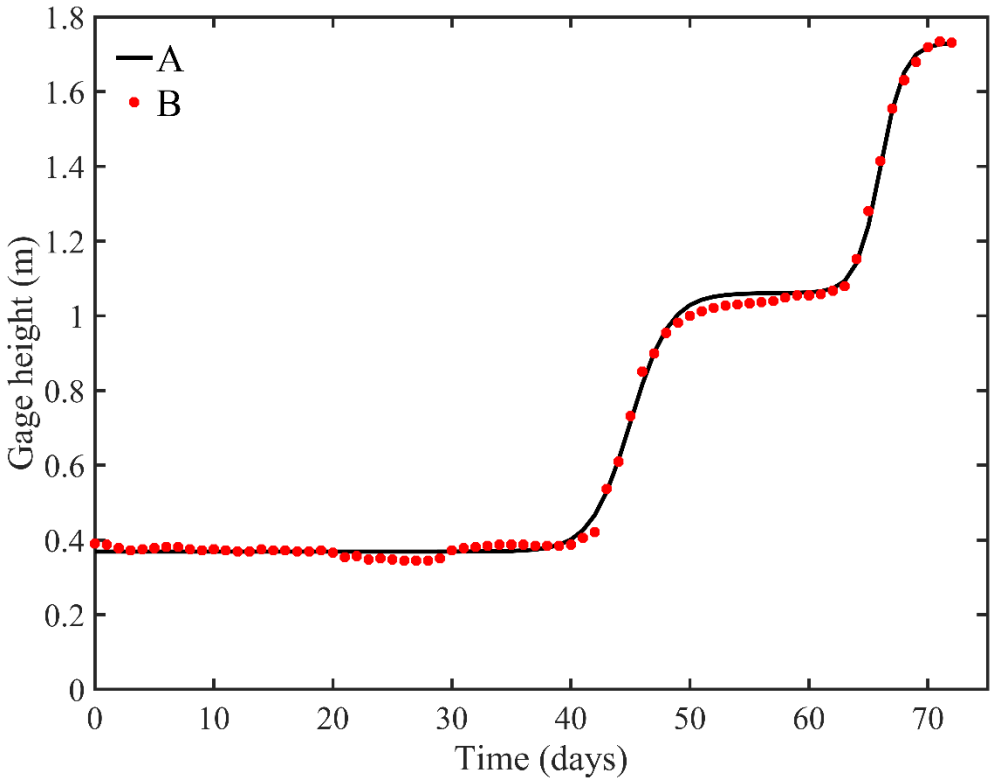

Fig. 4-1 A comparison of observed stages and simulated curve by Eq. (1) of Clear Lake in Lakeport, CA.

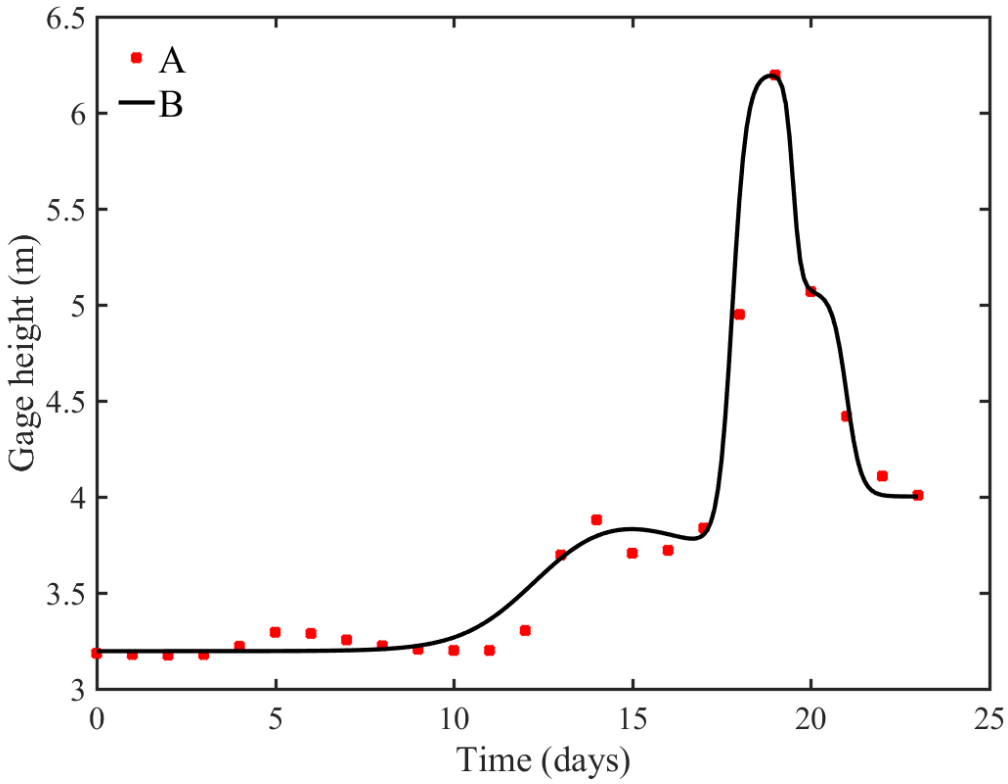

Fig. 4-2 A comparison of observed stages and simulated curve by Eq. (1) of Braden River in Lakewood Ranch, FL

When we study water flow in a sloping aquifer, we can set the stage of river constant at the beginning. After the groundwater reaches its pseudo-steady state after a long period of time, the stage of river stage starts to rise or fall. We can then investigate the water table response of such a rising or falling river stage. For this purpose, we may only need one sigmoid function in above Eq. (4-1) by allowing n=1 and p_1=1, and then adjust the values of a_1 and c_1 to fit the rising (or falling) river stage. An example is shown in Fig. 4-

3 below.

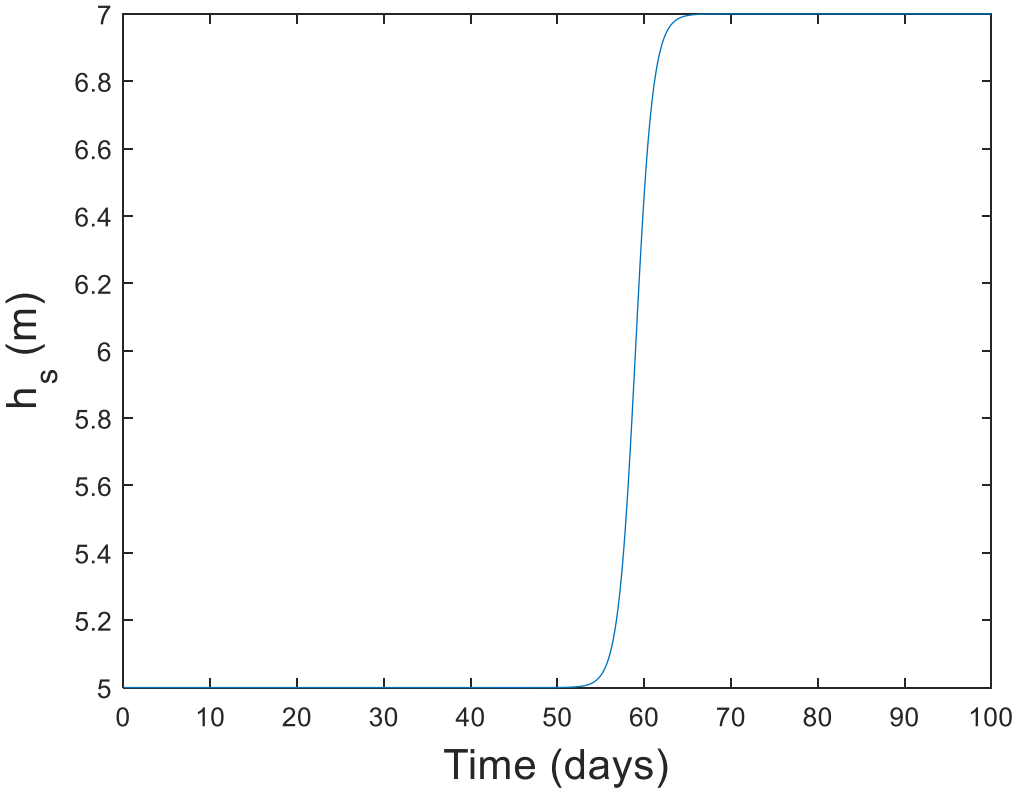

Fig. 4-3 The stage of river changes by Eq. (4-1) with a_1=1 d^{-1}, n=1, p_1=1 and c_1=59 d.

In Fig. 4-3, we set a_1=1 d^{-1}, n=1, p_1=1 and c_1=59 d. The stage of river is constant at 5 m from t=0 d to t=50 d, and then increases from 5 m to 7 m in a period of t=50 d to t=66 d. Be aware that the vertical axis in Fig. 4-3 starts from 5 m (not zero), and the stage of river at t=50 d is 5.002 m, the stage of river at t=66 d is 6.998 m. The time from t=0 d to t=50 d (with almost no change of river stage) in Fig. 4-3 is mostly for the system of investigated to reach its pseudo-steady state.

Based on Eqs. (2-1) to (2-5) in section 2.2 and Eq. (4-1), Eqs. (4-2a) to (4-2c) are obtained below.

$$h(x, t = 0) = h_i \tag{4-2a}$$

$$-Kh(x = 0^+, t)[(\frac{\partial h}{\partial x})_{x=0} - tan\theta] = -kh(x = 0^+, t)\frac{h(x=0^+,t)-h_s(t)}{b} \tag{4-2b}$$

$$\frac{\partial h}{\partial x}_{x=L} = 0 \tag{4-2c}$$

The Eq. (4-2a) represents the initial water table heights are h_i. The equation of the boundary condition at interface between the vertical clogging layer and aquifer is obtained in Eq. (4-2b). The right side of Eq. (4-2b) represents the flow rates in the clogging layers. The left sides of Eq. (4-2b) represents the flow rate at the interface between the clogging layer and aquifer. The Eq. (4-2c) means that the water table heights do not vary with the horizontal distance at the very long location x=L m.

Defining the following dimensionless terms, $h_D = \frac{h-h_i}{h_f-h_i}$, $x_D = \frac{x}{L}$, $t_D = \frac{Kh_a cos^2\theta t}{S_y L^2}$, $\alpha = \frac{Ltan\theta}{h_a}$, $W(t_D) = \frac{L^2 W(t)}{(h_f-h_i)Kh_a cos^2\theta}$, $R = \frac{Kb}{kL}$, $a_{kD} = \frac{S_y L^2 a_k}{Kh_a cos^2\theta}$, $c_{kD} = \frac{Kh_a cos^2\theta c_k}{S_y L^2}$, $m = \frac{Kbtan\theta}{(h_f-h_i)}$, $f_n = \sum_{k=1}^{n} \frac{p_k}{(1+\exp(a_{kD}(t_D-c_{kD})))}$, the dimensionless forms of Eq. (2-4) and Eqs. (4-2a) to (4-2c) are presented as below.

$$\frac{\partial^2 h_D}{\partial {x_D}^2} - \alpha\frac{\partial h_D}{\partial x_D} + W(t_D) = \frac{\partial h_D}{\partial t_D} \tag{4-3}$$

$$h_D(x_D, t_D = 0) = 0 \tag{4-4a}$$

$$R(\frac{\partial h_D}{\partial x_D})_{x_D=0} = h_D(x_D = 0^+, t_D) + f_n - 1 + m \tag{4-4b}$$

$$(\frac{\partial h}{\partial x_D})_{x_D=1} = 0 \tag{4-4c}$$

Define a new parameter $\varphi = h_D e^{-\frac{\alpha x_D}{2}}$, above four equations are changed to

$$\frac{\partial^2\varphi}{\partial {x_D}^2} - \frac{\alpha^2\varphi}{4} + e^{-\frac{\alpha x_D}{2}} W(t_D) = \frac{\partial\varphi}{\partial t_D} \tag{4-5a}$$

$$\varphi(x_D, t_D = 0) = 0 \tag{4-5b}$$

$$[R_1 \frac{\partial\varphi}{\partial x_D} + \left(\frac{R\alpha}{2} - 1\right)\varphi]|_{x_D=0} = f_n - 1 + m \tag{4-5c}$$

$$(\frac{\partial\varphi}{\partial x_D} + \frac{\alpha}{2}\varphi)|_{x_D=1} = 0 \tag{4-5d}$$

We need to point out that the derived procedures from Eq. (4-6a) to Eq. (18) is similar to those in section 2.2. However, as a very different equation is used to describe the more realistic river stage here, we like to document the derivation details in the following for the sake of completeness. The PDE of Eq. (4-5a) can be transformed into an ordinary different equation (ODE) by eliminating the *x* terms using an Integral transform method. The Integral transform of $\varphi(x_D, t_D)$ is defined as Eq. (4-6a) and the corresponding inversion formula is defined as Eq. (4-6b).

$$\bar{\varphi}(\omega_n, t_D) = \int_0^1 \varphi(x_D, t_D)\, K(\omega_n, x_D) dx_D \tag{4-6a}$$

$$\varphi(x_D, t_D) = \sum_{n=0}^{\infty} K(\omega_n, x_D)\, \bar{\varphi}(\omega_n, t_D) \tag{4-6b}$$

where $K(\omega_n, x_D)$ and ω_n are transform kernel and eigenvalue, respectively. The kernel $K(\omega_n, x_D)$ is the normalized eigenfunction of the following eigenvalue problem.

$$\frac{d^2k}{d{x_D}^2} + \omega_n^2 k = 0 \tag{4-7}$$

$$\left[\frac{\partial k}{\partial x_D} + \left(\frac{\alpha}{2} - \frac{1}{R_1}\right)k\right]|_{x_D=0} = 0 \tag{4-8a}$$

$$(\frac{\partial k}{\partial x_D} + \frac{\alpha}{2}k)|_{x_D=1} = 0 \tag{4-8b}$$

The kernel $K(\omega_n, x_D)$ is defined as

$$K(\omega_n, x_D) = A_n k(\omega_n, x_D) = A_n[\omega_n \cos(\omega_n x_D) + \left(\frac{1}{R} - \frac{\alpha}{2}\right) \sin(\omega_n x_D)] \tag{4-9}$$

where it has

$$A_n = \frac{\sqrt{2}}{\sqrt{\left[\omega_n^2 + (\frac{1}{R} - \frac{\alpha}{2})^2\right](1 + \frac{\frac{\alpha}{2}}{\omega_n^2 + \frac{1}{4}\alpha^2}) + \frac{1}{R} - \frac{\alpha}{2}}} \tag{4-10}$$

Taking integral transform on Eq. (4-5a) leads to

$$\int_0^1 K(\omega_n, x_D) e^{-\frac{\alpha x_D}{2}} W(t_D)\, dx_D + \int_0^1 K(\omega_n, x_D) \frac{\partial^2 \varphi}{\partial {x_D}^2} dx_D = \int_0^1 K(\omega_n, x_D) \frac{\partial \varphi}{\partial t_D} dx_D +$$

$$\alpha^2/4 \int_0^1 K(\omega_n, x_D) \varphi(x_D, t_D)\, dx_D \tag{4-11}$$

Based on function Green's theorem, the left side of Eq. (4-11) can be written as:

$$\int_0^1 K(\omega_n, x_D) e^{-\frac{\alpha x_D}{2}} W(t_D)\, dx_D + \int_0^1 K(\omega_n, x_D) \frac{\partial^2 \varphi}{\partial {x_D}^2} dx_D =$$

$$\int_0^1 K(\omega_n, x_D) e^{-\frac{\alpha x_D}{2}} W(t_D)\, dx_D - \omega_n^2 \bar{\varphi} - \frac{K_{x_D=0}(f_n - 1 + m)}{R} \tag{4-12}$$

Substituting Eqs. (4-6a), (4-8a), (4-8b) and (4-12) into Eq. (4-11), defining $\beta_n = \omega_n^2 + \alpha^2/4$, one has

$$\frac{\partial \bar{\varphi}}{\partial t_D} + \beta_n \bar{\varphi} = -\frac{K_{x_D=0}(f_n - 1 + m)}{R} + \frac{A_n}{\beta_n} W(t_D) \left\{ e^{-\frac{\alpha}{2}} \left[\beta_n \sin(\omega_n) - \frac{1}{R} \left(\frac{\alpha}{2} \sin(\omega_n) + \right. \right. \right.$$

$$\left. \left. \left. \omega_n \cos(\omega_n) \right) \right] + \frac{\omega_n}{R} \right\} \tag{4-13a}$$

$$\bar{\varphi}(0) = 0 \tag{4-13b}$$

Rearranging Eq. (4-13a) yield as

$$\frac{\partial \bar{\varphi}}{\partial t_D} + \beta_n \bar{\varphi} = B(t_D) \tag{4-14}$$

where

$$B(t_D) = -\frac{K_{x_D=0}(f_n - 1 + \mathrm{m})}{R} + \frac{A_n}{\beta_n} W(t_D) \left\{ e^{-\frac{\alpha}{2}} \left[\beta_n \sin(\omega_n) - \frac{1}{R_1} \left(\frac{\alpha}{2} \sin(\omega_n) + \omega_n \cos(\omega_n) \right) \right] + \frac{\omega_n}{R} \right\}$$

The solution of Eq. (19) subject to Eq. (18b) can be straightway obtained as

$$\bar{\varphi}(\omega_n, t_D) = \exp(-\beta_n t_D) \int_0^{t_D} B(t) \exp(\beta_n t)\, dt \tag{4-15}$$

Defining $\xi_1 = -\frac{1-m}{\beta_n}$,

$\xi_2 = \frac{1-\mathrm{m}}{\beta_n}$,

$$\xi_3 = \frac{A_n}{\beta_n} \left\{ e^{-\frac{\alpha}{2}} \left[\beta_n \sin(\omega_n) - \frac{1}{R} \left(\frac{\alpha}{2} \sin(\omega_n) + \omega_n \cos(\omega_n) \right) \right] + \frac{\omega_n}{R} \right\},$$

one obtains

$$\bar{\varphi}(\omega_n, t_D) = -\frac{A_n \omega_n}{R} [\quad_1 + \xi_2 \exp(-\beta_n t_D) + \int_0^{t_D} \exp(\beta_n (t - t_D)) f_n\, dt] - \xi_3 \exp(-\beta_n t_D) \int_0^{t_D} W(t_D) \exp(\beta_n t)\, dt \tag{4-16}$$

Substituting Eq. (4-16) into Eq. (11b), it has

$$\varphi(x_D, t_D) = \sum_{n=0}^{\infty} K(\omega_n, x_D) \left\{ -\frac{A_n \omega_n}{R} [\xi_1 + \xi_2 \exp(-\beta_n t_D) + \int_0^{t_D} \exp(\beta_n (t - t_D)) f_n\, dt] - \xi_3 \exp(-\beta_n t_D) \int_0^{t_D} W(t_D) \exp(\beta_n t)\, dt \right\} \tag{4-17}$$

The final solution (in dimensionless form) can be obtained by transformation.

$$h_D(x_D, t_D) = \varphi(x_D, t_D)\exp(\alpha x_D/2) \quad (4\text{-}18)$$

Eq. (4-18) serves as the working equation for computing the water table heights above the impermeable base at any given location and time with the more realistic river stage function. When the water table height is obtained, the river-aquifer flux can be computed using the modified Darcy's law for a sloping aquifer straightforwardly. We need to point out that the " $\int_0^{t_D} \exp(\beta_n(t - t_D))f_n\, dt$ " part in Eq. (17) is impossibly integral by an analytical method. A numerical method for integral is necessary and the codes are presented in Appendix C.

4.3 Results and Discussion

4.3.1 Comparison of the new analytical solution with numerical solutions

In this section, we will compare the new analytical solution using COMSOL numerical solution. The COMSOL program is built basing on a linearized modified Boussinesq equation as Eq. (2-4), an initial condition as Eq. (4-2a), the Boundary conditions as Eq. (4-2b) and (4-2c). The hydrological setting of analytical and numerical model are shown in the following. The stage of river is same to the stage in Fig. 4-3 with h_f=7 m, h_i=5 m, n=1, a_1=1 d^{-1}, n=1, p_1=1 and c_1=59 d. The thickness of the clogging layer is set as 1 m, and the hydraulic conductivity of the clogging layer is set as 0.248 m/d. The hydraulic conductivity of the aquifer along the sloping bed is set as 2.5 m/d, the specific yield of material in aquifer is set as 0.25 and the initial water head height of aquifer is set as 5 m. The vertical recharge is set as zero for the sake of illustration. Be consistent with

previous study in section 2.3.1, a horizontal aquifer is included as a reference of comparison, a sloping aquifer with a 5° sloping angle and a sloping aquifer with a 10° sloping angle are built. The time period is 100 days.

The design of COMSOL program is briefly illustrated as follows. The boundary condition is set by Eq. (4-2b) with the setting of a_1=1 d^{-1}, n=1, p_1=1 and c_1=59 d. The horizontal length L of the aquifer is 1000 m. The horizontal grid space is 0.1 m. We need to point out that we set a similar model with L=2000 m. The water table heights are identical with L=1000 m in a range of x=0 m to x=150 m. In this section, our focus is to investigate water head heights near the river from x=0 m to x=150 m. An analysis of grid convergence is carried out in three cases of COMSOL model, and it shows that the grid spacing does not affect the results of water head heights and river-aquifer fluxes.

Fig. 4-4 presents the water table heights at x=0, 50, 100 and 150 m with a period ranging from 0 d to 100 d. It is easy to see that the results of COMSOL program agree excellently with our analytical solution. The minor difference of water table heights between analytical solution and numerical solution is from 2 mm to 6 mm, and the RPD values between the analytical solution and COMSOL numerical solution are less than 0.15%.

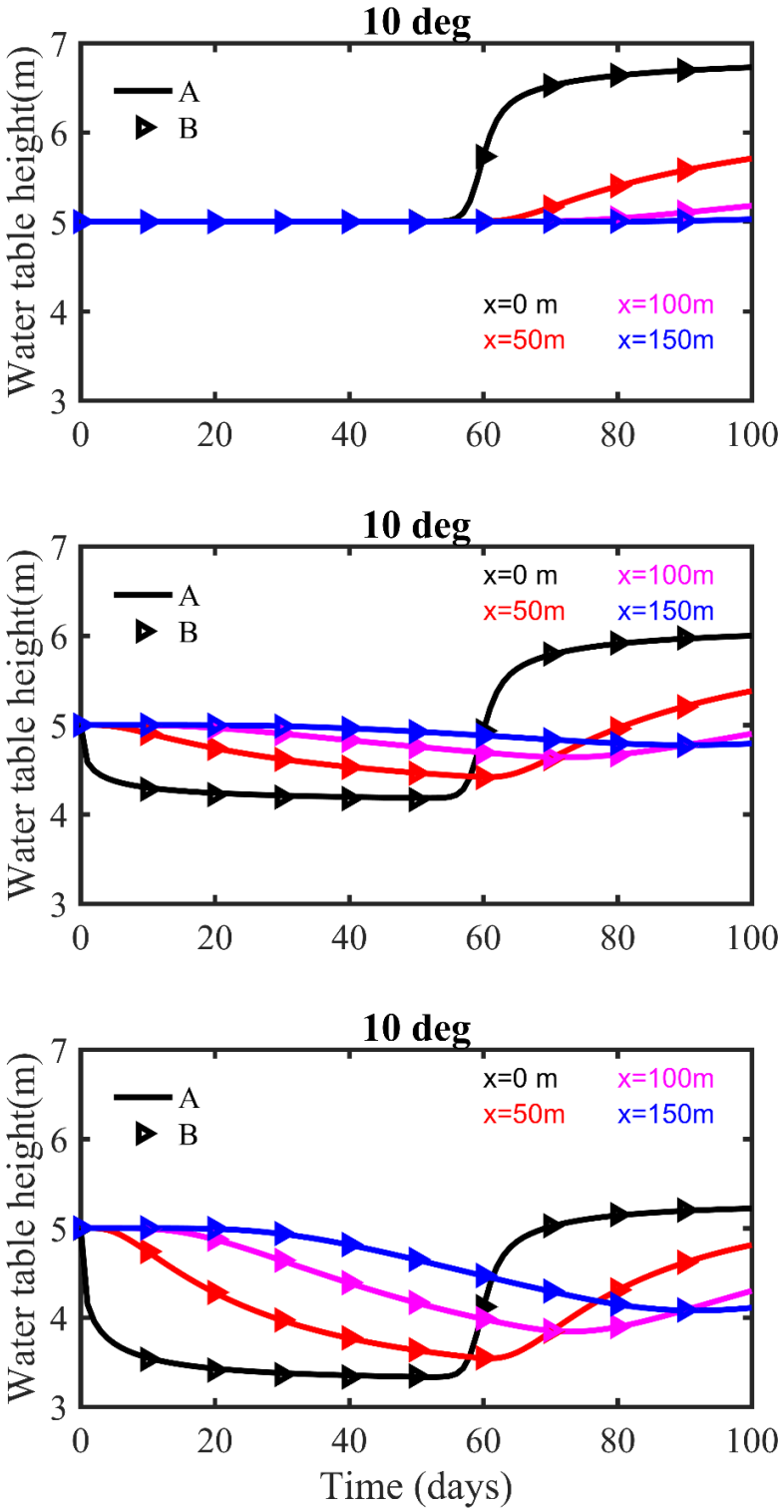

Fig. 4-4 Water table heights fluctuate with time at x=0, 50, 100 and 150 m in a horizontal aquifer, a 5° sloping aquifer, and a 10° sloping aquifer with a river changing by Eq. (4-1) with a_1=1 d^{-1} , n=1, p_1=1 and c_1=59 d.

4.3.2 Comparison of the analytical solutions with transient initial condition and steady-state initial condition

In section 4.3.1., Fig. 4-4 displays that water tables of the two sloping aquifers have not yet reach their steady-state at t=50 d. Indeed, water table height at x=150 m needs a long time to arrive at its steady state. With an attempt to obtain a steady state groundwater table in a range of x=0 m to x =150 m, we set the fitting parameter a_1=1 d^{-1}, n=1, p_1=1, c_1=1009 d and L=2000 m. These values of a_1 and c_1 will result in a much longer of time during which the river stage barely increases, thus provide more time for the system investigated to reach its pseudo-steady state. Specially, the use of a_1=1 d^{-1}, and c_1 =1009 d here represents a situation that river stage will not increase substantially until the 1000^{th} day. This is much different from the previous situation of a_1=1 d^{-1} and c_1=59 d in which river stage will not increase substantially only until the 50^{th} day. The initial and final stages of river are the same as in section 4.3.1. Fig. 4-5 presents water table heights at x=0, 50, 100 and 150 m over a 2000 days period. The stage of river is constant at 5 m in a period of t=0 d to t=1000 d, then the stage rises to 7 m from t=1000 d to t=1016 d. We need to point out that a similar model with a different aquifer length L=3000 m has been tested, the results display that the differences of water table heights at x=0 m to x=150 m are less than 2 mm between the setting of L=2000 m and L=3000 m in 2000 day period. Thus the length of 2000 m is long enough for the purpose here.

A few interesting observations can be made from Fig. (4-3). First, the water table heights are nearly identical at different locations in steady state for the two sloping aquifer cases. Second, when the sloping angle becomes smaller, the water table will requires longer time to reach steady state after variation of the river stage.

In dealing with the issue of river-aquifer system in a presence of a sloping bed, the analytical solutions in chapters 2 and 3 are limited. Figs. (4-6) to (4-9) compare water table heights obtained by a river rising at the identical groundwater initial condition h_i=5 m and at the steady-state initial condition which is similar to the water table heads in Fig. 4-5 at t=1000 d in a range of x=0 m to x=150 m at t=0, 10, 50 and 100 d. The legend A represents the results of h_i=5 m and the legend B represents the results of the steady-state initial condition. We call the result of h_i=5 m as case A and the result of the steady-state initial condition as case B. The hydrological parameters of aquifer and vertical layer are set as same as section 4.3.1. The stage of river with case B is set by Eq. (4-1) with a_1=1 d^{-1}, n=1, p_1=1, c_1=9 d, h_i=5 m, h_f=7 m. The water table heights in Fig. 4-5 reaches its pseudo-steady state at t=1000 d with the river stage of 5 m. The river stage increases quite rapidly from t=1000 d to t=1016 d. Fig. 4-6 displays the water table heights for cases A and B. Without surprise, the water table heights for cases A and B are identical for a horizontal aquifer. However, for a sloping aquifer with a 15º sloping angle, the water table height for case B is about 0.87 m higher than that for case A. For a sloping aquifer with a 10º sloping angle, the water table height for case B is about 1.72 m higher than that for case A.

Fig. 4-7 presents water table heights at t=10 d in a range of x=0 m to x=150 m. Water table heights of case A increase with the rise of river in a range of x=0 m to x=40 m for sloping aquifers. Water table heights of case B decrease with the rise of river in a range of x=0 m to x=70 m for sloping aquifers. It is seen that water table heights of case A fluctuate more rapidly than case B. The differences of water table heights between case A and case B are from 0.16 m to 0.87 m for a sloping aquifer with a 5º sloping angle. The

differences of water table heights between case A and case B are from 0.16 m to 0.87 m for a sloping aquifer with 5º sloping angle. The differences of water table heights between case A and case B are from 0.25 m to 1.72 m for a sloping aquifer with 10º sloping angle.

Fig 4-8 displays water table heights at t=50 d in a range of x=0 m to x=150 m. The differences of water table heights between case A and case B are from 0.05 m to 0.80 m for a sloping aquifer with 5º sloping angle. The differences of water table heights between case A and case B are from 0.04 m to 1.37 m for a sloping aquifer with 10º sloping angle. Fig 4-9 displays water table heights at t=100 d in a range of x=0 m to x=150 m. The differences of water table heights between case A and case B are from 0.02 m to 0.57 m for a sloping aquifer with 5º sloping angle. The differences of water table heights between case A and case B are from 0.01 m to 0.60 m for a sloping aquifer with 10º sloping angle.

Fig. 4-10 presents water table heights at x=0 m with time. Water table heights of case A and case B move closely with time and becomes essentially indistinguishable after t=40 d. Fig. 4-11 presents water table heights at x=50 m with time. After short transient stage, water table heights of case A increase at t=10 d. The period of transient stage at x=100 m is about twenty days and the period of transient stage at x=150m is about forty days in Figs. 4-12 and 4-13. It is seen that in general, the ground water table takes time to achieve steady state.

The comparison between case A and B implies that cautions should be taken for using an idealized constant initial water table heights above the impermeable base when

studying groundwater flow in an unconfined sloping aquifer. In section 4.3.4 we will discuss how to use our new method to predict ground water table in a sloping aquifer.

4.3.3 Response of peak flow to groundwater table and river-aquifer fluxes

In this section, we will investigate the influences of peak flow in a river on groundwater table height and river-aquifer flux for sloping aquifers with different sloping angles of 0°, 5°, and 10°. A river stage may vary over time after a precipitation event. Fig. 4-14 is an example of a peak flow in a river. We will use Eq. (4-1) to describe a river stage which is relatively stable from t=0 d to t=1005 d, and then rises sharply at t=1005 d to reach a peak value of h_s=10 m at t=1010 d, followed by a sharp decline limb (see Fig. 4-14). After such a spike, the river stage falls back to previous stable value after t=1015 d. Fig. 4-15 and Fig. 4-16 present the water table heights at x=0, 50, 100 and 150 m for a horizontal aquifer and sloping aquifers with 5º and 10º sloping angles in a period of t=1000 d to t=1150 d, respectively. Before the arrival of the river stage spike, the groundwater flow system reach its steady-state at t=1005 d at least for the near river region of x between 0 and 150 m. When the river spike arrives, we can see that the water table height at x=0 m increases about 3 meters. When the distance to river becomes larger, the response time of water table height to the river spike becomes longer. It is interesting to note that when the distance to river becomes larger, although the magnitude of water table response to the river spike becomes smaller, the duration of such a response becomes longer. This is caused by the propagation and hydraulic diffusivity of the river spike signal in the aquifer.

When the sloping angle increases from 0º to 10º, the water table heights increase remarkably for x=50, 100 and 150 m. Fig. 4-17 displays the influences of peak flow on the river-aquifer fluxes for a horizontal aquifer and sloping aquifers with 5º and 10º sloping angles. The positive values of river-aquifer fluxes represent that river recharges the aquifer, and the negative values of river-aquifer fluxes represent that aquifer recharges the river. When the river stage increases, the river-aquifer fluxes increase as well. The river-aquifer fluxes for 5° sloping aquifer are complex. First, the groundwater is recharged by the river before the arrival of the river stage spike. Second, the groundwater recharge from the river increases rapidly with the arrival of the river stage spike. Such a recharge rate decreases when the river stage falls back. Third, after the river stage spike, the recharge rate from river to the aquifer gradually drops to zero, the flow direction is reversed and the aquifer starts to recharge the river. A few days later, the flow direction is reversed again and river starts to recharge the aquifer.

These observations can be understood as follows. The river-aquifer flux is driven by two forces: one is the sloping bed which tends to drive flow down-gradient (away from the river to the aquifer), and the other is the rise of river stage. The former (or first) driving force is presented all the time while the later (or second) driving force is temporary and depends on the magnitude and duration of the river stage spike. Before the arrival of the river stage spike, the first driving force prevails and the second driving force is absent, thus flow is from river to aquifer. When the arrival of the river stage spike, the second driving force is dominating, leading to a spike of river recharge to the aquifer. Right after the river stage spike, the river stage drops quickly, but the drop of groundwater level in the aquifer is not as fast as the drop of river stage, thus leading to a

situation that the water table in the aquifer near the river is greater than the river stage, thus generating flow from the aquifer to the river. However, such a situation cannot last much longer as the water table in the aquifer continuously declines, resulting to the declining flow from the aquifer to the river. Eventually, the water table declines so much that the first driving force starts to become the dominating factor again, resulting in flow from river to the aquifer again.

Similar observations have been made for the 10° sloping aquifer, except that the flow direction has not been reversed with the arrival of river stage spike (see Fig. 4-17). This is because the first driving force (i.e., the sloping bed) is so strong that the second driving force (i.e., the rise of the river stage) is not strong enough to affect the flow direction. If one wants to compute the baseflow to a certain reach of the river, one can simply multiplying the discharge of flow from aquifer to the river per unit length by the total length of the river.

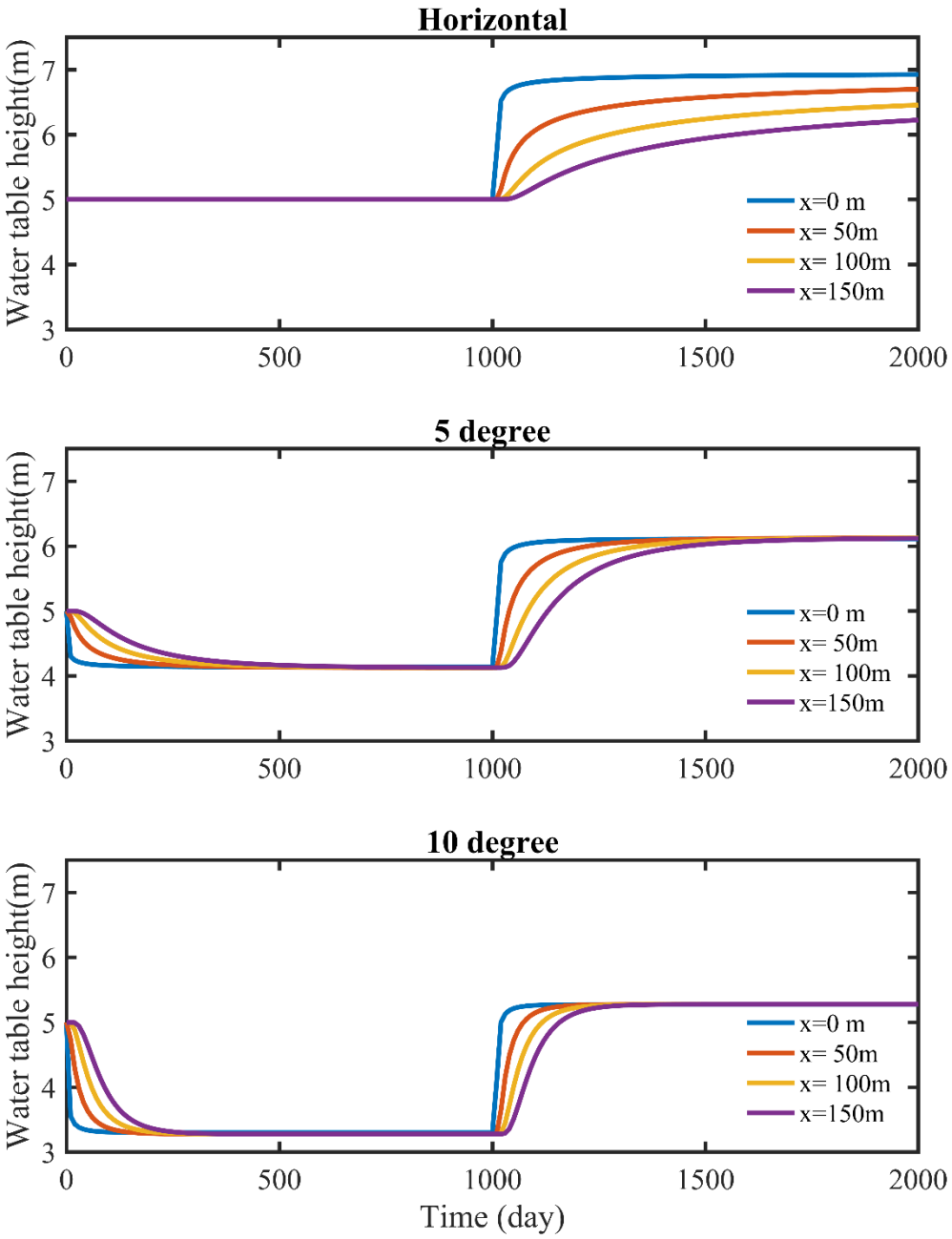

Fig. 4-5 Water table heights fluctuate with time at x=0, 50, 100 and 150 m in a horizontal aquifer, a 5° sloping aquifer, and a 10° sloping aquifer with a river changing by Eq. (4-1) with a=1 d^{-1} , n=1, p_1=1and c_1=1009 d.

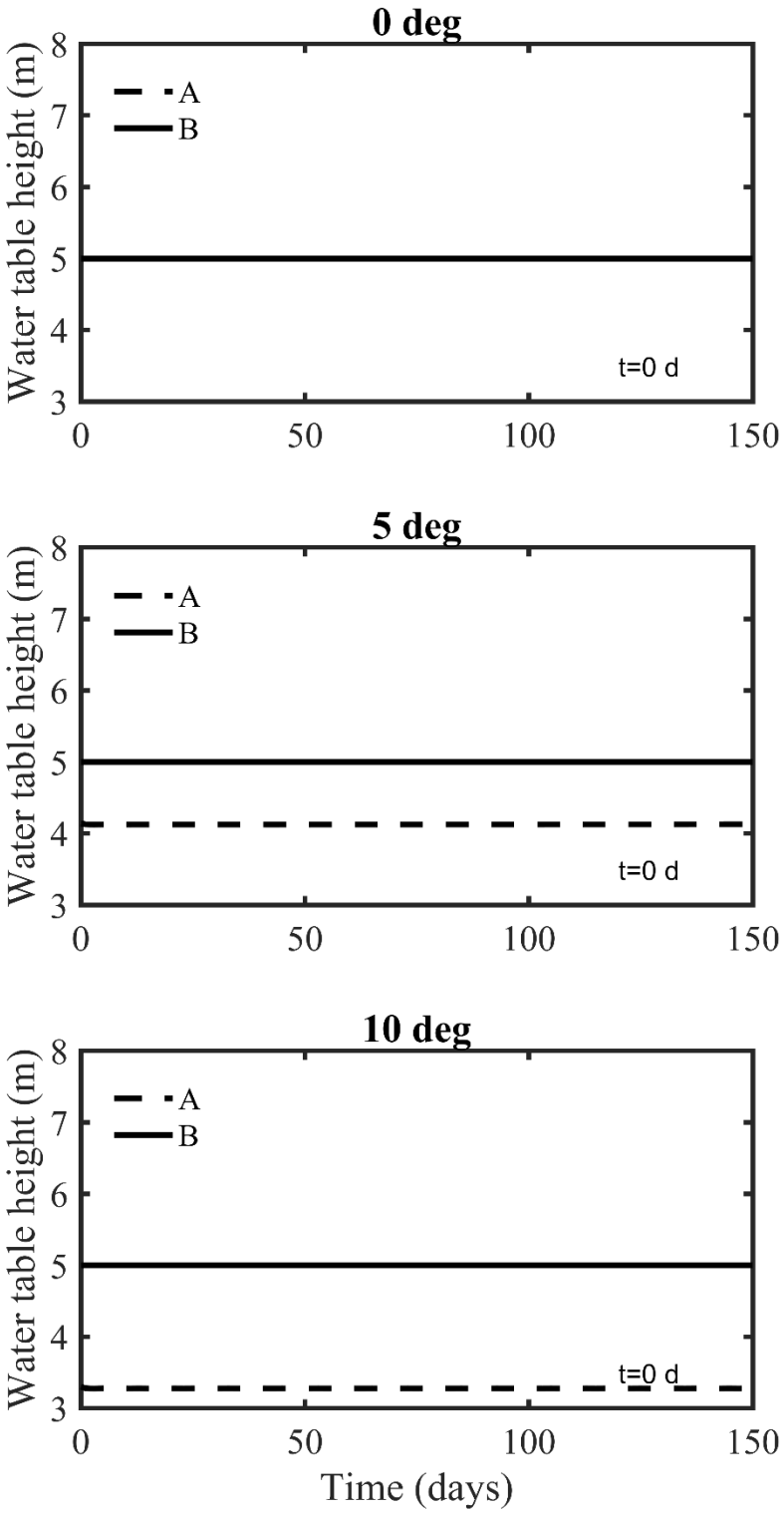

Fig. 4-6 Comparison of water table heights above the impermeable bed at *t*=0 d for a horizontal aquifer, a 5° sloping aquifer, and a 10° sloping aquifer between a classical initial head (B) and a steady state initial head (A).

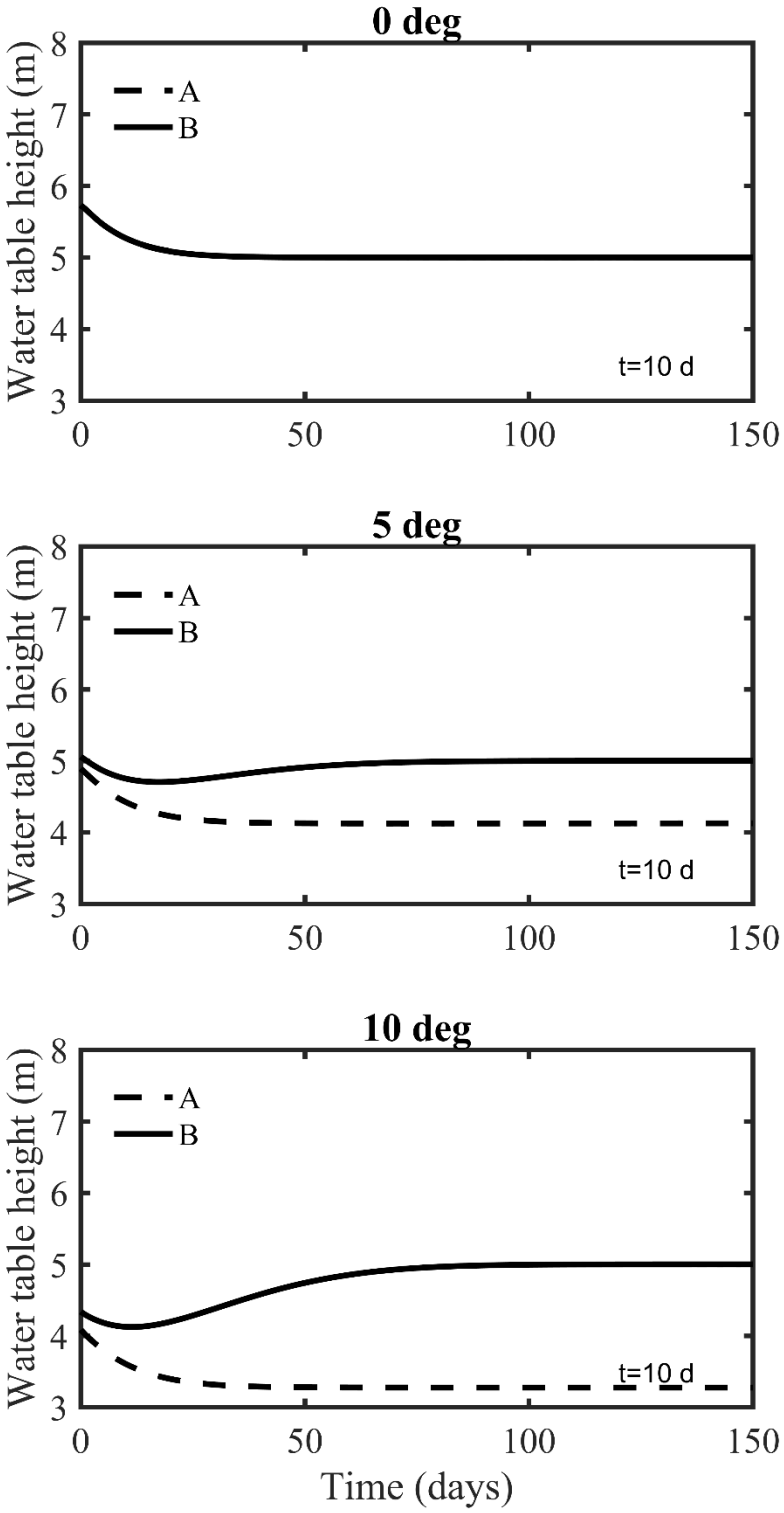

Fig. 4-7 Comparison of water table heights above the impermeable bed at *t*=10 d for a horizontal aquifer, a 5° sloping aquifer, and a 10° sloping aquifer between a general initial head (B) and a steady state initial head (A).

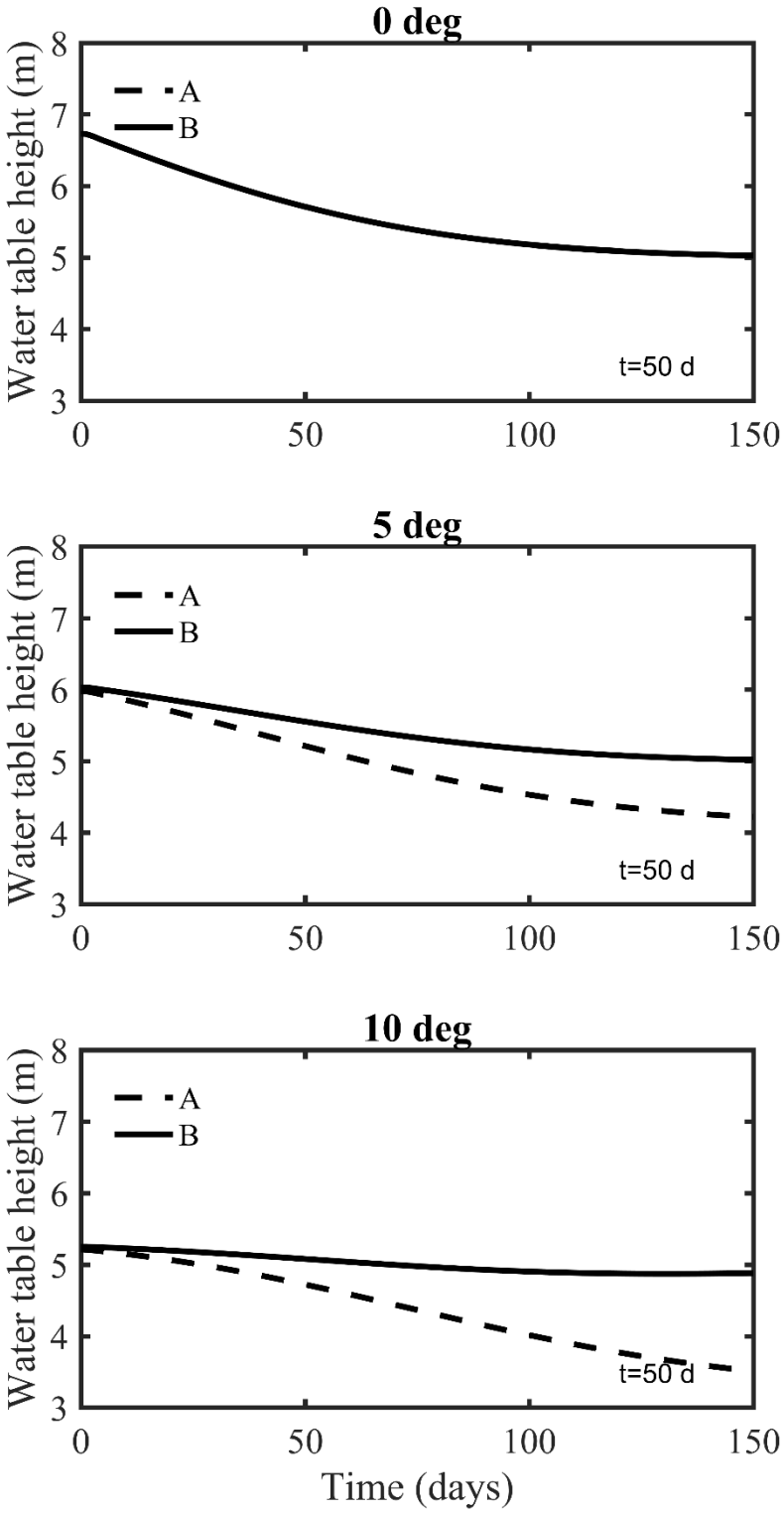

Fig. 4-8 Comparison of water table heights above the impermeable bed at *t*=50 d for a horizontal aquifer, a 5° sloping aquifer, and a 10° sloping aquifer between a general initial head (B) and a steady state initial head (A).

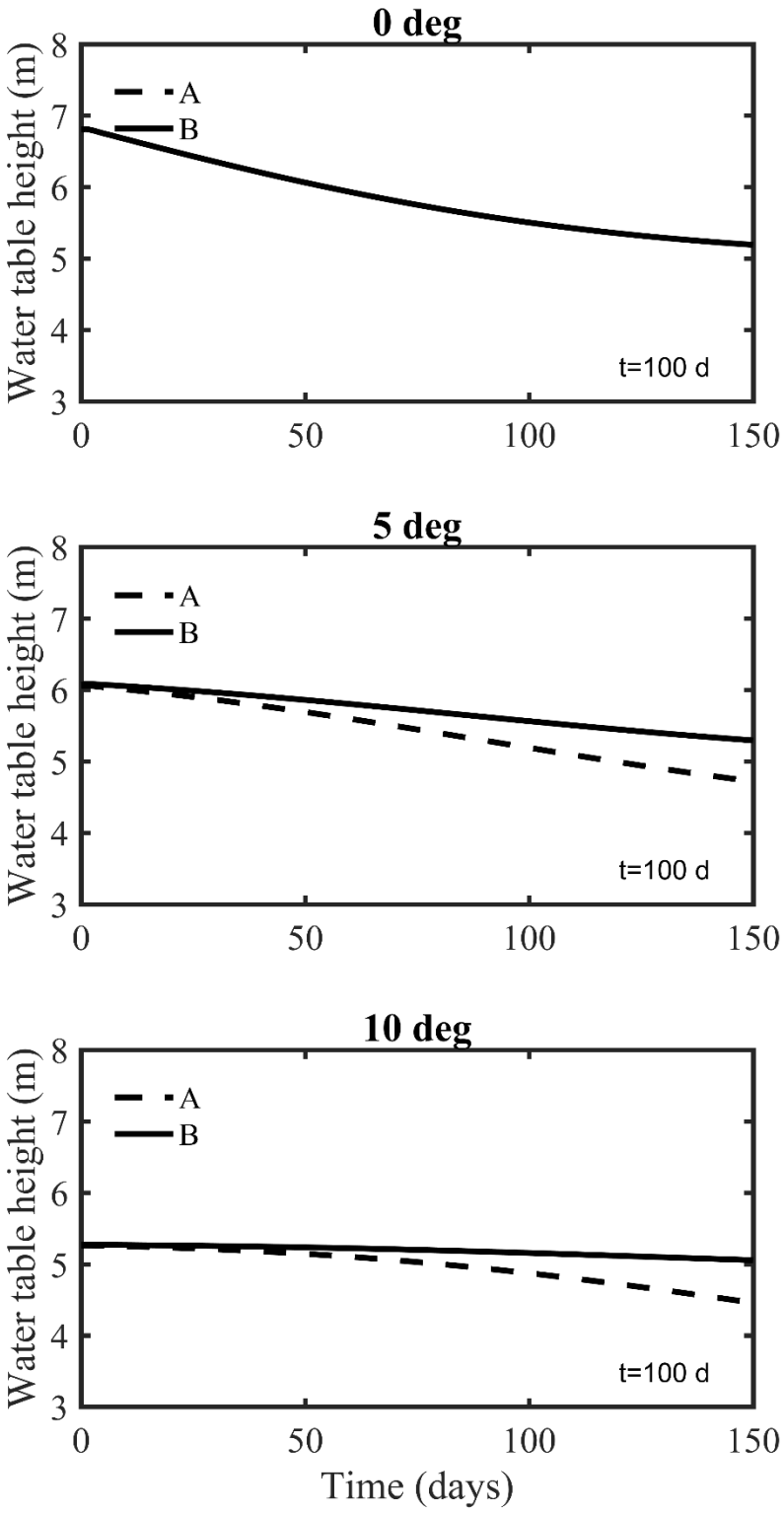

Fig. 4-9 Comparison of water table heights above the impermeable bed at *t*=100 d for a horizontal aquifer, a 5° sloping aquifer, and a 10° sloping aquifer between a general initial head (B) and a steady state initial head (A).

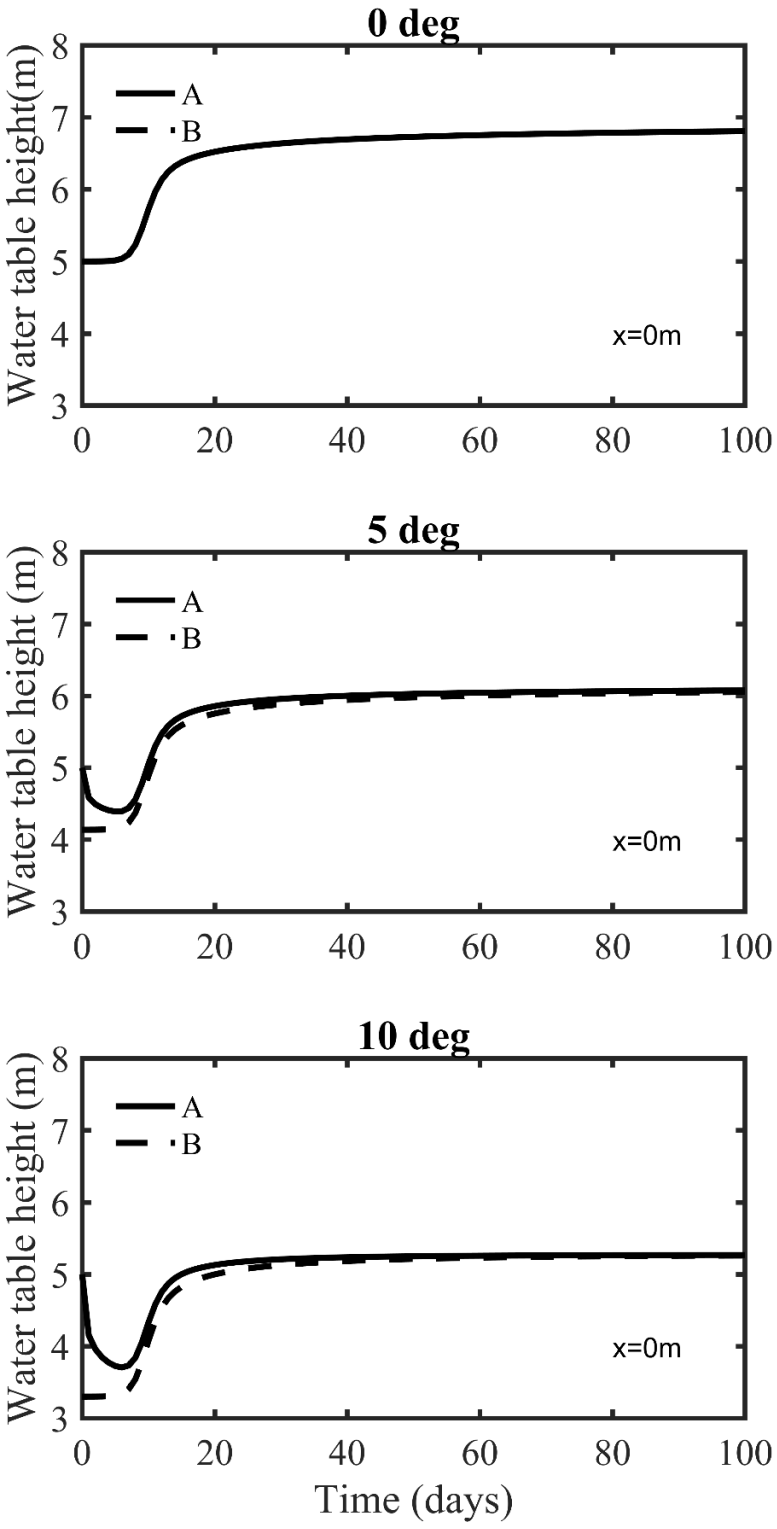

Fig. 4-10 Comparison of water table heights with time at *x*=0 m for a horizontal aquifer, a 5° sloping aquifer, and a 10° sloping aquifer between a general initial head (B) and a steady state initial head (A).

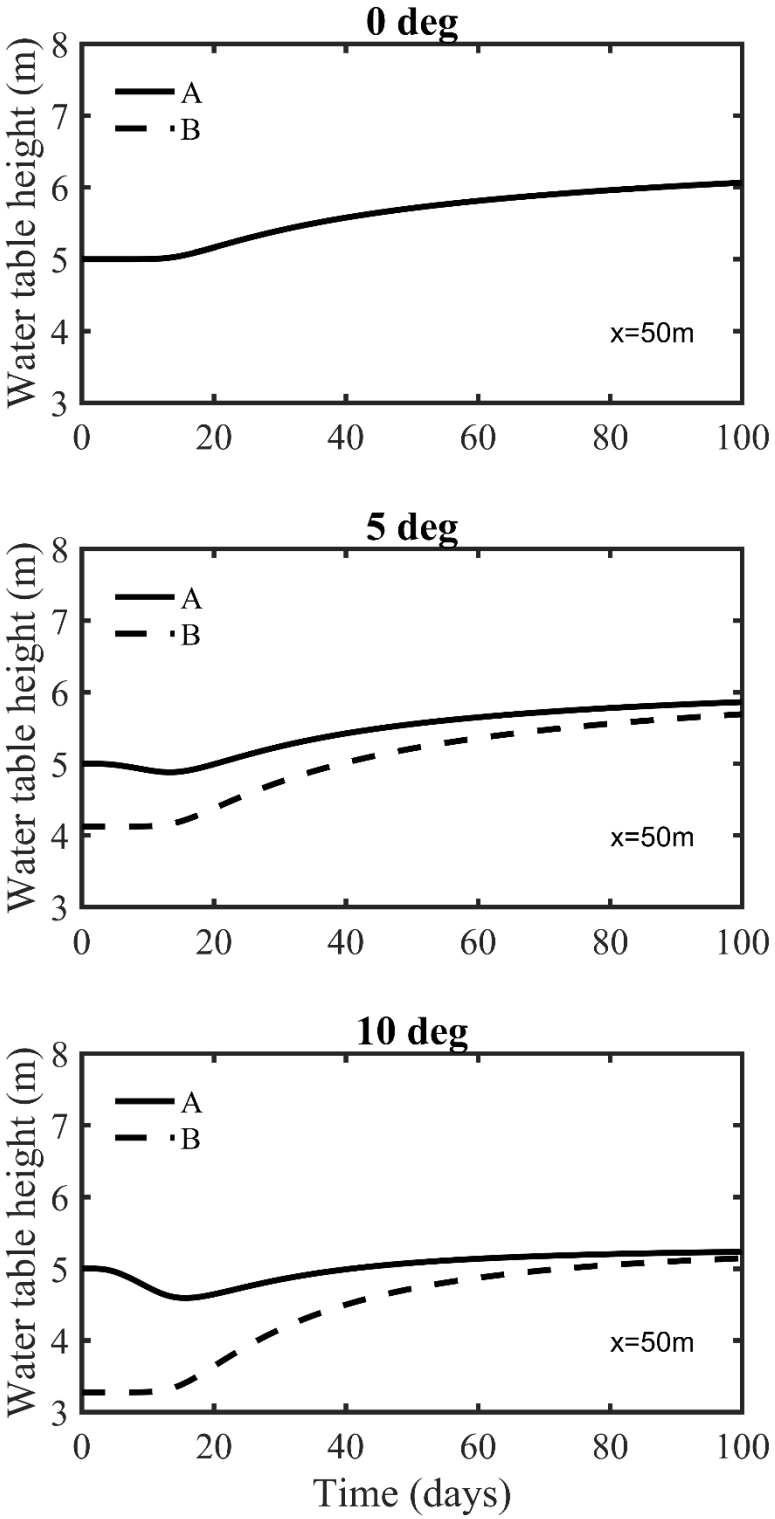

Fig. 4-11 Comparison of water table heights with time at *x*=50 m for a horizontal aquifer, a 5° sloping aquifer, and a 10° sloping aquifer between a general initial head (B) and a steady state initial head (A).

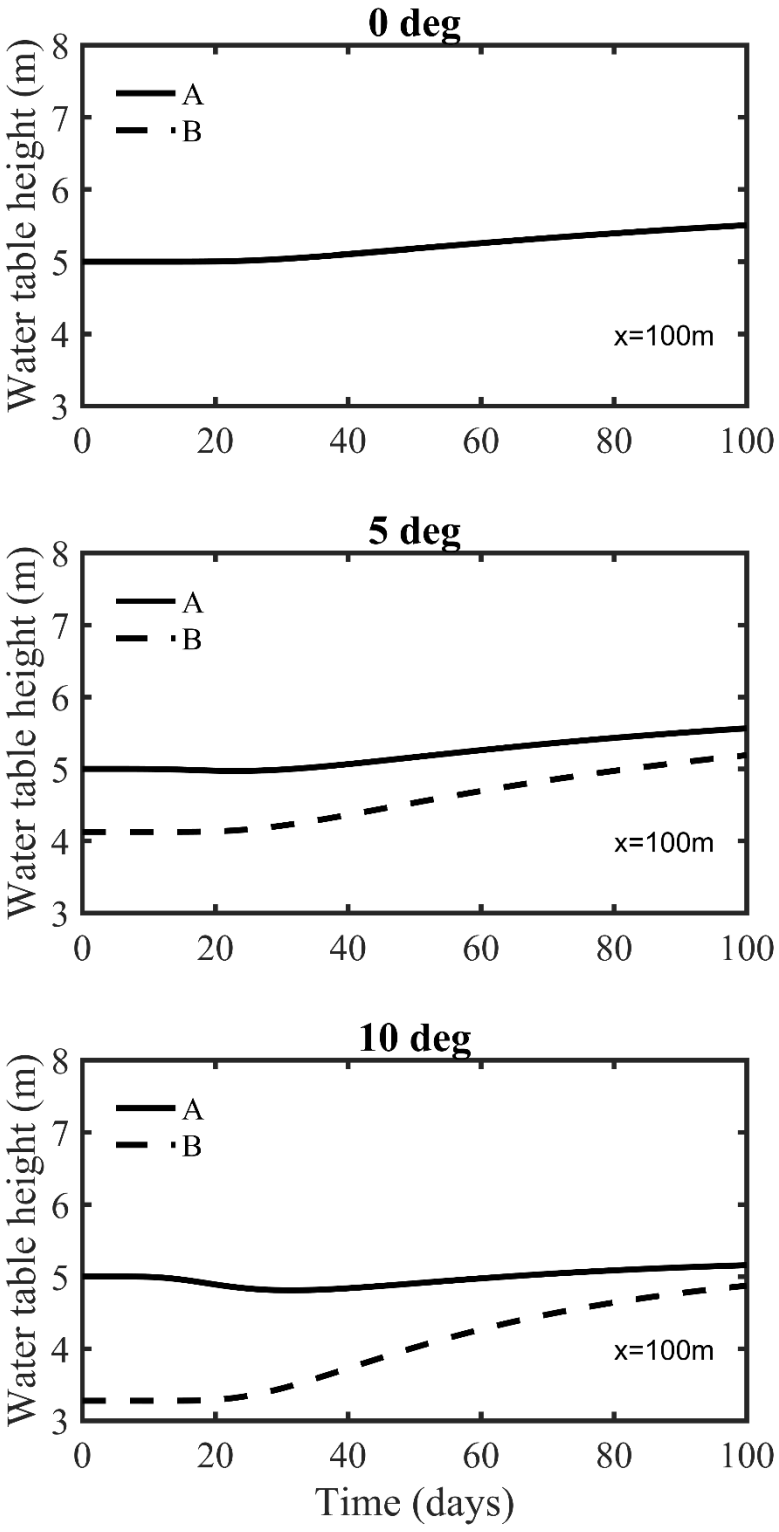

Fig. 4-12 Comparison of water table heights with time at *x*=100 m for a horizontal aquifer, a 5° sloping aquifer, and a 10° sloping aquifer between a general initial head (B) and a steady state initial head (A).

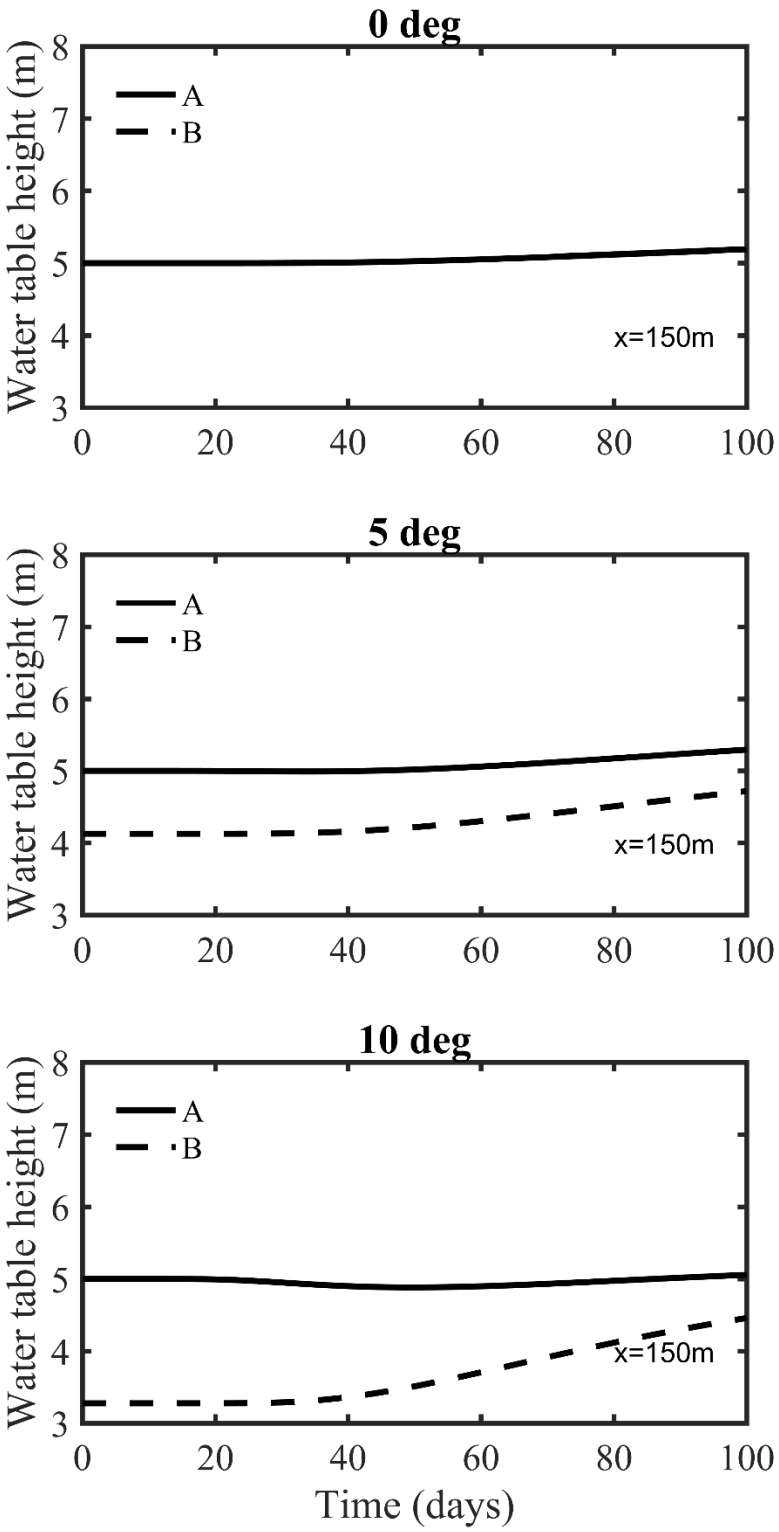

Fig. 4-13 Comparison of water table heights with time at *x*=150 m for a horizontal aquifer, a 5° sloping aquifer, and a 10° sloping aquifer between a general initial head (B) and a steady state initial head (A).

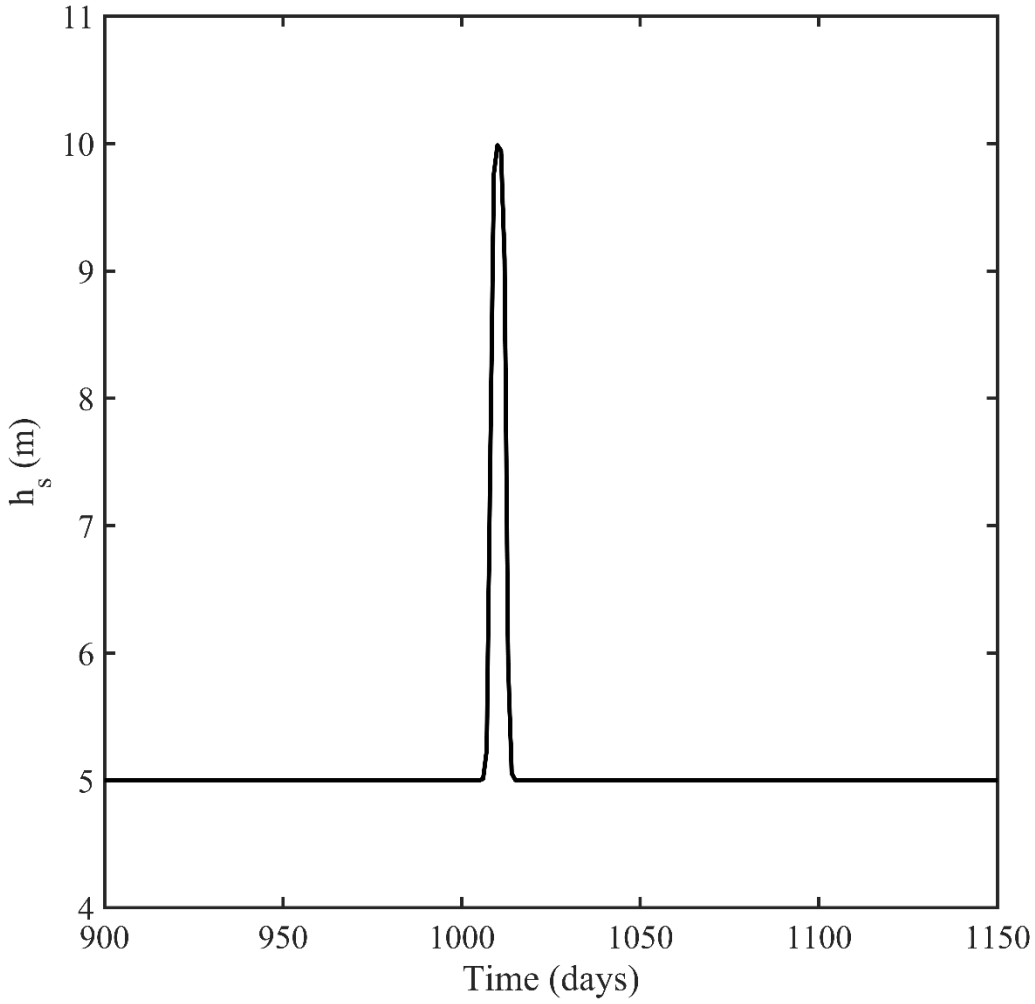

Fig. 4-14 The stage of river with a peak flow described by Eq. (4-1).

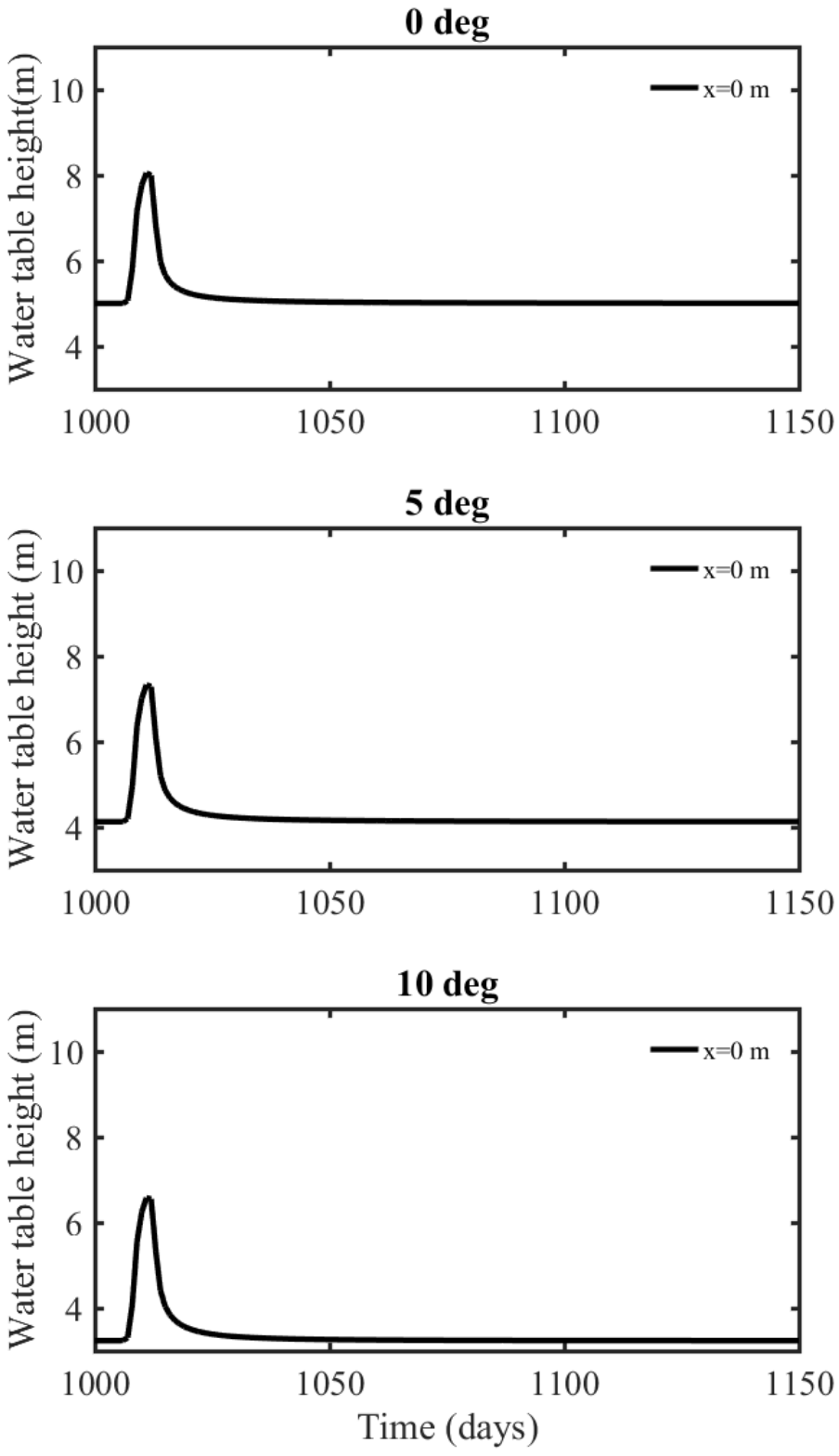

Fig. 4-15 The water table heights with time at x=0 m in a horizontal aquifer, a 5° sloping aquifer, and a 10° sloping aquifer for a river with a peak flow.

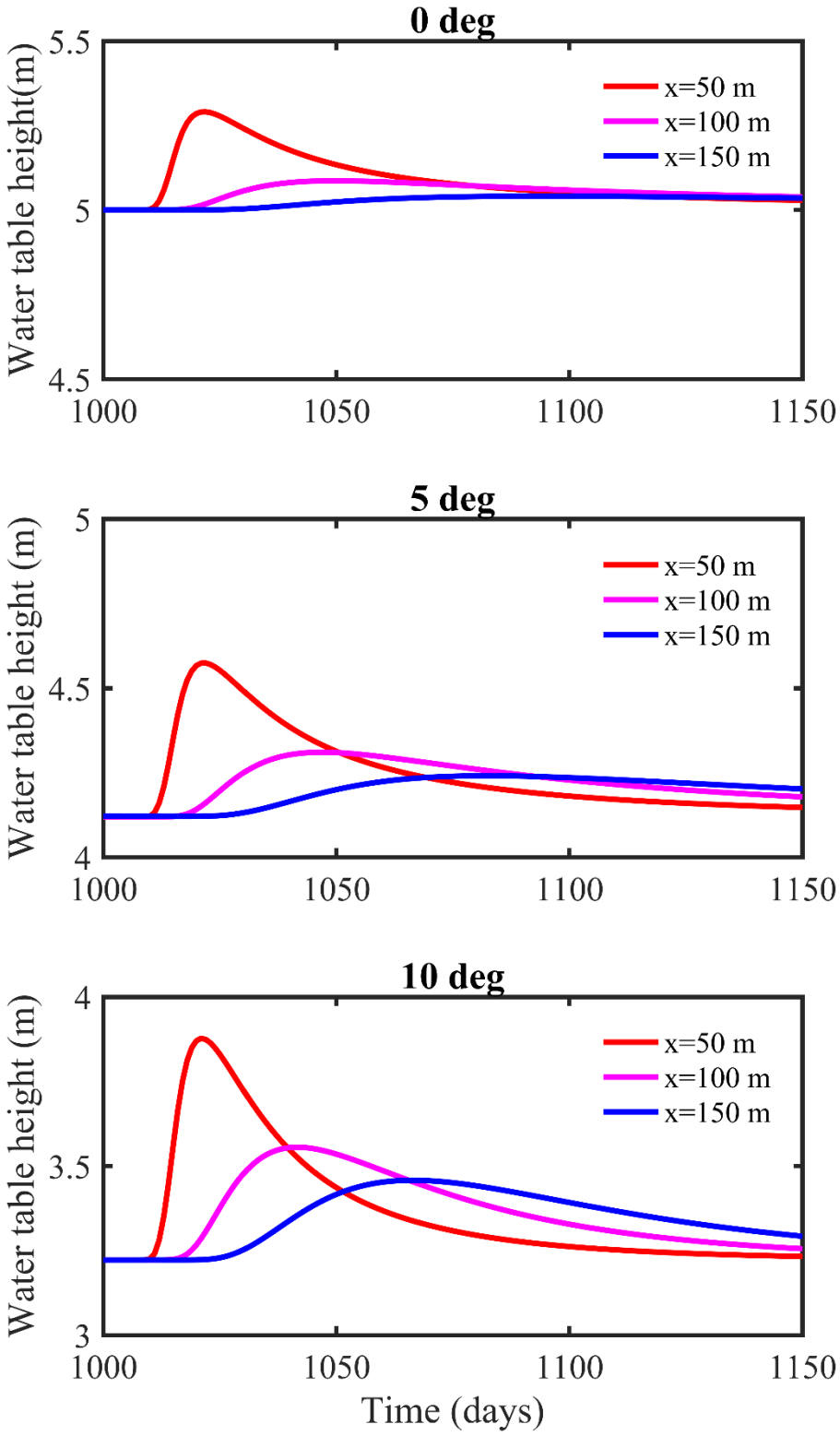

Fig. 4-16 The water table heights with time at *x*=50, 100 and 150 m in a horizontal aquifer, a 5° sloping aquifer, and a 10° sloping aquifer for a river with a peak flow.

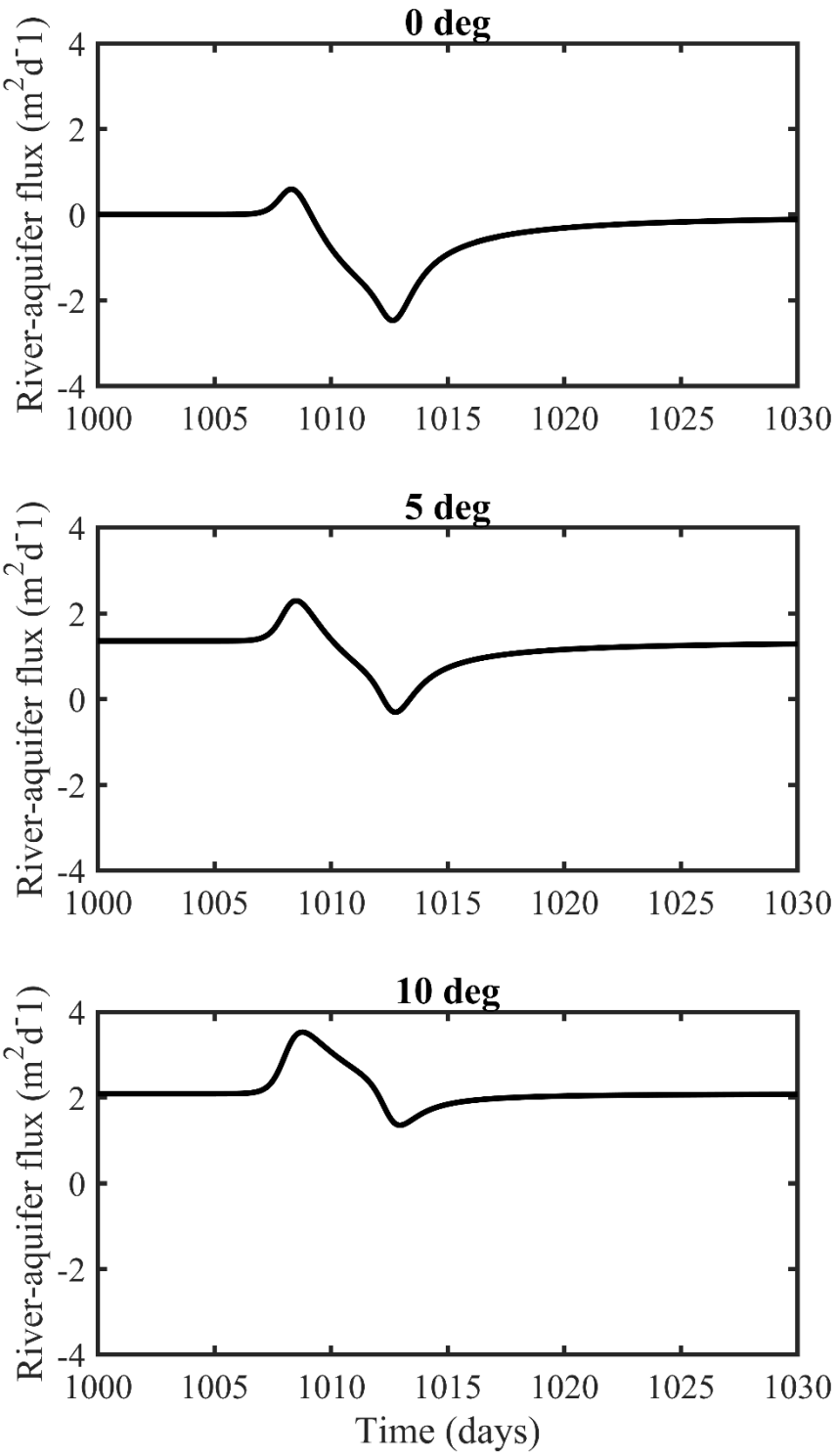

Fig. 4-17 The river-aquifer fluxes with time at the interface between vertical clay and aquifer in a horizontal aquifer, a 5° sloping aquifer, and a 10° sloping aquifer for a river with a peak flow.

4.3.4 Analysis of the h_a impact

In our analytical method, we use the average thickness of aquifer h_a instead of h in Eq. (2-4) to linearize the problem. This approximation is widely adopted in analytical solutions to a linearized Boussinesq equation for horizontal aquifers before (Marino, 1973; Liang and Zhang, 2012). The most common methods to select the value of h_a for horizontal aquifers are to let h_a=h_i or let h_a equal to the average value of the initial heads at the left and right boundaries. However, those methods do not consider a rapidly varied river stage. They also do not consider a sloping bed. In this section, we will investigate the influences of water table fluctuation in the presence of a sloping bed and a changing river stage with different h_a values.

We have computed the arithmetic averaged thicknesses of aquifer based on Fig. 2-3 for horizontal, 5º sloping and 10º sloping aquifers using the analytical solution. Such averaged thicknesses are 5.25, 5.89 and 6.37 m for t=10, 30 and 50 d, respectively for the horizontal aquifer; such averaged thicknesses are 5.17, 5.92 and 6.57 m for t=10, 30 and 50 d, respectively for the 5º sloping aquifer; such averaged thicknesses are 5.05, 5.81 and 6.57 m for t=10, 30 and 50 d, respectively for the10º sloping aquifer. The average thicknesses of aquifers are estimated basing on h_a=5 m for the linearized analytical solution. The results show that the values of h_a are underestimated, when the river stage rises with time. Furthermore, the range of change of the averaged thickness becomes greater when the sloping angle gets larger.

Recognizing that the averaged aquifer thickness is underestimated for setting h_a=5 m, we then change h_a=6 m and repeat above computation of the water table heights. We find

that the averaged thicknesses of the horizontal aquifer are 5.28, 6.00 and 6.51 m for t=10, 30 and 50 d, respectively; the averaged thicknesses of the 5º sloping aquifer are 5.19, 6.00 and 6.67 m for t=10, 30 and 50 d, respectively; the averaged thicknesses of the10º sloping aquifer are 5.05, 5.86 and 6.63 m for t=10, 30 and 50 d, respectively. The computed water table heights for three aquifers for two different h_a values (5 m and 6 m) with a rising river stage are shown in Fig. 4-18. It is shown that when the sloping angle increases, the influences of h_a to water table heights decrease. When the river stage increases from 5 to 10 m, the discrepancies of water table heights between h_a=5 m and h_a =6 m for three aquifers range from 0.008 to 0.14 m.

Above analysis concerns a rising river stage, now we will discuss a falling river stage. The river stage decreases from 5 to 3 m with λ=0.1 d^{-1}. The initial water table heights is 5 m, the average thickness of aquifer is 5 m, and the hydraulic parameters of aquifer and vertical clogging layer are same as their counterparts in section 2.3.1. For such a falling river stage, the averaged thicknesses of the horizontal aquifer are 4.90, 4.64 and 4.45 m for t=10, 30 and 50 d, respectively; the averaged thicknesses of the 5º sloping aquifer are 4.75, 4.23 and 3.80 m for t=10, 30 and 50 d, respectively; the averaged thicknesses of the 10º sloping aquifer are 4.55, 3.62 and 2.83 m for t=10, 30 and 50 d, respectively. The results show that the values of h_a are overestimated when the river stage declines with time.

After above analysis, the value of h_a is dropped from 5 to 4 m for the case of a falling river stage. When the river stage decreases from 5 to 3 m with λ=0.1 d^{-1} and other parameters remaining the same as the model above, the averaged thicknesses of the horizontal aquifer are 4.91, 4.69 and 4.52 m for t=10, 30 and 50 d, respectively; the

averaged thicknesses of the 5º sloping aquifer are 4.78, 4.30 and 3.89 m for t=10, 30 and 50 d, respectively; the averaged thicknesses of the 10º sloping aquifer are 4.59, 3.70 and 2.89 m for t=10, 30 and 50 d, respectively. The water table heights for three aquifers for two different h_a values (5 m and 4 m) with a falling river stage are shown in Fig. 4-19. When the river stage decreases from 5 to 3 m, the discrepancies of water table heights between h_a=5 m and h_a =4 m for three aquifers range from 0.014 m to 0.083 m.

In section 4.3.2, we obtained water table heights in a period of 2000 days for three aquifers at x=0, 50, 100 and 150 m. The average thicknesses of sloping aquifers are less than 5 m in the period of t=0 d to t=1000 d. In this case, we use h_a=5 m and obtained the steady state water table heights 4.12 m and 3.22 m for 5º sloping aquifer and 10º sloping aquifer respectively. The steady state water table heights are not affected by the values of h_a. A demonstrate is shown in the following.

From Figs. 4-18 and 4-19, one can see that the use of different h_a values does not appear to affect the overall water table heights greatly. Therefore, we recommend to choose the value of h_a based on the average of the initial heads on the left and right boundaries.

The steady-state water table heights can be estimated by Eq. (2-4). When the infiltrated recharge is zero and the river stage is constant, one can have the steady-state governing equation of flow as:

$$\frac{\partial^2 h}{\partial x^2} - \frac{tan\theta}{h_a}\frac{\partial h}{\partial x} = 0. \qquad (4\text{-}19)$$

The general solution of Eq. (4-19) can be obtained straightforwardly as

$$h = C_1\, exp\left(\frac{tan\theta}{h_a}x\right) + C_2 \quad . \tag{4-20}$$

where C_1 and C_2 are two constants to be determined. Basing on the boundary condition of Eqs. (2-7b) and (2-7c), we can obtain C_1=0 and C_2=h_s-(K/k_1)*tanθ.

It is easily seen that the steady-state water table heights in a sloping aquifer are not related to the value of h_a. Furthermore, such steady-state water table heights are independent of x, meaning that they are uniform over the domain of interest. Specifically, the steady-state water table heights of the 5º sloping aquifer and the 10º sloping aquifer are 4.12 m and 3.22 m, respectively, which are the same as the steady-state water table heights in Fig. 4-5.

From Fig. 4-5, one can see that it takes approximately 250 days for water table to approach its steady state at x=150 m when the sloping angle is 10º. Such an observation is consistent with a quantitative analysis using the concept of hydraulic diffusivity (D) defined as:

$$D = \frac{Kh_a}{S_y} \tag{4-21}$$

Based on such a hydraulic diffusivity, one may recall the following equation to estimate the characteristic time (T) for dissipating a pore pressure (or hydraulic head) anomaly (Bear, 1972):

$$T = \frac{x^2}{2D} \tag{4-22}$$

Such a characteristic time should be in the same order of magnitude with the time required to approximate the steady-state. Given the values of K=2.5 m/day, h_a=3.22 m

(see the steady-state h_a above for the 10º sloping aquifer), S_y=0.25, and x=150 m, one will obtain T=349 days for the 10º sloping aquifer. Such an estimated characteristic time is within the same order of magnitude as the time of approaching the steady state observed from Fig. 4-5, which is 250 days.

4.3.5 Application of new analytical solution

In section 4.3.2, we compare water table heights calculated using an idealized initial condition, and we find that the system requires a long time to achieve steady state, especially in a horizontal aquifer. In this section, we will discuss how to use our solution to estimate ground water table and river-aquifer flux for a variable river stage in a sloping aquifer. We need to point out that this method only works for a special case below, i.e., the river stage is nearly constant for an extensive period of time before start to rise relatively rapidly.

Before predicting the ground water table, some field works are necessary to gather the necessary information. For instance, we need several pressure transducers and an observation well near the river to record the stage of river and the elevation of water table at the observation well. The hydraulic conductivities of the clogging layer may be tested using a slug test, and the aquifer hydraulic conductivity may be obtained using a pumping test or a slug test. The porosity and specific yield of the aquifer may be obtained from laboratory test using samples taken from the aquifer investigated. The thickness of the clogging layer can be obtained from coring, and the inclined angle of the impermeable base can be obtained using geological map or geophysical survey.

Assuming that the stage of river stays on a level of h_{i1} for a known period of time and then rises rapidly to h_{f1} in a short period of time (for instance by flood, snowmelt or precipitation in the upstream). The stage curve of river is recorded by sensor. We can fit the stage curve of river by Eq. (4-1) and obtain the value of fitting parameter a_1. For instance, if the stage of river increases from 5 m to 7 m in 2, 5 and 10 d, the corresponding parameter of a can be set as 1.4, 2.8 and 7 d^{-1}. The stage curves are shown in Fig. 4-20.

At first, we set a great value of fitting parameter c_1 (meaning that the system has experienced a long period of time with a nearly constant river stage, thus has already reach its pseudo-steady state) and use Eq. (4-1) and our solution to calculate water table height distribution at the location of the observation well. The initial value of river and water table heights in aquifer are set by the value of h_i. Second, we can calibrate the value of h_i by comparing the observed water table height h_1 at the observation well with the calculated pseudo-steady state water table height at the observation well. After this step, we can calculate the water table by our solution with the calibrated initial value h_i of river stage for all the following times.

For instance, the stage of river stays on 5 m for a long time and the distance between river and an observation well is 50 m. The hydrological parameters of model are the same as in the 5º sloping angle case in section 4.3.2. If we observe the water table height is 4.30 m at the observation well, the corresponding time can be found in Fig. 4-21. We can describe the ground water table at the beginning time of river rise by the results at t=97 days. If the stage of river rises from 5 m to 7 m in 5 days, a new equation will be built as below: $h_s(t) = 7 - 2/(1 + e^{2.8t-106})$ (4-19)

We can obtain groundwater table with time using Eq. (4-19). The part of t=0 d to t=97 d is use to obtain the ground water table at the beginning time of river rise. The part of t>97 d can be used to predict the water table fluctuation after river rise.

The attempt here is to simulate a realistic river stage function when studying a river-aquifer system in a sloping aquifer framework. However, we have to point out that above discussion is still limited to a relatively simple scenario of the river stage variation, i.e., a relatively long period of time of relatively stable river stage, followed by a rapid rise of the river stage. The methodology established here is important and it can be used to simulate more realistic river stage fluctuation functions. For instance, if a falling river stage also exists after the rising phase, then another sigmoid function can be added into the river stage function, i.e., there are two terms in the summation of Eq. (4-1). The rest derivation procedures are nearly identical to what has been presented in this chapter except that the formula will get more complex. Furthermore, if the river stage fluctuates with a number of rising limbs and falling limbs, a sequential sigmoid functions can be used to mimic the shape of the river stage fluctuation, and the rest derivation procedures are straightforward (albeit a little bit tedious). In this way, we can essentially derive the analytical model for a wide range of possible river stage fluctuations.

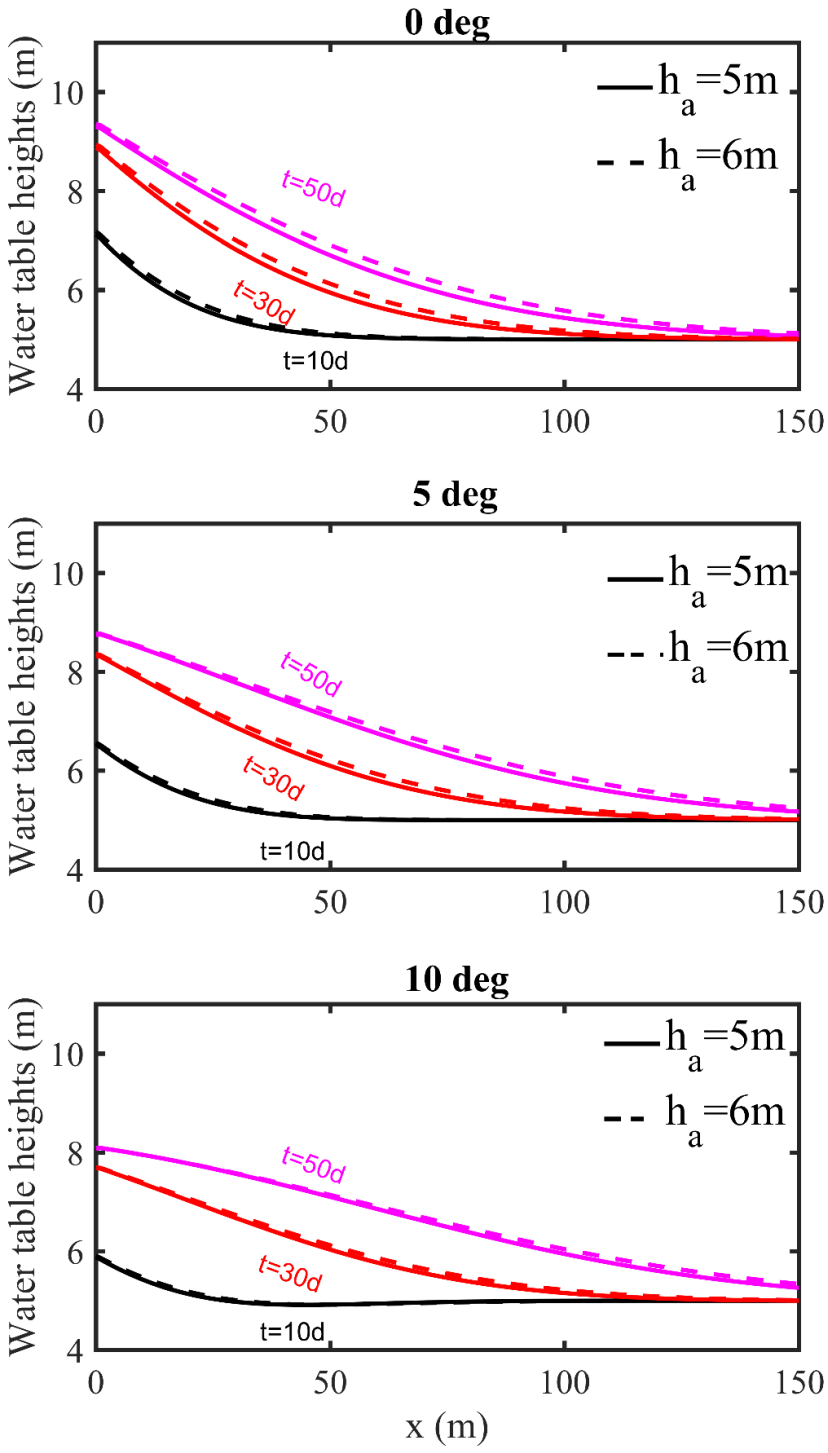

Fig. 4-18 Comparison of water table heights above the impermeable bed at *t*=10, 30 and 50 d for a horizontal aquifer, a 5° sloping aquifer, and a 10° sloping aquifer with a rising river stage between h_a=5 m and h_a=6 m.

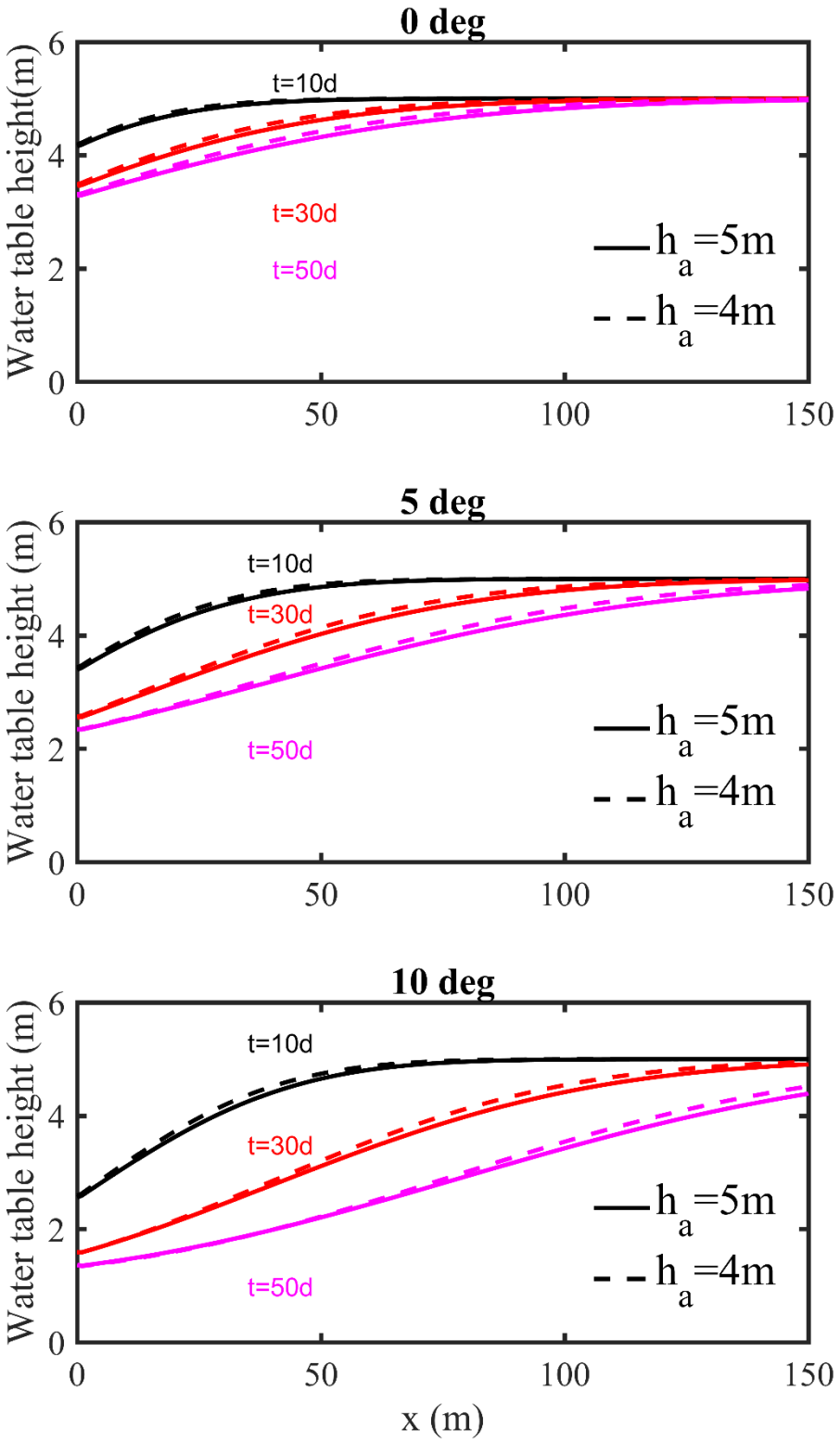

Fig. 4-19 Comparison of water table heights above the impermeable bed at t=10, 30 and 50 d for a horizontal aquifer, a 5° sloping aquifer, and a 10° sloping aquifer with a declining river stage between h_a=5 m and h_a=4 m.

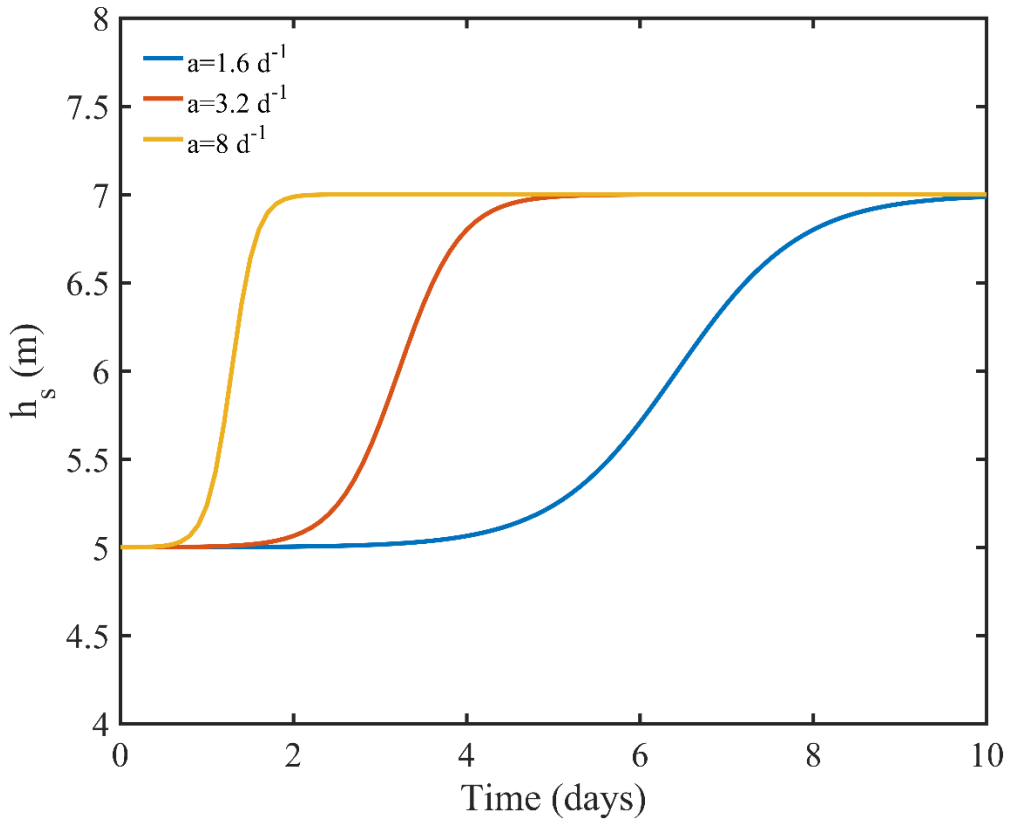

Fig. 4-20 the curves of river stage increase from 5 m to 7 m in 2, 5 and 10 d.

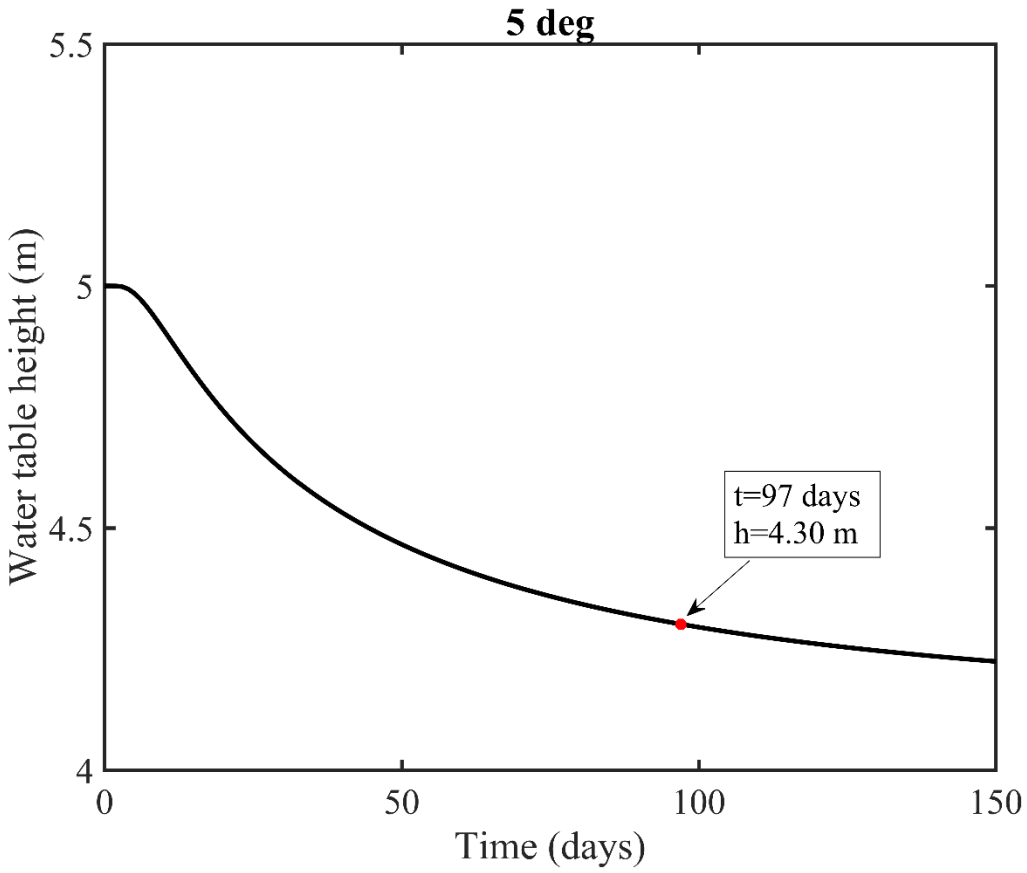

Fig. 4-21 Water table height fluctuates at *x*=50 m with a constant stage of river.

4.4 Conclusion

A new semi-analytical solution is developed to estimate the ground water table distribution in a sloping aquifer with one water interacted river and potential time-dependent recharge from infiltration on the top. The semi-analytical solution is derived by a new method to describe the realistic river stage variations using a sequential sigmoid functions. The new method allows the stage of river changes as an "S" shaped curve and this important feature can be used to overcome the problem of using an idealized and

likely unrealistic initial condition of a constant water table heights above the sloping base in previous numerous studies.

We compare our new semi-analytical solution with a 1D finite-element numerical model developed in COMSOL and find that our analytical solution agrees greatly with COMSOL simulations. The water table heights simulated from above mentioned idealized initial head would change rapidly at the beginning of simulation, and requires a long period of time to reach its pseudo-state state status.

The unique feature of the proposed new sigmoid functions for describing the river stage will allow system to reach its pre-rising pseudo-steady state condition, thus is more close to what happens in an actual river-aquifer system when the river stage remains nearly the same level for a long period of time before rising. We investigate the response of peak flow to groundwater table and river-aquifer flux. We investigate the influences of h_a to the groundwater table in a sloping aquifer with a river and semi-infinite extent by the analytical method.

The developed analytical solution of this chapter is expected to be more realistic to describe the river-aquifer system in a sloping aquifer framework, and it can be used as an important base for investigating other complex river stage variations in the future.

CHAPTER 5

SUMMARY AND CONCLUSIONS

5.1 Summary and conclusions

In this dissertation, we have investigated the influences of sloping bed, dynamic river stage, the vertical clogging layer and time-dependent infiltration recharge on the groundwater table fluctuations and river-aquifer flux under various hydrological conditions.

Hydrodynamics in an unconfined sloping aquifer has been a concern among several previous researchers. But the previous studies have several problems in multiple aspects such as treatment of the boundary condition associated with the clogging layer, exclusion of the infiltration recharge in the Boussinesq equation, etc. To advance the science of hydrodynamics in a sloping unconfined aquifer, a new semi-analytical solution was developed by setting the dynamic river stage and infiltration recharge on the top. The comparison displays that the analytical solution of previous study by Bansal et al. (2016) is not suited for describing the hydrodynamics in an unconfined sloping aquifer.

The new analytical solution was compared with the finite element method of numerical simulations by COMSOL program and HydroGeoSphere. The COMSOL program was built by the same linearized Boussinesq equation and it fits greatly with the analytical solution. The HydroGeoSphere program couples the flow processes in the unsaturated zone and the saturated zone. The results display that the accuracy of analytical solution will decrease with the increase of sloping angles. The responses of infiltration recharge to water table fluctuations and river-aquifer flux demonstrate that

sporadic recharge events (possibly occurring in arid and semi-arid regions) do not play an important role in affecting the response of water table and river-aquifer flux, when compared to the river stage variations and sloping angles.

Water flow in an unconfined sloping aquifer between two parallel rivers with water infiltrated recharge has also been studied in a few limited previous studies. But the previous studies did not consider the influences of 1) the clogging layer between river and aquifer, 2) the various stages of rivers, and 3) infiltrated recharge on the top. An analytical solution included these factors has been developed in this dissertation based on the linearized Boussinesq equation. Similarly, for such a two river and one aquifer system, the water table heights and river-aquifer fluxes obtained by the analytical solution, and two numerical programs of COMSOL and HydroGeoSphere are compared. Our results show the analytical solution agree greatly with COMSOL program. The comparison displays that the factors of the unsaturated zone process and the linearized approach used in the analytical solution may cause negligible errors for a sloping aquifer with a 10^{o} sloping angle. Greater discrepancy will be resulted when the sloping angle becomes larger.

The variations of water profile in an unconfined aquifer is much different from the variations of water profile in a horizontal aquifer, especially in an unconfined aquifer with two parallel rivers. The water table profile can evolve from a straight line parallel with the sloping at the beginning to a convex shape without any recharge or evaporation on the top of aquifer.

The different hydraulic parameters may cause different influences on water table fluctuations and river-aquifer fluxes in an unconfined sloping aquifer. The influences of hydraulic parameters for an unconfined sloping aquifer with one river or two river are similar but different in some extents.

The previous studies of the analytical solutions in an unconfined sloping aquifer are limited by the idealized initial condition. We have developed a new method to avoid the limitation of idealized initial condition by using a sequential sigmoid functions to describe the river stage variations. The benefit of using the sigmoid functions permits the system to reach its pseudo-steady state after a long period of stable river stage before the rapid rise of the river stage, thus avoid the difficulty of selecting the proper initial condition, which is often complex and unknown for a sloping aquifer. We find that when the sloping angle becomes greater, the water table will achieve steady state more quickly.

5.2 Future work

Up to now, most of studies on the water flow in an unconfined sloping aquifer only consider the influences of saturated zone. We build a model with unsaturated zone and saturated zone by HydroGeoSphere, but that the unsaturated zone processes have not been fully explored in great details. For instance, how are the different soil types, water table depth, and surface infiltration going to affect the overall hydrodynamics of flow in an unconfined sloping aquifer?

The recharge events discussed in this dissertation are sporadic, which is suitable for dealing with extreme precipitation events in arid and semi-arid regions, but may not be

suitable for more humid environment in which a sustainable recharge event can last for a long period of time. This issue should also explored in details in the future.

To align with previous studies, this dissertation primarily focus on single rising or falling limb of the river stage, although the proposed sequential sigmoid functions is capable of dealing with complex river stage fluctuations. In the future, it will be nice to explore the variation of water table and surface water-groundwater interaction when the river stage rises and falls in more realistic patterns observed in real world.

The aquifer heterogeneity has not been considered in this study and should be explored in the future. For instance, multiple sedimentary layers with vastly different hydraulic properties may exist in the field. It will be interesting to find out how is such layering feature will impact the hydrodynamics in a sloping aquifer framework.

The investigation conducted is a two-dimensional cross-section approach. It means that we have not considered the river stage variation along the river channel. A three-dimensional approach honoring river stage variation not only with time but also along the river channel will be very valuable for assessing the interaction of river with a sloping angles.

The assumption adopted in this study is that the river stage can be described using a prescribed function of time. In reality, one may have to incorporate the open channel flow in the river and the groundwater flow in the sloping aquifer into an integrated system.

The single river case discussed here assumes that the river is straight at least with the domain of interest. In reality, the river channel is meandering. The two rivers discussed are assumed to be parallel with each in this study. In reality, the two rivers may be in any

geometrical setting (parallel or not). Therefore, the interaction of a sloping aquifer with two non-parallel rivers will be the concern.

The clogging layer morphology discussed here is highly idealized. In the future, more realistic river bed clogging layer should be considered. Furthermore, such a clogging layer may even vary with space and time continuously (because of the periodic flooding events in the river channel). It is worthwhile to explore the interaction of river with a sloping aquifer with the presence of such clogging layers.

The rivers are fully penetrating in this dissertation. In the future, partially penetrating rivers should be investigated, particularly for river in the down-gradient site where a greater depth to the impermeable bed is seen.

This study does not consider any pumping or injection wells in the sloping aquifer. In reality, those wells may be functioned, and their influence will be checked. For instance, it will be interesting to find out what is the difference for river bank pumping in a sloping aquifer from that in a horizontal aquifer? Is the stream depleting rate the same in a sloping aquifer as that in a horizontal aquifer when one or multiple river bank pumping wells are installed.

Despite the long list of unexplored problems outlined above, this dissertation provides some fundamental knowledge and analytical solutions that are easy to use. The solution has been tested and the conditions for the use of those solutions have also been explained. With this in mind, we believe that this body of work represents a significant advancement in hydrodynamics of sloping unconfined aquifers.

REFERENCES

Akylas, E., Koussis, A.D., 2007. Response of sloping unconfined aquifer to stage changes in adjacent stream. I. Theoretical analysis and derivation of system response functions. Journal of Hydrology, 338(1): 85-95. DOI:https://doi.org/10.1016/j.jhydrol.2007.02.021

Ashjari, J., Raeisi, E., 2006. Influences of anticlinal structure on regional flow, Zagros, Iran. Journal of cave and karst studies, 68(3): 118-129.

Bansal, R.K., Lande, C.K., Warke, A., 2016. Unsteady groundwater flow over sloping beds: analytical quantification of stream–aquifer interaction in presence of thin vertical clogging layer. Journal of Hydrologic Engineering, 21(7): 04016017.

Bear, J., 1972. Dynamics of fluids in porous materials. Society of Petroleum Engineers: Dallas, TX, USA.

Boussinesq, J., 1877. Du mouvement non permanent des eaux souterraines. Essai sur le theorie des courantes, Imprimerie Nationale, Paris, 680.

Bouwer, H., 2002. Artificial recharge of groundwater: hydrogeology and engineering. Hydrogeology Journal, 10(1): 121-142.

Brutsaert, W., 1994. The unit response of groundwater outflow from a hillslope. Water Resources Research, 30(10): 2759-2763.

Cabrera, M., Custodio, E., 2004. Groundwater flow in a volcanic–sedimentary coastal aquifer: Telde area, Gran Canaria, Canary Islands, Spain. Hydrogeology Journal, 12(3): 305-320.

Calver, A., 2001. Riverbed permeabilities: Information from pooled data. Groundwater, 39(4): 546-553.

Carsel, R.F., Parrish, R.S., 1988. Developing joint probability distributions of soil water retention characteristics. Water resources research, 24(5): 755-769.

Chapman, T., 1980. Modeling groundwater flow over sloping beds. Water Resources Research, 16(6): 1114-1118.

Chauhan, H., Schwab, G., Hamdy, M., 1968. Analytical and computer solutions of transient water tables for drainage of sloping land. Water Resources Research, 4(3): 573-579.

Chen, X., 2000. Measurement of streambed hydraulic conductivity and its anisotropy. Environmental Geology, 39(12): 1317-1324.

Chen, Z., Li, J., Shen, H., Zhanghua, W., 2001. Yangtze River of China: historical analysis of discharge variability and sediment flux. Geomorphology, 41(2-3): 77-91.

Chen, X., 2004. Streambed hydraulic conductivity for rivers in south-central Nebraska. Journal of the American Water Resources Association, 40(3): 561-573.

Childs, E., 1971. Drainage of groundwater resting on a sloping bed. Water Resources Research, 7(5): 1256-1263.

Domenico, P.A., Schwartz, F.W., 1998. Physical and chemical hydrogeology, 506. Wiley New York.

Dutton, A.R., Harden, B., Nicot, J.P., O'Rourke, D., Harden, B., O'Rourke, D., Harden, R.W., 2003. Groundwater availability model for the central part of the Carrizo-

Wilcox aquifer in Texas. Contract report to the Texas Water Development Board, TWDB, Austin, TX, 295.

Fetter, C., 1999. Contaminant hydrogeology.

Ghosh, N.C. et al., 2015. Semi-analytical model for estimation of unsteady seepage from a large water body influenced by variable flows. Water resources management, 29(9): 3111-3129.

Glover, R.E., Balmer, G.G., 1954. River depletion resulting from pumping a well near a river. Eos, Transactions American Geophysical Union, 35(3): 468-470.

Hantush, M.S., 1967. Growth and decay of groundwater-mounds in response to uniform percolation. Water Resources Research, 3(1): 227-234.

Imrie, C., Durucan, S., Korre, A., 2000. River flow prediction using artificial neural networks: generalisation beyond the calibration range. Journal of hydrology, 233(1-4): 138-153.

Ingebritsen, S., Scholl, M., 1993. The hydrogeology of Kilauea volcano. Geothermics, 22(4): 255-270.

Join, J.-L., Folio, J.-L., Robineau, B., 2005. Aquifers and groundwater within active shield volcanoes. Evolution of conceptual models in the Piton de la Fournaise volcano. Journal of Volcanology and Geothermal Research, 147(1-2): 187-201.

Koussis, A.D., Lien, L.T., 1982. Linear theory of subsurface storm flow. Water Resources Research, 18(6): 1738-1740.

Koussis, A.D., Smith, M.E., Akylas, E., Tombrou, M., 1998. Groundwater drainage flow in a soil layer resting on an inclined leaky bed. Water resources research, 34(11): 2879-2887.

Leek, R., Wu, J.Q., Wang, L., Hanrahan, T.P., Barber, M.E., Qiu, H., 2009. Heterogeneous characteristics of streambed saturated hydraulic conductivity of the Touchet River, south eastern Washington, USA. Hydrological Processes: An International Journal, 23(8): 1236-1246.

Li, Q., Ito, K., Wu, Z., Lowry, C.S., Loheide II, S.P., 2009. COMSOL Multiphysics: A novel approach to ground water modeling. Groundwater, 47(4): 480-487.

Liang, X., Zhang, Y.K., 2012. Analytical solution for drainage and recession from an unconfined aquifer. Groundwater, 50(5): 793-798.

Luthin, J.N., Guitjens, J.C., 1967. Transient solutions for drainage of sloping land. Journal of Irrigation and Drainage Engineering.

Mahoney, J.M., Rood, S.B., 1998. Streamflow requirements for cottonwood seedling recruitment—an integrative model. Wetlands, 18(4): 634-645.

Manglik, A., Rai, S., Singh, R., 1997. Response of an unconfined aquifer induced by time varying recharge from a rectangular basin. Water resources management, 11(3): 185-196.

Marei, S., Towner, G., 1975. A Hele-Shaw Analog Study of the seepage of groundwater resting on a sloping bed. Water Resources Research, 11(4): 589-594.

Marino, M., 1973. Water-table fluctuation in semipervious stream-unconfined aquifer systems. Journal of Hydrology, 19(1): 43-52.

Moutsopoulos, K.N., 2013. Solutions of the Boussinesq equation subject to a nonlinear Robin boundary condition. Water Resources Research, 49(1): 7-18.

Mustafa, S., 1987. Water table rise in a semiconfined aquifer due to surface infiltration and canal recharge. Journal of hydrology, 95(3-4): 269-276.

Plan, L., Filipponi, M., Behm, M., Seebacher, R., Jeutter, P., 2009. Constraints on alpine speleogenesis from cave morphology—a case study from the eastern Totes Gebirge (Northern Calcareous Alps, Austria). Geomorphology, 106(1-2): 118-129.

Polubarinova, P.Y., Kochina, N., 1962. Theory of ground water movement. Princeton University Press.

Rai, S., Singh, R., 1992. Water table fluctuations in an aquifer system owing to time-varying surface infiltration and canal recharge. Journal of Hydrology, 136(1-4): 381-387.

Rai, S., Singh, R., 1995. An analytical solution for water-table fluctuation in a finite aquifer due to transient recharge from a strip basin. Water resources management, 9(1): 27-37.

Ram, S., Jaiswal, C., Chauhan, H., 1994. Transient water table rise with canal seepage and recharge. Journal of hydrology, 163(3-4): 197-202.

Rhodes, K.A., Proffitt, T., Rowley, T., Knappett, P.S., Montiel, D., Dimova, N., Tebo, D., Miller, G.R., 2017. The importance of bank storage in supplying baseflow to rivers flowing through compartmentalized, alluvial aquifers. Water Resources Research, 53(12): 10539-10557.

Sauro, F., Zampieri, D., Filipponi, M., 2013. Development of a deep karst system within a transpressional structure of the Dolomites in north-east Italy. Geomorphology, 184: 51-63.

Schmid, P., Luthin, J., 1964. The drainage of sloping lands. Journal of Geophysical Research, 69(8): 1525-1529.

Sebok, E., Duque, C., Engesgaard, P., Boegh, E., 2015. Spatial variability in streambed hydraulic conductivity of contrasting stream morphologies: channel bend and straight channel. Hydrological processes, 29(3): 458-472.

Sedghi, M.M. and Zhan, H., 2016. Hydraulic response of an unconfined-fractured two-aquifer system driven by dual tidal or stream fluctuations. Advances in water resources, 97, pp.266-278.

Shukla, K., Chauhan, H., Srivastava, V., 1990. Finite difference solution of Boussinesq unsteady-state equation for highly sloping lands. Journal of Irrigation and Drainage Engineering, 116(1): 107-113.

Sun, J., Miao, X., 2017. Water-isolating capacity of an inclined coal seam floor based on the theory of water-resistant key strata. Mine Water and the Environment, 36(2): 310-322.

Tang, Q., Kurtz, W., Schilling, O.S., Brunner, P., Vereecken, H., Franssen, H.J.H., 2017. The influence of riverbed heterogeneity patterns on river-aquifer exchange fluxes under different connection regimes. Journal of Hydrology, 554: 383-396.

Teloglou, I.S., Bansal, R.K., 2012. Transient solution for stream–unconfined aquifer interaction due to time varying stream head and in the presence of leakage. Journal of hydrology, 428: 68-79.

Theis, C.V., 1941. The effect of a well on the flow of a nearby stream. Eos, Transactions American Geophysical Union, 22(3): 734-738.

Therrien, R., McLaren, R., Sudicky, E., Panday, S., 2006. HydroGeoSphere, Groundwater Simul. Group. Univ. of Waterloo,(Link to software: http://hydrogeosphere.org/.).

Troch, P.A., Paniconi, C., Emiel van Loon, E., 2003. Hillslope-storage Boussinesq model for subsurface flow and variable source areas along complex hillslopes: 1. Formulation and characteristic response. Water Resources Research, 39(11).

Upadhyaya, A., Chauhan, H., 1998. Solutions of Boussinesq equation in semiinfinite flow region. Journal of irrigation and drainage engineering, 124(5): 265-270.

Upadhyaya, A., Chauhan, H., 2002. Water table rise in sloping aquifer due to canal seepage and constant recharge. Journal of irrigation and drainage engineering, 128(3): 160-167.

Van Der Valk, A.G., 2005. Water-level fluctuations in North American prairie wetlands. Hydrobiologia, 539(1): 171-188.

Van Genuchten, M.T., 1980. A closed-form equation for predicting the hydraulic conductivity of unsaturated soils 1. Soil science society of America journal, 44(5): 892-898.

Verhoest, N.E., Troch, P.A., 2000. Some analytical solutions of the linearized Boussinesq equation with recharge for a sloping aquifer. Water Resources Research, 36(3): 793-800.

Wang, F. et al., 2017. Impacts of injection pressure of a dip-angle sloping strata reservoir with low porosity and permeability on CO2 injection amount. Greenhouse Gases: Science and Technology, 7(1): 92-105.

Wooding, R., Chapman, T., 1966. Groundwater flow over a sloping impermeable layer: 1. Application of the Dupuit-Forchheimer assumption. Journal of Geophysical Research, 71(12): 2895-2902.

Workman, S., Serrano, S., Liberty, K., 1997. Development and application of an analytical model of stream/aquifer interaction. Journal of Hydrology, 200(1-4): 149-163.

Zhang, J., Shen, B., 2004. Coal mining under aquifers in China: a case study. International Journal of Rock Mechanics and Mining Sciences, 41(4): 629-639.

Zissis, T., Teloglou, I., Terzidis, G., 2001. Response of a sloping aquifer to constant replenishment and to stream varying water level. Journal of hydrology, 243(3-4): 180-191.

APPENDIX A

MATLAB SCRIPT FILES FOR COMPUTING THE WATER TABLE HEIGHTS IN SECTION 2.2

%Part 1 This part is to prepare the input of the corresponding parameters, to obtain the values of h_D (hh1 for horizontal, hh2 for 3 deg angle, hh3 for 5 deg angle, hh4 for 10 deg angle) and to calculate the values of water table heights hhhh1 and hydraulic heads hhh1.

```
clear;

W1=[2.0153, 0, 0.20153, 0.020153, 1.00765, 2.0153];
W2=[2.0153, 0, 0.20153, 0.020153, 1.00765, 2.0153];
W3=[2.0153, 0, 0.20153, 0.020153, 1.00765, 2.0153];
W4=[2.0153, 0, 0.20153, 0.020153, 1.00765, 2.0153];
W5=[2.0153, 0, 0.20153, 0.020153, 1.00765, 2.0153];

t1=0.0025*0.2;
t2=0.0025*0.4;
t3=0.0025*0.6;
t4=0.0025*0.8;
t5=0.0025;

t21=0.00248100969*0.2;
t22=0.00248100969*0.4;
t23=0.00248100969*0.6;
t24=0.00248100969*0.8;
t25=0.00248100969;

t31=0.00242461578*0.2;
t32=0.00242461578*0.4;
t33=0.00242461578*0.6;
t34=0.00242461578*0.8;
t35=0.00242461578;

x=[0, 0.02, 0.05, 0.08, 0.1, 0.15];
tt1=0:0.0025*0.002:t5;
tt2=0:0.00248100969*0.002:t25;
tt3=0:0.00242461578*0.002:t35;
%
% tt1=[t1 t2 t3 t4 t5];
% tt2=[t21 t22 t23 t24 t25];
% tt3=[t31 t32 t33 t34 t35];
```

```
x=0:0.001:0.15;
% t=[t1 t2 t3 t4 t5];
R1=[0.01008, 0.01005, 0.01000, 0.00978];
% R1=[0.02016, 0.02011, 0.02001, 0.01955];
t=0:1:50;

alpha=[0, 10.4816, 17.4977, 35.2654];
% alpha=[0, 10.4816, -17.4977, -35.2654];

lambda1=[2000, 2005.49, 2015.31, 2062.18];

hf1=[10, 3];
hi=5;
ha=5;
Ka=2.5;
L=1000;
theta=[0 3 5 10]*pi/180;

m1=[0 0.10537 0.17639 0.3555];

for i=1:length(tt1)
for j=1:length(x)

hh1(i,j)=h1(x(j),tt1(i),R1(1),alpha(1),lambda1(1),t1,t2,t3,t4,t5,m1(1),W1(2),W2(2),W3(2)
,W4(2),W5(2));
   hhh1(i,j)=hh1(i,j)*(hf1(1)-hi)+hi+tan(theta(1))*100*(1-x(j));
   hhhh1(i,j)=hh1(i,j)*(hf1(1)-hi)+hi;

end
end

for i=1:length(tt2)

for j=1:length(x)

hh3(i,j)=h1(x(j),tt2(i),R1(1),alpha(3),lambda1(3),t21,t22,t23,t24,t25,m1(3),W1(2),W2(2),
W3(2),W4(2),W5(2));
   hhh3(i,j)=hh3(i,j)*(hf1(1)-hi)+hi+tan(theta(3))*100*(1-x(j));
   hhhh3(i,j)=hh3(i,j)*(hf1(1)-hi)+hi;

end
end

for i=1:length(tt3)
```

```
for j=1:length(x)
hh4(i,j)=h1(x(j),tt3(i),R1(1),alpha(4),lambda1(4),t31,t32,t33,t34,t35,m1(4),W1(2),W2(2),
W3(2),W4(2),W5(2));
   hhh4(i,j)=hh4(i,j)*(hf1(1)-hi)+hi+tan(theta(4))*100*(1-x(j));
   hhhh4(i,j)=hh4(i,j)*(hf1(1)-hi)+hi;

end
end
```

Part 2

This part is a subroutine program to obtain the values of h_d and ω_n.

```
function [ val ] = h1(x,t,R1,alpha,lambda1,t1,t2,t3,t4,t5,m1,W1,W2,W3,W4,W5)

N=3000;
omega=get_omega(R1,alpha,N);
omega_n=omega(2:N);

beta_n=omega_n.^2+alpha^2/4;
An=(2./((omega_n.^2+(alpha/2-1/R1)^2).*(1+(alpha/2)./(omega_n.^2+(alpha/2)^2))-
alpha/2+1/R1)).^0.5;%%revised
xix=-An.*omega_n./R1;

xi1=-(1-m1)./beta_n;

xi2=1./(beta_n-lambda1);

xi4=-1./(beta_n-lambda1)+(1-m1)./beta_n;

xi5=(An./beta_n).*(exp(-alpha/2)*(beta_n.*sin(omega_n)-
(1/R1)*((alpha/2)*sin(omega_n)+omega_n.*cos(omega_n)))+(1/R1)*omega_n);

if (t<=t5) && (t>t4)
   Iwt=W5.*(exp(beta_n*(t-t))-exp(beta_n*(t4-t)))+W4.*(exp(beta_n*(t4-t))-
exp(beta_n*(t3-t)))+W3.*(exp(beta_n*(t3-t))-exp(beta_n*(t2-t)))+W2.*(exp(beta_n*(t2-
t))-exp(beta_n*(t1-t)))+W1.*(exp(beta_n*(t1-t))-exp(beta_n*(0-t)));
  %  Iwt(isnan(Iwt))=0;
elseif  (t<=t4) && (t>t3)
   Iwt=W4.*(exp(beta_n*(t-t))-exp(beta_n*(t3-t)))+W3.*(exp(beta_n*(t3-t))-
exp(beta_n*(t2-t)))+W2.*(exp(beta_n*(t2-t))-exp(beta_n*(t1-t)))+W1.*(exp(beta_n*(t1-
t))-exp(beta_n*(0-t)));
   % Iwt(isnan(Iwt))=0;
elseif (t<=t3 && t>t2)
   Iwt=W3.*(exp(beta_n*(t-t))-exp(beta_n*(t2-t)))+W2.*(exp(beta_n*(t2-t))-
exp(beta_n*(t1-t)))+W1.*(exp(beta_n*(t1-t))-exp(beta_n*(0-t)));
```

```
    %  Iwt(isnan(Iwt))=0;
elseif (t<=t2 && t>t1)
   Iwt=W2.*(exp(beta_n*(t-t))-exp(beta_n*(t1-t)))+W1.*(exp(beta_n*(t1-t))-
exp(beta_n*(0-t)));
     % Iwt(isnan(Iwt))=0;
elseif (t<=t1 && t>=0)
   Iwt=W1.*(exp(beta_n*(t-t))-exp(beta_n*(0-t)));

end
phi=xix.*(xi1+xi2*exp(-lambda1*t)+xi4.*exp(-
beta_n*t))+(xi5./beta_n).*Iwt;%(W3.*(exp(beta_n*(0.5-t))-exp(beta_n*(0.3-
t)))+W2.*(exp(beta_n*(0.3-t))-exp(beta_n*(0.1-t)))+W1.*(exp(beta_n*(0.1-t))-
exp(beta_n*(0-t))));
K=An.*(omega_n.*cos(omega_n*x)+(-alpha/2+1/R1)*sin(omega_n*x));%%revised
temp=K.*phi;
val=exp(x*alpha/2)*sum(temp);
end
% test=(xi5./beta_n).*(W3.*(exp(beta_n*(0.5-t))-exp(beta_n*(0.3-
t)))+W2.*(exp(beta_n*(0.3-t))-exp(beta_n*(0.1-t)))+W1.*(exp(beta_n*(0.1-t))-
exp(beta_n*(0-t))));
% test1=W3*(exp(beta_n*t));
% %disp(test);

function [val]=get_omega(R1,alpha,N)
% syms p_o R1 R2 alpha
% f=tan(p_o)-p_o*(1/R1+1/R2)/(p_o^2+(alpha/2-1/R1)*(alpha/2+1/R2));
% p_n=p_o-f/diff(f,p_o)
sing=sqrt(-(alpha/2-1/R1)*(alpha/2));
va=[0 0];
for ii=1:N

   if sing<(ii-1)*pi+pi/2 && sing>(ii-1)*pi-pi/2
      va=singular(ii,R1,alpha,sing);
      val(ii)=va(1);
      NN=ii;
      ii=ii+1;
   end
   p_o=pi*(ii-1)+eps;
   tol=1e-12;
   for kk=1:100
      p_n =p_o - (tan(p_o) - (p_o*(1/R1))/((alpha/2 - 1/R1)*(alpha/2) +
p_o^2))/(tan(p_o)^2 - 1/(R1*(p_o^2 + (alpha*(alpha/2 - 1/R1))/2)) +
(2*p_o^2)/(R1*(p_o^2 + (alpha*(alpha/2 - 1/R1))/2)^2) + 1);
      err=abs(p_n-p_o);
      %giving constraint
      if p_n>=(ii-1)*pi+pi/2
```

```
        p_n=(ii-1)*pi+pi/2-10000000*eps;
      end
      if p_n<=(ii-1)*pi-pi/2
        p_n=(ii-1)*pi-pi/2+10000000*eps;
      end
      p_o=p_n;
      if (err<tol)
        break;
      end
    end
    %break point
    val(ii)=p_o;
end
if va(2)~=0
    val=[val(1:NN),va(2),val(NN+1:end)];
end
end

%calculate omeiga at signular point
function va= singular(ii,R1,alpha,sing)
%first point
p_o=(sing+pi*(ii-1)-pi/2)/2;
tol=1e-12;
for kk=1:100
    p_n =p_o - (tan(p_o) - (p_o*(1/R1))/((alpha/2 - 1/R1)*(alpha/2) + p_o^2))/(tan(p_o)^2
- 1/(R1*(p_o^2 + (alpha*(alpha/2 - 1/R1))/2)) + (2*p_o^2)/(R1*(p_o^2 +
(alpha*(alpha/2 - 1/R1))/2)^2) + 1);
    err=abs(p_n-p_o);
    %giving constraint
    if p_n>=sing
      p_n=sing-10000000*eps;
    end
    if p_n<=(ii-1)*pi-pi/2
      p_n=(ii-1)*pi-pi/2+10000000*eps;
    end
    p_o=p_n;
    if (err<tol)
      break;
    end
end
va(1)=p_o;

%second point
p_o=(sing+pi*(ii-1)+pi/2)/2;
tol=1e-12;
for kk=1:100
```

```
    p_n =p_o - (tan(p_o) - (p_o*(1/R1))/((alpha/2 - 1/R1)*(alpha/2) + p_o^2))/(tan(p_o)^2
- 1/(R1*(p_o^2 + (alpha*(alpha/2 - 1/R1))/2)) + (2*p_o^2)/(R1*(p_o^2 +
(alpha*(alpha/2 - 1/R1))/2)^2) + 1);
    err=abs(p_n-p_o);
    %giving constraint
    if p_n<=sing
        p_n=sing+10000000*eps;
    end
    if p_n>=(ii-1)*pi+pi/2
        p_n=(ii-1)*pi+pi/2-10000000*eps;
    end
    p_o=p_n;
    if (err<tol)
        break;
    end
end
va(2)=p_o;
end
```

APPENDIX B

MATLAB SCRIPT FILES FOR COMPUTING THE WATER TABLE HEIGHTS IN

SECTION 3.2

%Part 1 This part is to prepare the input of corresponding parameters, to obtain the values of h_D (hh1 for horizontal, hh2 for 3 deg angle, hh3 for 5 deg angle, hh4 for 10 deg angle) and to calculate the values of water table heights hhhh1 and hydraulic heads hhh1.

```
clear;
clc

W1=[2.0153, 0, 2.0153, 0.020153, 1.00765, 2.0153];
W2=[2.0153, 0, 2.0153, 0.020153, 1.00765, 2.0153];
W3=[2.0153, 0, 2.0153, 0.020153, 1.00765, 2.0153];
W4=[2.0153, 0, 2.0153, 0.020153, 1.00765, 2.0153];
W5=[2.0153, 0, 2.0153, 0.020153, 1.00765, 2.0153];
t1=0.0606153944;
t2=0.06667693;
t3=0.121230789;
t4=0.127292328;
t5=0.303076972;

x=0:0.01:1;
t=[t1, t2, t3, t4, t5];

R1=[0.10081, 0.10053, 0.00992, 0.09777, 0.1];
R2=[0.10081, 0.10053, 0.00992, 0.09777, 0.1];

% alpha=[0, 1.04816, 1.74977, 3.52654, 1.80001];  % ha=5m
alpha=[0, 0.83852, 1.399818616, 2.82123, 1.44001];  % ha=6.25m

mu=[1, -0.18421];

lambda1=[16, 16.0439, 16.12246826, 16.4975];  % ha=6.25m

hf1=[10, 5];
hi=5;
ha=6.25;
L=100;
theta=[0 3 5 10 5.1428]*pi/180;

m1=[0 0.10537 0.17639 0.3555 0.17999];
```

```
m2=[0 0.10537 0.17639 0.3555 0.17999];

for i=1:length(t)
%     for i=1:length(theta)
for j=1:length(x)

hh1(i,j)=h(x(j),t(i),R1(1),R2(1),alpha(1),mu(1),lambda1(1),0,t1,t2,t3,t4,t5,m1(1),m2(1),
W1(2),W2(2),W3(2),W4(2),W5(2));
   hhh1(i,j)=hh1(i,j)*(hf1(1)-hi)+hi+tan(theta(1))*100*(1-x(j));
   hhhh1(i,j)=hh1(i,j)*(hf1(1)-hi)+hi;
end
end

for i=1:length(t)
%     for i=1:length(theta)
for j=1:length(x)
   %     xD, hhh

hh2(i,j)=h(x(j),t(i),R1(1),R2(1),alpha(2),mu(1),lambda1(2),0,t1,t2,t3,t4,t5,m1(2),m2(2),
W1(2),W2(2),W3(2),W4(2),W5(2));
   hhh2(i,j)=hh2(i,j)*(hf1(1)-hi)+hi+tan(theta(2))*100*(1-x(j));
   hhhh2(i,j)=hh2(i,j)*(hf1(1)-hi)+hi;
%     +tan(theta(3))*100*(1-x(j));
   tt(i)=t(i)*100.765;

end
end

for i=1:length(t)
%     for i=1:length(theta)
for j=1:length(x)
   %     xD, hhh

hh3(i,j)=h(x(j),t(i),R1(1),R2(1),alpha(3),mu(1),lambda1(3),0,t1,t2,t3,t4,t5,m1(3),m2(3),
W1(2),W2(2),W3(2),W4(2),W5(2));
   hhh3(i,j)=hh3(i,j)*(hf1(1)-hi)+hi+tan(theta(3))*100*(1-x(j));
   hhhh3(i,j)=hh3(i,j)*(hf1(1)-hi)+hi;
%     +tan(theta(3))*100*(1-x(j));
   tt(i)=t(i)*100.765;

end
end

for i=1:length(t)
%     for i=1:length(theta)
for j=1:length(x)
```

```
    %     xD, hhh

hh4(i,j)=h(x(j),t(i),R1(1),R2(1),alpha(4),mu(1),lambda1(4),0,t1,t2,t3,t4,t5,m1(4),m2(4),
W1(2),W2(2),W3(2),W4(2),W5(2));
    hhh4(i,j)=hh4(i,j)*(hf1(1)-hi)+hi+tan(theta(4))*100*(1-x(j));
    hhhh4(i,j)=hh4(i,j)*(hf1(1)-hi)+hi;
%     +tan(theta(3))*100*(1-x(j));
    tt(i)=t(i)*100.765;

end
end
```

%Part 2

This part is a subroutine program to obtain the values of h_d and ω_n.

```
function [ val ] =
h(x,t,R1,R2,alpha,mu,lambda1,lambda2,t1,t2,t3,t4,t5,m1,m2,W1,W2,W3,W4,W5)

N=3000;
omega=get_omega(R1,R2,alpha,N);
omega_n=omega(2:N);

beta_n=omega_n.^2+alpha^2/4;
An=(2./((omega_n.^2+(alpha/2-
1/R1)^2).*(1+(alpha/2+1/R2)./(omega_n.^2+(alpha/2+1/R2)^2))-
alpha/2+1/R1)).^0.5;%%revised

a=omega_n.*R2*exp(alpha/2)*(1-m1)+(mu+m2)*R1*(omega_n.*cos(omega_n)+(-
alpha/2+1/R1)*sin(omega_n));%%revised
b=R1*R2*beta_n*exp(alpha/2);
xi1=a./b;

xi2=omega_n./(R1*(beta_n-lambda1));

a=mu*(omega_n.*cos(omega_n)+(-alpha/2+1/R1)*sin(omega_n));%%revised
b=(beta_n-lambda2)*R2*exp(alpha/2);
xi3=a./b;

a=R2*(lambda1+m1.*(beta_n-lambda1)).*omega_n.*(beta_n-
lambda2)*exp(alpha/2)+R1*(mu.*lambda2-m2.*(beta_n-lambda2)).*(beta_n-
lambda1).*(omega_n.*cos(omega_n)+(-alpha/2+1/R1)*sin(omega_n));%%revised
b=beta_n*R1*R2.*(beta_n-lambda1).*(beta_n-lambda2)*exp(alpha/2);
xi4=a./b;

xi5=(An./beta_n).*(exp(-alpha/2)*(beta_n.*sin(omega_n)-
(1/R1)*((alpha/2)*sin(omega_n)+omega_n.*cos(omega_n)))+(1/R1)*omega_n);

if (t<=t5) && (t>t4)
   Iwt=W5.*(exp(beta_n*(t-t))-exp(beta_n*(t4-t)))+W4.*(exp(beta_n*(t4-t))-
exp(beta_n*(t3-t)))+W3.*(exp(beta_n*(t3-t))-exp(beta_n*(t2-t)))+W2.*(exp(beta_n*(t2-
t))-exp(beta_n*(t1-t)))+W1.*(exp(beta_n*(t1-t))-exp(beta_n*(0-t)));
elseif  (t<=t4) && (t>t3)
   Iwt=W4.*(exp(beta_n*(t-t))-exp(beta_n*(t3-t)))+W3.*(exp(beta_n*(t3-t))-
exp(beta_n*(t2-t)))+W2.*(exp(beta_n*(t2-t))-exp(beta_n*(t1-t)))+W1.*(exp(beta_n*(t1-
t))-exp(beta_n*(0-t)));
elseif (t<=t3 && t>t2)
```

```
   Iwt=W3.*(exp(beta_n*(t-t))-exp(beta_n*(t2-t)))+W2.*(exp(beta_n*(t2-t))-
exp(beta_n*(t1-t)))+W1.*(exp(beta_n*(t1-t))-exp(beta_n*(0-t)));
     %  Iwt(isnan(Iwt))=0;
elseif (t<=t2 && t>t1)
   Iwt=W2.*(exp(beta_n*(t-t))-exp(beta_n*(t1-t)))+W1.*(exp(beta_n*(t1-t))-
exp(beta_n*(0-t)));
      % Iwt(isnan(Iwt))=0;
elseif (t<=t1 && t>=0)
   Iwt=W1.*(exp(beta_n*(t-t))-exp(beta_n*(0-t)));

end
phi=An.*(xi1-xi2*exp(-lambda1*t)-xi3*exp(-lambda2*t)+xi4.*exp(-
beta_n*t))+(xi5./beta_n).*Iwt;%(W3.*(exp(beta_n*(0.5-t))-exp(beta_n*(0.3-
t)))+W2.*(exp(beta_n*(0.3-t))-exp(beta_n*(0.1-t)))+W1.*(exp(beta_n*(0.1-t))-
exp(beta_n*(0-t))));
K=An.*(omega_n.*cos(omega_n*x)+(-alpha/2+1/R1)*sin(omega_n*x));%%revised
temp=K.*phi;
val=exp(x*alpha/2)*sum(temp);
end

function [val]=get_omega(R1,R2,alpha,N)

sing=sqrt(-(alpha/2-1/R1)*(alpha/2+1/R2));
va=[0 0];
for ii=1:N

   if sing<(ii-1)*pi+pi/2 && sing>(ii-1)*pi-pi/2
      va=singular(ii,R1,R2,alpha,sing);
      val(ii)=va(1);
      NN=ii;
      ii=ii+1;
   end
   p_o=pi*(ii-1)+eps;
   tol=1e-12;

   for kk=1:100
      p_n =p_o - (tan(p_o) - (p_o*(1/R1 + 1/R2))/((alpha/2 - 1/R1)*(alpha/2 + 1/R2) +
p_o^2))/(tan(p_o)^2 - (1/R1 + 1/R2)/((alpha/2 - 1/R1)*(alpha/2 + 1/R2) + p_o^2) +
(2*p_o^2*(1/R1 + 1/R2))/(p_o^2 + (alpha/2 - 1/R1)*(alpha/2 + 1/R2))^2 + 1);
      err=abs(p_n-p_o);
      %giving constraint
      if p_n>=(ii-1)*pi+pi/2
         p_n=(ii-1)*pi+pi/2-10000000*eps;
      end
      if p_n<=(ii-1)*pi-pi/2
         p_n=(ii-1)*pi-pi/2+10000000*eps;
```

```
        end
        p_o=p_n;
        if (err<tol)
           break;
        end
    end
    %break point
    val(ii)=p_o;
end
if va(2)~=0
    val=[val(1:NN),va(2),val(NN+1:end)];
end
end

%calculate omeiga at signular point
function va= singular(ii,R1,R2,alpha,sing)
%first point
p_o=(sing+pi*(ii-1)-pi/2)/2;
tol=1e-12;
for kk=1:100
    p_n =p_o - (tan(p_o) - (p_o*(1/R1 + 1/R2))/((alpha/2 - 1/R1)*(alpha/2 + 1/R2) +
p_o^2))/(tan(p_o)^2 - (1/R1 + 1/R2)/((alpha/2 - 1/R1)*(alpha/2 + 1/R2) + p_o^2) +
(2*p_o^2*(1/R1 + 1/R2))/(p_o^2 + (alpha/2 - 1/R1)*(alpha/2 + 1/R2))^2 + 1);
    err=abs(p_n-p_o);
    %giving constraint
    if p_n>=sing
        p_n=sing-10000000*eps;
    end
    if p_n<=(ii-1)*pi-pi/2
        p_n=(ii-1)*pi-pi/2+10000000*eps;
    end
    p_o=p_n;
    if (err<tol)
        break;
    end
end
va(1)=p_o;

%second point
p_o=(sing+pi*(ii-1)+pi/2)/2;
tol=1e-12;
for kk=1:100
    p_n =p_o - (tan(p_o) - (p_o*(1/R1 + 1/R2))/((alpha/2 - 1/R1)*(alpha/2 + 1/R2) +
p_o^2))/(tan(p_o)^2 - (1/R1 + 1/R2)/((alpha/2 - 1/R1)*(alpha/2 + 1/R2) + p_o^2) +
(2*p_o^2*(1/R1 + 1/R2))/(p_o^2 + (alpha/2 - 1/R1)*(alpha/2 + 1/R2))^2 + 1);
    err=abs(p_n-p_o);
```

```
    %giving constraint
    if p_n<=sing
        p_n=sing+10000000*eps;
    end
    if p_n>=(ii-1)*pi+pi/2
        p_n=(ii-1)*pi+pi/2-10000000*eps;
    end
    p_o=p_n;
    if (err<tol)
        break;
    end
end
va(2)=p_o;
end

% %get Wt
% function [val]=get_Wt(t)
% if (t>=0&t<0.1)
%     val=3.1;
% elseif(t>=0.1&t<0.3)
%     val=6.2;
% else(t>=0.3&t<=0.5)
%     val=0;
% end
% end
```

APPENDIX C

MATLAB SCRIPT FILES FOR COMPUTING THE WATER TABLE HEIGHTS IN SECTION 4.2

%Part 1 This part is to prepare the input of corresponding parameters, to obtain the values of h_D (hh1 for horizontal, hh2 for 3 deg angle, hh3 for 5 deg angle, hh4 for 10 deg angle) and to calculate the values of water table heights hhhh1 and hydraulic heads hhh1.

```
clear;

W1=[2.0153, 0, 0.20153, 0.020153, 1.00765, 2.0153];
W2=[2.0153, 0, 0.20153, 0.020153, 1.00765, 2.0153];
W3=[2.0153, 0, 0.20153, 0.020153, 1.00765, 2.0153];
W4=[2.0153, 0, 0.20153, 0.020153, 1.00765, 2.0153];
W5=[2.0153, 0, 0.20153, 0.020153, 1.00765, 2.0153];

t1=0.0025*0.2;
t2=0.0025*0.4;
t3=0.0025*0.6;
t4=0.0025*0.8;
t5=0.0025*2;

t21=0.00248100969*0.2;
t22=0.00248100969*0.4;
t23=0.00248100969*0.6;
t24=0.00248100969*0.8;
t25=0.00248100969*2;

% t31=0.00242461578*0.2;
% t32=0.00242461578*0.4;
% t33=0.00242461578*0.6;
% t34=0.00242461578*0.8;
% t35=0.00242461578*1;

t31=0.00026940175*0.2;
t32=0.00026940175*0.4;
t33=0.00026940175*0.6;
t34=0.00026940175*0.8;
t35=0.00026940175*2; %L=3000m

% x=[0, 0.025, 0.05, 0.075];
x=[0, 0.05, 0.1, 0.15];
```

```
% x=[0, 0.01666667, 0.0333333, 0.05];

% x=0:0.0005:0.075;
tt1=0:0.0025*0.02:t5;
tt2=0:0.00248100969*0.02:t25;
tt3=0:0.00242461578*0.02:t35;

% tt1=0:0.0025*0.02:t5;
% tt2=0:0.00248100969*0.02:t25;
% tt3=0:0.00026940175*0.02:t35;

% % 2000m
% tt1=0:0.000625*0.002:t5;
% tt2=0:0.00062025242*0.002:t25;
% tt3=0:0.00060615394*0.002:t35;

% tt1=[t1 t2 t3 t4 t5];
% tt2=[t21 t22 t23 t24 t25];
% tt3=[t31 t32 t33 t34 t35];

t=0:1:1000;
% x=0:0.001:0.15;
% t=[t1 t2 t3 t4 t5];
% t=0.025;
R1=[0.01008, 0.01005, 0.01000, 0.00978];
% R1=[0.02016, 0.02011, 0.02001, 0.01955];
% R1=[0.00504, 0.00503, 0.005, 0.00489]; % L=2000m
% R1=[0.00326, 0.01005, 0.01000, 0.00978];% L=3000m


%
alpha=[0, 10.4816, 17.4977, 35.2654];
% alpha=[0, 10.4816, -17.4977, -35.2654];
% alpha=[0, 20.96311171, 34.99546541, 70.53079228]; %L=2000m
% alpha=[0, 10.4816, 17.4977, 105.796];

% lambda1=[2000, 2005.49, 2015.31, 2062.18];
% lambda1=[0, 0, 0, 0];
% lambda1=[1000, 1002.75, 1007.65, 1031.09];
% lambda1=[2800, 1002.75, 2821.43, 2887.06];

hf1=[7, 3];
hi=5;
ha=5;
Ka=2.5;
L=1000;
```

```
theta=[0 3 5 10]*pi/180;
% a=[20000, 20054.9, 20153.1, 20621.8];
% a=[80000, 80219.7, 80612, 82487];
a=[20000, 20054.9, 20153.1, 20621.8];
% c=-1009;
c=-59;
% theta=[0 3 -5 -10]*pi/180;

% m1=[0 0.10537 0.175049 0.34478];
% m1=[0 0.10537 -0.175049 -0.34478];
% m1=[0 0.21074 0.350097 0.68956];
% m1=[0 0.10537  0.43762   0.86195];
% m2=[0 0.10537 -0.43762 -0.86195];
m1=[0 0.10537  0.44097   0.8887];

for i=1:length(tt1)
%     for i=1:length(theta)
for j=1:length(x)
   %     xD, hhh

hh1(i,j)=h2(x(j),tt1(i),R1(1),alpha(1),t1,t2,t3,t4,t5,m1(1),W1(2),W2(2),W3(2),W4(2),W5
(2),a(1),c);

   hhh1(i,j)=hh1(i,j)*(hf1(1)-hi)+hi+tan(theta(1))*1000*(1-x(j));
   hhhh1(i,j)=hh1(i,j)*(hf1(1)-hi)+hi;

end
end

for i=1:length(tt2)

for j=1:length(x)

hh3(i,j)=h2(x(j),tt2(i),R1(1),alpha(3),t21,t22,t23,t24,t25,m1(3),W1(2),W2(2),W3(2),W4(
2),W5(2),a(3),c);
   hhh3(i,j)=hh3(i,j)*(hf1(1)-hi)+hi+tan(theta(3))*1000*(1-x(j));
   hhhh3(i,j)=hh3(i,j)*(hf1(1)-hi)+hi;

end
end

for i=1:length(tt3)

for j=1:length(x)
hh4(i,j)=h2(x(j),tt3(i),R1(1),alpha(4),t31,t32,t33,t34,t35,m1(4),W1(2),W2(2),W3(2),W4(
2),W5(2),a(4),c);
```

```
    hhh4(i,j)=hh4(i,j)*(hf1(1)-hi)+hi+tan(theta(4))*1000*(1-x(j));
    hhhh4(i,j)=hh4(i,j)*(hf1(1)-hi)+hi;

end
end

 %Part 2
```

This part is a subroutine program to obtain the values of h_d and ω_n.

```
function [ val ] = h2(x,t,R1,alpha,t1,t2,t3,t4,t5,m1,W1,W2,W3,W4,W5,a,c)

N=3000;
omega=get_omega(R1,alpha,N);
omega_n=omega(2:N);

beta_n=omega_n.^2+alpha^2/4;
An=(2./((omega_n.^2+(alpha/2-1/R1)^2).*(1+(alpha/2)./(omega_n.^2+(alpha/2)^2))-
alpha/2+1/R1)).^0.5;%%revised
xix=-An.*omega_n./R1;

xi1=-(1-m1)./beta_n;

% for kkk=1:length(t)
fun = @(x) exp(beta_n.*(x-t))./(1+exp(a*x+c));

xi2=integral(fun,0,t,'ArrayValued',true);

xi4=(1-m1)./beta_n;

xi5=(An./beta_n).*(exp(-alpha/2)*(beta_n.*sin(omega_n)-
(1/R1)*((alpha/2)*sin(omega_n)+omega_n.*cos(omega_n)))+(1/R1)*omega_n);

if (t<=t5) && (t>t4)
    Iwt=W5.*(exp(beta_n*(t-t))-exp(beta_n*(t4-t)))+W4.*(exp(beta_n*(t4-t))-
exp(beta_n*(t3-t)))+W3.*(exp(beta_n*(t3-t))-exp(beta_n*(t2-t)))+W2.*(exp(beta_n*(t2-
t))-exp(beta_n*(t1-t)))+W1.*(exp(beta_n*(t1-t))-exp(beta_n*(0-t)));
  %  Iwt(isnan(Iwt))=0;
elseif  (t<=t4) && (t>t3)
    Iwt=W4.*(exp(beta_n*(t-t))-exp(beta_n*(t3-t)))+W3.*(exp(beta_n*(t3-t))-
exp(beta_n*(t2-t)))+W2.*(exp(beta_n*(t2-t))-exp(beta_n*(t1-t)))+W1.*(exp(beta_n*(t1-
t))-exp(beta_n*(0-t)));
   % Iwt(isnan(Iwt))=0;
elseif (t<=t3 && t>t2)
    Iwt=W3.*(exp(beta_n*(t-t))-exp(beta_n*(t2-t)))+W2.*(exp(beta_n*(t2-t))-
exp(beta_n*(t1-t)))+W1.*(exp(beta_n*(t1-t))-exp(beta_n*(0-t)));
     %  Iwt(isnan(Iwt))=0;
```

```
elseif (t<=t2 && t>t1)
   Iwt=W2.*(exp(beta_n*(t-t))-exp(beta_n*(t1-t)))+W1.*(exp(beta_n*(t1-t))-
exp(beta_n*(0-t)));
      % Iwt(isnan(Iwt))=0;
elseif (t<=t1 && t>=0)
   Iwt=W1.*(exp(beta_n*(t-t))-exp(beta_n*(0-t)));
      %Iwt(isnan(Iwt))=0;

end
phi=xix.*(xi1+xi2+xi4.*exp(-beta_n*t))+(xi5./beta_n).*Iwt;
%(W3.*(exp(beta_n*(0.5-t))-exp(beta_n*(0.3-t)))+W2.*(exp(beta_n*(0.3-t))-
exp(beta_n*(0.1-t)))+W1.*(exp(beta_n*(0.1-t))-exp(beta_n*(0-t))));
K=An.*(omega_n.*cos(omega_n*x)+(-alpha/2+1/R1)*sin(omega_n*x));%%revised
temp=K.*phi;
val=exp(x*alpha/2)*sum(temp);
end

function [val]=get_omega(R1,alpha,N)
% syms p_o R1 R2 alpha
% f=tan(p_o)-p_o*(1/R1+1/R2)/(p_o^2+(alpha/2-1/R1)*(alpha/2+1/R2));
% p_n=p_o-f/diff(f,p_o)
sing=sqrt(-(alpha/2-1/R1)*(alpha/2));
va=[0 0];
for ii=1:N

   if sing<(ii-1)*pi+pi/2 && sing>(ii-1)*pi-pi/2
      va=singular(ii,R1,alpha,sing);
      val(ii)=va(1);
      NN=ii;
      ii=ii+1;
   end
   p_o=pi*(ii-1)+eps;
   tol=1e-12;

   for kk=1:100
      p_n =p_o - (tan(p_o) - (p_o*(1/R1))/((alpha/2 - 1/R1)*(alpha/2) +
p_o^2))/(tan(p_o)^2 - 1/(R1*(p_o^2 + (alpha*(alpha/2 - 1/R1))/2)) +
(2*p_o^2)/(R1*(p_o^2 + (alpha*(alpha/2 - 1/R1))/2)^2) + 1);
      err=abs(p_n-p_o);
      %giving constraint
      if p_n>=(ii-1)*pi+pi/2
         p_n=(ii-1)*pi+pi/2-10000000*eps;
      end
      if p_n<=(ii-1)*pi-pi/2
         p_n=(ii-1)*pi-pi/2+10000000*eps;
      end
```

```
        p_o=p_n;
        if (err<tol)
           break;
        end
    end
    %break point
    val(ii)=p_o;
end
if va(2)~=0
    val=[val(1:NN),va(2),val(NN+1:end)];
end
end

%calculate omeiga at signular point
function va= singular(ii,R1,alpha,sing)
%first point
p_o=(sing+pi*(ii-1)-pi/2)/2;
tol=1e-12;
for kk=1:100
    p_n =p_o - (tan(p_o) - (p_o*(1/R1))/((alpha/2 - 1/R1)*(alpha/2) + p_o^2))/(tan(p_o)^2
- 1/(R1*(p_o^2 + (alpha*(alpha/2 - 1/R1))/2)) + (2*p_o^2)/(R1*(p_o^2 +
(alpha*(alpha/2 - 1/R1))/2)^2) + 1);
    err=abs(p_n-p_o);
    %giving constraint
    if p_n>=sing
        p_n=sing-10000000*eps;
    end
    if p_n<=(ii-1)*pi-pi/2
        p_n=(ii-1)*pi-pi/2+10000000*eps;
    end
    p_o=p_n;
    if (err<tol)
        break;
    end
end
va(1)=p_o;

%second point
p_o=(sing+pi*(ii-1)+pi/2)/2;
tol=1e-12;
for kk=1:100
    p_n =p_o - (tan(p_o) - (p_o*(1/R1))/((alpha/2 - 1/R1)*(alpha/2) + p_o^2))/(tan(p_o)^2
- 1/(R1*(p_o^2 + (alpha*(alpha/2 - 1/R1))/2)) + (2*p_o^2)/(R1*(p_o^2 +
(alpha*(alpha/2 - 1/R1))/2)^2) + 1);
    err=abs(p_n-p_o);
    %giving constraint
```

```
    if p_n<=sing
        p_n=sing+10000000*eps;
    end
    if p_n>=(ii-1)*pi+pi/2
        p_n=(ii-1)*pi+pi/2-10000000*eps;
    end
    p_o=p_n;
    if (err<tol)
        break;
    end
end
va(2)=p_o;
end
```

APPENDIX D

DERIVATION OF MODIFIED DARCY'S LAW FOR A SLOPING AQUIFER

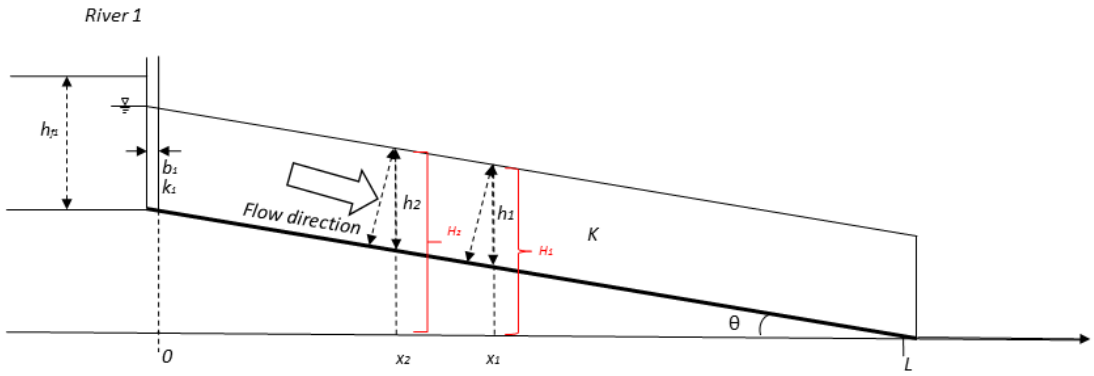

Fig. A-1 A diagram of water flow in an unconfined aquifer.

Fig. A-1 is the schematic diagram showing groundwater flow in a sloping aquifer. The coordinate system setup in Fig. A-1 and the symbols are the same as in section 2.2. The flow direction in an unconfined sloping aquifer is parallel to the sloping bed. In this part, q is the discharge over the entire unconfined aquifer per unit width. The parameter "h" represents water table height and the parameter "H" represent hydraulic head. The subscripts 1 and 2 represent a down-gradient point (point 1) and an up-gradient point (point 2) that are very close with each other with a small horizontal interval of $\Delta x = x_1 - x_2$, where x_1 and x_2 are the horizontal coordinates of point 1 and 2, respectively.

Water flows through a cross section, and the aquifer saturated thickness perpendicular to the flow direction (which is parallel to the sloping bed) is $hcos\theta$. The hydraulic gradient in the direction of the sloping bed is $\frac{dH}{dx/cos\theta}$, where the term of "dx/cosθ" is the difference of length in the direction of the sloping bed. The Darcy's law in a sloping aquifer can be expressed as below:

$$q(x,t) = -Khcos\theta \frac{H_2 - H_1}{(x_2 - x_1)/cos\theta}. \quad \text{(A-1)}$$

The hydraulic head can be described by water table height and the sloping angle in the following.

$$H = h + (L - x)\tan\theta \quad \text{(A-2)}$$

Substituting Eq. (A-2) into Eq. (A-1), one has

$$q(x,t) = -Khcos\theta \frac{h_2 + (L - x_2)tan\theta - [h_1 + (L - x_1)tan\theta]}{(x_2 - x_1)/cos\theta} \quad \text{(A-3)}$$

Eq. (A-3) can be simplified easily in the following.

$$q(x,t) = -Khcos^2\theta\left(\frac{h_2 - h_1}{x_2 - x_1} - tan\theta\right) \quad \text{(A-4)}$$

where the term of $\frac{h_2 - h_1}{x_2 - x_1}$ can be expressed as $\frac{\partial h}{\partial x}$, and the modified Darcy's law for a sloping aquifer is obtained below:

$$q(x,t) = -Kh\left(\frac{\partial h}{\partial x} - tan\theta\right)cos^2\theta \quad \text{(A-5)}$$